
**Universidad Pontificia Comillas de Madrid**
**Escuela Técnica Superior de Ingeniería (ICAI)**

**Instituto de Investigación Tecnológica (IIT)**

# DC segmentation of electrical grids to improve power system stability

**Author:** Mathieu Robin

**Supervisors:** Dr. Francisco Javier Renedo Anglada
Prof. Dr. Aurelio García Cerrada
Dr. Juan Carlos Gonzalez Torres

October 23, 2024

Madrid, Spain

# Summary

In recent decades, electrical transmission grids have seen a shift from conventional High Voltage Alternating Current (HVAC) transmission systems to hybrid power systems with a growing share of High Voltage Direct Current (HVDC) transmission (hybrid HVAC/HVDC systems). In parallel with the development of HVDC links, power systems have also become more and more interconnected creating large AC synchronous electrical grids, increasing their total inertia and thus enhancing their frequency stability and overall reliability.

However, with the continuous industrial growth and the introduction of new economical objectives, power systems are operated closer to their stability limits. Consequently, the risk of severe disruptions is increasing. Indeed, in the last decades, various events have shown that electromechanical oscillations, transient stability and stability issues in general are a threat for large power systems.

This doctoral dissertation investigates a promising application of HVDC systems to tackle severe instability problems: DC segmentation. DC segmentation is the action of going from one large AC synchronous grid into a set of smaller AC asynchronous grids connected by HVDC links. Specifically, this research focuses on the study and the improvements of the effects of DC segmentation using HVDC systems based on Voltage Source Converters (VSC-HVDC) on power system stability.The power system-stability phenomena studied in this PhD being angle stability under small disturbances (electromechanical oscillations), angle stability under large disturbances (transient stability) and frequency stability.

The main findings of this PhD thesis can be summarised as follows:

- DC segmentation can be very effective to suppress critical inter-area oscillations in stressed AC power systems. Thus, a new DC segmentation algorithm has been proposed to mitigate inter-area electromechanical

oscillations. The proposed algorithm obtains a DC-segmentation architecture for an initial HVAC system.

- DC segmentation with VSC-HVDC systems controlled with constant power references has small impact on intra-area electromechanical oscillations. Thus, Power Oscillation Damping (POD) controllers for the reactive-power injections of the converter stations of the VSC-HVDC segments (POD-Q controllers) have been proposed and implemented in order to damp intra-area oscillations in a DC-segmented test system. POD-Q controllers using local and global measurements have been analysed, proving that they can help to damp intra-area oscillations.

- DC segmentation with VSC-HVDC systems controlled with constant power references jeopardises frequency stability of the overall system. Thus, an active-power supplementary controller for frequency support has been implemented in the VSC-HVDC segments in order to mitigate this issue.

- Altogether, the use of DC segmentation, frequency support and POD-Q control brings an important improvement of the overall stability of power systems compared to the initial AC system. DC segmentation could be of interest in stressed large-scale power systems in which angle stability is critical.

# Acknowledgments

A PhD thesis is a very long journey filled with hopes and doubts, joys and struggles, and that is impossible to fulfil without the support and guidance of others. Thus, before jumping into the scientific content of this manuscript, I ought to thank the people that have been part of this journey with their time, expertise and love.

First of all, I would like to express my deepest gratitude to my PhD thesis supervisors Dr. Francisco Javier Renedo Anglada, Prof. Dr. Aurelio García Cerrada and Dr. Juan Carlos Gonzalez Torres. Javier, your enthusiasm, guidance and mentorship throughout these years have been crucial to the success of this PhD. Thank you for having always managed to make yourself available when needed! Even when the distance and the circumstances weren't on our side. Aurelio, your feedback has been invaluable, thank you for bringing your experience and diligence to the table. Juan Carlos, you are the one that introduced me to the world of AC/DC stability and RMS simulation, thank you for your diligence and your friendliness. The valuable ideas, suggestions and comments provided by the three of you have been essential for the development and successful completion of this thesis. Without your perseverance, knowledge and trust, I would definitely not have been able to complete this project. ¡Muchísimas gracias a los tres!

I was also lucky to be part of Dr. Abdelkrim Benchaib's team. Thank you Abdelkrim, for having built such a great working environment and for


believing in our work every day, it was truly supportive to work with you. In addition, I would also like to say thank you to Dr. Pablo García González for his guidance, wise remarks and feedback.

However, a PhD journey is not just about the supervisory team, and in my case, I had the opportunity to join an incredible research group in SuperGrid Institute (the "Control and Stability Group") to pursue my work. Hind, Rayane, Kosei, Paul, Miguel, Lucas, and Gianni—thank you for your collaboration and support. During my years in the institute, I also had the privilege to meet amazing people outside of my working group. To Antoine, Myriam, Pascal, Helena, Nicolas, Shafie, William, Guilherme, Diego, Gustavo, Regina, Titouan, Mohamed, Phong, Daniel, Ying, Filipe, Nathan, Eugène, Kirsty, Matthieu, Louis, Aubin, Jing, Seddik, and all the others I met there: thank you! You have contributed to making my stay a great and enriching experience.

I am grateful for the support I received from Comillas Pontifical University, Madrid, going from the administrative staff to the skilled researchers from IIT (Instituto de Investigación Tecnológica) with whom I had the chance to discuss many technical aspects. Thank you, Luis, Lukas, Ajda and Enrique for the help and the welcome in Comillas. Then, I would like to thank SuperGrid Institute and its management board for having funded my research project and having believed in me. Likewise, I would like to thank the French Government that has supported this work with a grant overseen by the French National Research Agency (ANR) as part of the "Investissements d'Avenir" Program (ANE-ITE-002-01).

On a more personal note, I want to thank those who made these years enjoyable outside of work as well. To my many roommates: Vincent, Floriane, Joanna, Apolline, Leyre, Coralie, Inés and Marine, thank you for your friendship and support. You made my time in Lyon memorable, and I am very grateful to have met you. As my PhD has been an international endeavour, I would also like to thank some of my Spanish friends: Eloy, Serra and Vicente for you friendship and support. Thank you also to my favourite climbing partners: Josselin, William, Domagoj, for our many adventures that helped me to escape the difficult times of the PhD. And thank you to Ari, despite the many kilometres between us, your friendship and love means a lot to me.

Finally, I would like to thank the ones that have always been there for me: my parents and brother, thank you for your unconditional love and support, I would never have done half of this work without you!

# Contents

# List of Tables

# List of Figures

# Acronyms

**CCT:** Critical Clearing Time.

**COI:** Centre Of Inertia.

**EMT:** Electromagnetic Transient.

**FACTS:** Flexible Alternating Current Transmission System.

**FC:** Frequency Control.

**GFL-VSC:** Grid-Following Voltage Source Converter.

**GFM-VSC:** Grid-Forming Voltage Source Converter.

**HVAC:** High Voltage Alternating Current.

**HVDC:** High Voltage Direct Current.

**LCC:** Line Commutated Converter.

**MTDC:** Multi-Terminal HVDC system.

**MMC:** Modular Multilevel Converter.

**OHL:** Overhead transmission Lines.

**PLL:** Phase-Locked Loop.

**POD:** Power-Oscillation Damping.

**PSS:** Power System Stabilisers.

**Q-LF:** reactive-Power control strategy based on Local Frequency.

**Q-FCOI:** reactive-Power control strategy based on the Frequency of the Centre Of Inertia.

**RES:** Renewable Energy Sources.

**RMS:** Root-Mean-Square.

**SG:** Synchronous Generator.

**SSA:** Small-Signal Analysis.

**TSO:** Transmission System Operator.

**VSC:** Voltage Source Converter.

**WAF:** Weighted-Average of the Frequencies measured at the AC terminals of a VSC-MTDC system.

# Chapter 1

# Introduction

## 1.1 HVAC and HVDC transmission

The genesis of electric power systems was marked by a passionate competition (sometimes theatrically called the War of the Currents) between two technologies of power transmission: the Alternating Current (AC) technology, promoted by George Westinghouse and Nikola Tesla and the Direct Current (DC) supported - among others - by Thomas A. Edison.

During the 20th century, AC technology progressively became the prevalent technology for the transmission and distribution of electricity driven, mainly, by the existence of the transformer that made voltage step-up possible and thus reduce line losses in long-distance electricity transmission. Such thing was not possible for DC systems since no technology existed at the time to increase DC voltage.

Initially, the first AC grids were of limited size, but they gradually expanded to regional, national, and even continental scales, forming wide-area synchronous grids. One example of those grids is the Continental Europe synchronous grid (see Fig. 1.1) supplying over 400 million people in 24 countries.

While AC technology still is the dominant technology for the transmission and distribution of electricity, it is limited by some technical aspects that can be overcome by the DC technology developed in the last decades [5].

Indeed, in face of the growing need to decarbonise the economy while satisfying public needs, power grids are currently facing the following main challenges:

- The increase of the total load - and thus generation - in order to electrify

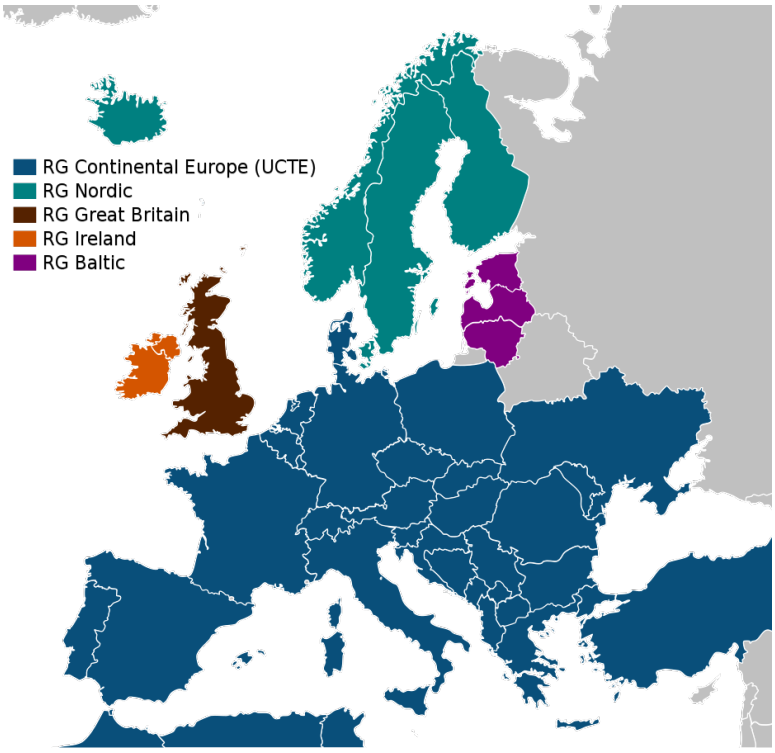


Figure 1.1: Main synchronous grids of Europe [1].

some historically non-electrified sectors (especially the transport sector with the rise of electrical vehicles).

- The rise of renewable-but-intermittent energy sources (RES), mainly wind and solar.
- The often large distance between the energy production centres and the energy consumption.
- The increase of distributed generation (notice that this point is contradictory to the previous one).
- The growing public resentment over overhead transmission lines (OHL) leading to an increase of the use of underground cables.

Overcoming these challenges would require a substantial evolution of current electrical grids with the construction of many new transmission lines for the transmission of electricity over long distances, either to increase the interconnection between countries and regions, or to connect bulk sources of production to the rest of the grid. Additionally, many of these transmission lines would actually be underground or underwater cables due to geographical constraints (manly for the connection of offshore wind farms or distant countries) or public acceptance issues.

In many of these applications, HVDC transmission is better suited than HVAC transmission (or even the only solution). For example, no AC link would ever connect two asynchronous grids. Additionally, due to the capacitive effect and the need of reactive power compensation, it is nearly impossible to use underground or undersea AC cables for long distances. Finally, over a certain distance, known as the break-even distance, HVDC transmission becomes cheaper than HVAC transmission. This is due to the lower losses, lower amount of cables needed and the absence of reactive power compensation for HVDC, even with the initial high cost of the AC/DC converter stations (see Fig. 1.2). The break even distance is typically around 600km for OHL and 50km for underground or submarine cables [6, 7].

Summarising, the main applications were HVDC transmission may be more appropriate than HVAC transmission are:

- Connection of asynchronous AC power networks.
- Transmission of bulk power via OHL over long distances.
- Transmission of power via isolated cables (submarine and underground) over medium-to-long distances.

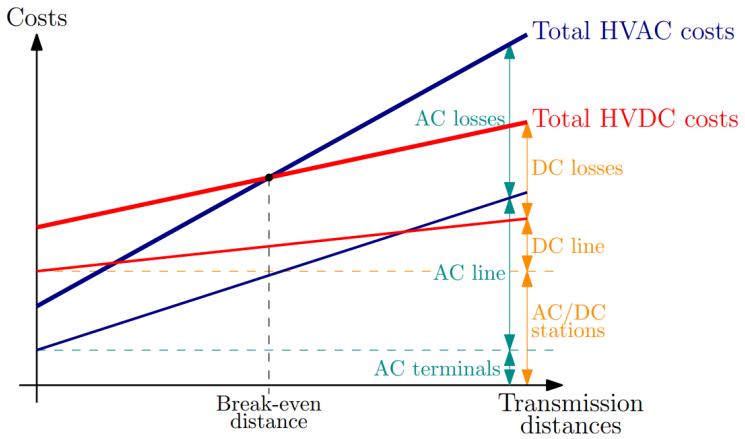


Figure 1.2: Cost comparison between HVAC and HVDC transmission systems. Figure from [2].

## 1.2 HVDC transmission technologies

HVDC transmission can be based on two converter technologies: thyristor-based **Line-Commutated Converters (LCCs)** and IGBT-based self- commutated **Voltage Source Converters (VSCs)**.

LCC technology is a more mature technology with most of the existing HVDC links using this kind of converters. However, VSC-based technology is currently becoming the preferred technology thanks to its superior controllability and flexibility. In particular, VSCs have a constant DC voltage, can control reactive power independently of active power at the AC side, can rapidly change the power direction, can be connected to weak grids, and can offer black-start capability.

VSC technology takes different forms, from the conventional **2-level VSC** to the more recent **Modular Multilevel Converter (MMC)** [8–10]. MMC topology possesses all the advantages of the 2-level VSC while limiting many of its problems. Indeed, in comparison with the 2-level VSC, MMC have higher power ratings, smoother outputs with much lower amount of harmonics (and thus do not require expensive harmonic filters), a much better electromagnetic compatibility and lower losses.

A VSC-HVDC converter can be controlled in various manners, the two most common ones being grid-following and grid-forming control.

**Grid-following** (GFL-VSC) also known as current-source control is the

traditional method. GFL-VSC power converters behave as a current source. They impose both the active and reactive power by controlling the current injection to the AC grid. To do so, a GFL-VSC locates the voltage space vector at the AC connection point using a Phase-Locked Loop (PLL) and orientates its output current according to the active- and reactive-power set points. Thus, a GFL-VSC must always be connected to a functioning AC grid.

**Grid-forming** (GFM-VSC), also known as voltage-source control, has emerged more recently. Originally, it was intended for islanded applications [11] but it is also becoming a common request from TSOs of bulk power systems [12–14]. In this control mode, the VSC operates as a voltage source behind a series impedance and thus, imposes the voltage magnitude and frequency at the point of connection. Since more than one GFM-VSC or several synchronous generators (SGs) may also be connected to the same grid, some form of synchronisation mechanism has to be provided. This strategy is the most appropriate to connect VSCs to weak grids. GFM-VSCs need a self-synchronisation strategy to operate in power systems with other conventional synchronous generation or GFM-VSC generation [11–14].

Supplementary controllers can be implement in both grid-following and grid-forming VSCs in order to improve the stability of the system. As an example, embedded VSC-HVDC systems (i.e. VSC-HVDC systems with both VSCs connected in the same AC grid) can participate in the damping of the system [15] while VSC connected to small asynchronous regions [16] can provide frequency support. A review of the supplementary controllers of VSCs is presented in Section 2.3.

For the remainder of this work, unless stated otherwise, all the systems studied will be VSC-HVDC controlled in grid-following mode.

## 1.3 Existing and future HVDC links

Table 1.1 [17] presents a list of the HVDC links commissioned since 2021. (All the links of the table were last accessed in May 2024).

In general, new HVDC projects involve the installation of new conductor lines, which can be either overhead lines or underground cables. However, when the construction of new overhead lines faces strong public opposition or when the cost of new underground AC or DC cables is prohibitive, converting existing AC overhead lines to DC becomes the only feasible option to increase power exchange capacity [18, 19]. An example of such conversion is the

Table 1.1: New VSC-HVDC links commissioned since 2021

| Name | Year commissioned | Power (MW) | Voltage DC (kV) | Voltage AC (kV) | Transmission length (km) | Converter manufacturer | Type of connection |
|---|---|---|---|---|---|---|---|
| IFA2, UK-France | 2021 | 1000 | ±320 | 400/400 | 240 subsea | Hitachi ABB | Asynchronous |
| | https://www.hitachienergy.com/about-us/customer-success-stories/ifa2, https://ifa1interconnector.com/ifa2/ | | | | | | |
| SW Link, Sweden | 2021 | 2x720 | ±300 | 400 | 190 underground, 60 OHL | GE | Embedded |
| | https://www.gevernova.com/grid-solutions/products/applications/hvdc/south-west-link-hvdc-case-study-en-2015-10-grid-pea-0574.pdf<br>https://www.svk.se/sydvastlanken | | | | | | |
| Rudong offshore wind farm, China | 2021 | 1100 | ±400 | 220/500 | 100 underwater | XJ Group RXHK, | Embedded |
| | https://www.rxhk.co.uk/corporate/news/rudong-owf-hvdc-link-goes-live/<br>https://www.nrec.com/en/index.php/about/newsInfo/107.html | | | | | | |
| North Sea Link, Norway-UK | 2021 | 1400 | ±515 | 420/400 | 720 subsea | Hitachi ABB | Asynchronous |
| | https://www.hitachienergy.com/about-us/customer-success-stories/nsl-link<br>http://www.northsealink.com/ | | | | | | |
| Pugalur-Thrissur, India | 2021 | 2x1000 | ±320 | 400 | 32 underground, 170 OHL | Siemens Energy | Embedded |
| | https://www.nsenergybusiness.com/projects/raigarh-pugalur-trichur-high-voltage-direct-current-hvdc-transmission-project/ | | | | | | |
| ElecLink, UK-France | 2022 | 1000 | ±320 | 400/400 | 51 subsea | Siemens Energy | Asynchronous |
| | https://www.eleclink.co.uk/ | | | | | | |
| Guangdong-Guangzhou, China | 2022 | 2x1500 | ±300 | / | Back-to-back | RXHK, NR Electric | Asynchronous |
| | https://www.rxhk.co.uk/corporate/news/baihetan-jiangsu-uhvdc-transmission-project-contract-award/<br>https://www.nrec.com/en/index.php/about/newsInfo/117.html<br>http://global.chinadaily.com.cn/a/202206/14/WS62a7f8a3a310fd2b29e629e8.html | | | | | | |
| Baihetan-Jiangsu UHVDC, China | 2022 | 3x1334 | ±400 | 510 | 2080 OHL | RXHK, NR C-EPRI - Electric | Asynchronous |
| | https://www.rxhk.co.uk/corporate/news/baihetan-jiangsu-uhvdc-transmission-project-contract-award/<br>https://nrec.com/en/index.php/about/newsInfo/125.html<br>http://news.jschina.com.cn/qyxw/202207/t20220706_3031103.shtml | | | | | | |
| Johan Sverdrup Phase 2, Norway | 2022 | 200 | ±80 | 110/300 | 200 underwater | Siemens Energy | Embedded |
| | https://energy.ec.europa.eu/system/files/2020-05/10._sharifabadi_kamran_-_multivendor_hvdc_links_supplying_oil_and_gas_installations_0.pdf | | | | | | |
| Savoie-Piedmont, Italy-France | 2022 | 2x600 | ±320 | / | 190 underground | GE | Embedded |
| | https://www.rte-france.com/en/projects/savoie-piemont-190-km-of-european-solidarity-from-chambery-to-turin<br>https://www.gegridsolutions.com/products/applications/hvdc/france-italy-hvdc-link-casestudy-en-2018-02-grid-pea-1641.pdf | | | | | | |
| DolWin6, Germany | 2023 | 900 | ±320 | / | 45 subsea, 45 underground | Siemens Energy | Embedded |
| | https://www.tennet.eu/projects/dolwin6 | | | | | | |
| Viking Link, UK-Denmark | 2023 | 800 | ±525 | 400/400 | 630 subsea, 135 underground | Siemens Energy | Asynchronous |
| | https://www.viking-link.com/ | | | | | | |

Ultranet project[1], a 2 GW, ±380kV, 340km OHL link to be commissioned in 2026.

## 1.4 Power system stability

Power system stability terms, definitions and classification were presented by a IEEE/CIGRE Joint Task Force in [20] and recently updated in [3, 4]. In those references, power system stability is defined as [4]:

> *The ability of an electric power system, for a given initial operating condition, to regain a state of operating equilibrium after being subjected to a physical disturbance, with most system variables bounded so that practically the entire system remains intact*

Traditionally [20], the stability of power system was classified into three types: rotor angle stability, frequency stability and voltage stability. More recently, a new task force was established in order to extend the classification to take into account the effects of electronic power devices [4]. This work added the concepts of *resonance stability* and *converter-driven* stability as presented in Fig. 1.3.

This PhD thesis focuses on frequency stability and rotor angle stability (divided into transient and small signal stability).

### 1.4.1 Rotor angle stability

According to the IEEE/CIGRE Joint Task Force on Stability Terms and Definitions, angle stability is defined as [4]

> *The ability of the interconnected synchronous machines in a power system to remain in synchronism under normal operating conditions and to regain synchronism after being subjected to a small or large disturbance.*

It can be classified into two types:

- Large-disturbance angle stability (transient stability) [20]:

[1] https://www.amprion.net/Grid-expansion/Our-Projects/Ultranet/

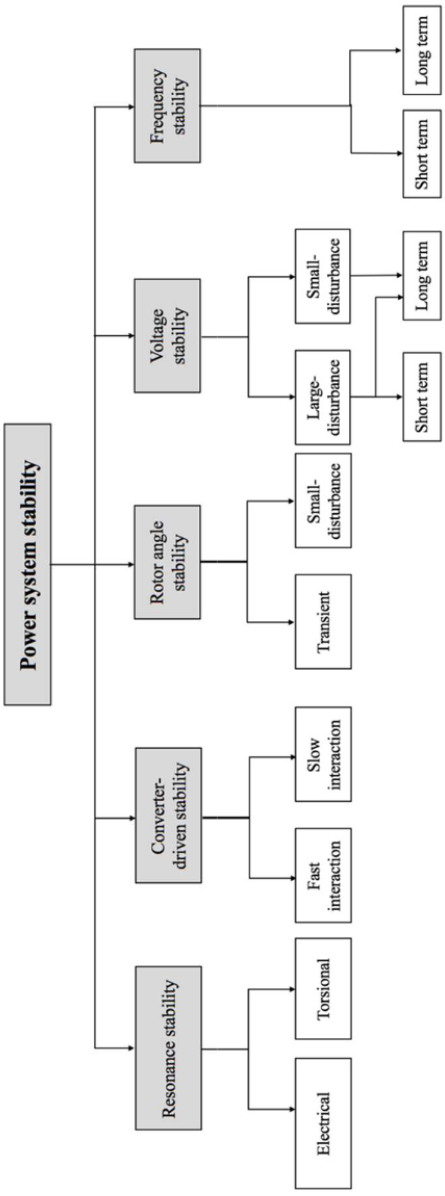


Figure 1.3: Classification of power system stability [3, 4].

> *The ability of the power system to maintain synchronism when subjected to a severe disturbance, such as a short circuit on a transmission line. The resulting system response involves large excursions of generator rotor angles and is influenced by the nonlinear power-angle relationship.*

- Small-disturbance (or small-signal) angle stability [20]:

> *The ability of the power system to maintain synchronism under small disturbances. The disturbances are considered to be sufficiently small so that the system of equations can be linearised for analysis purposes.*

**Transient stability**

Transient stability is related to loss-of-synchronism phenomenon in power systems caused by large disturbances. Most common threats to transient stability are short circuit in stressed power systems with the subsequent cascading disconnection of parallel lines due to overloading. This can cause the separation of a power system in two or more asynchronous zones. Some of them may have a production deficit that would cause under frequency while others may have a production surplus that would cause over frequency. A typical example of this events has been the Continental Europe Synchronous Area Separation on the 8th of January of 2021 [21]: a strong power flow from east to west in Europe caused an overload in a substation in Croatia, causing cascading outages, leading to the separation of the grid in two asynchronous area. In the North-west area, the frequency dropped down to 49.7Hz leading to the disconnection of many industrial loads in France and Italy. In the South-East area, the frequency rose up to 50.6 Hz causing the disconnection of generators.

A similar sequence of events caused a Blackout in Turkey on March the 31st, 2015 [22] and another Continental Europe Synchronous Area Separation on 24 July 2021 [21] showing that transient stability is still an issue for large power systems.

**Small-signal angle stability**

In small signal angle stability, the main focus is on the study of electromechanical oscillations (also known as power oscillations), i.e, the electromechanical modes associated to the angles and speeds of the synchronous machines. The analysis relies on a linearised version of the system of interest.

In large power system, electromechanical oscillations are still an issue as shown by the inter-area oscillations event on the 1st of December of 2016 [23] when a poorly-damped inter-area oscillation was triggered by a line disconnection in France, close to the border with Spain.

Traditionally, electromechanical oscillations have been tackled using Power System Stabilisers (PSS) in some of the generators of the system [24] . More recently, Power Oscillation Damping (POD) controllers are being installed in FACTS [25, 26] or in HVDC converters [27], for the same purpose.

This PhD thesis illustrates how DC segmentation can be used to suppress inter-area oscillation modes (Chapter 6), while the remaining local modes are tackled using POD controllers on reactive power (POD-Q) in the HVDC converters used for the segmentation (Chapter 7).

### 1.4.2 Frequency stability

According to the IEEE/CIGRE Joint Task Force on Stability Terms and Definitions [20],

> *Frequency stability refers to the ability of a power system to maintain steady frequency following a severe system upset resulting in a significant imbalance between generation and load. It depends on the ability to maintain/restore equilibrium between system generation and load, with minimum unintentional loss of load.*

In order to improve frequency stability in power systems, so far, the trend has been to connect together local or national grids in order to increase their total inertia. This has led to the creation of continental-size power systems such as the continental European grid reaching from Portugal to Ukraine. Thus, frequency stability has been less of an issue in large power system while it is still the primary issue for isolated power systems [28].

Applying DC segmentation to a large power system will lead to reduction of the inertia for each of the new asynchronous areas and thus could threat their frequency stability. This phenomenon is studied in Chapter 4 and a frequency-support control strategy is proposed in Chapter 7 in order to mitigate this issue.

## 1.5 DC segmentation of power systems

As seen in Section 1.4, the large size (and thus total inertia) of large interconnected power systems has allowed them to greatly improve their frequency

stability. However, their size has become an issue for their angle stability and for cascading outages that can cause important outages.

Thus, one may wonder if there exist a perfect size for power system in which global stability is optimised. The research in [29] suggests that there is indeed a size for which the balance between total inertia (for improving frequency stability) and risk of large scale blackout is optimised.

However, future power grids cannot be built from scratch to fit this theoretical perfect size and must adapt to the existing grids and the geographical characteristics of each region. One concept that could be used to approach this balance is DC segmentation.

DC segmentation was first proposed in [30] with the following definition:

> *DC segmentation involves breaking large grids [...] into smaller sectors interconnected by Back-to-Back HVDC links and HVDC transmission lines.*

DC segmentation is regarded as a promising application of VSC-HVDC to tackle, once and for all, severe instability problems or to improve the operation of the system [31].

It is worth pointing out that DC segmentation is a planning action that creates permanent AC asynchronous regions (called clusters) linked by DC links. Thus, it must not be mixed up with temporary measures (for example intentional islanding) even if they also create AC asynchronous regions.

Fig. 1.4 depicts the DC segmentation of a power system in three asynchronous clusters.

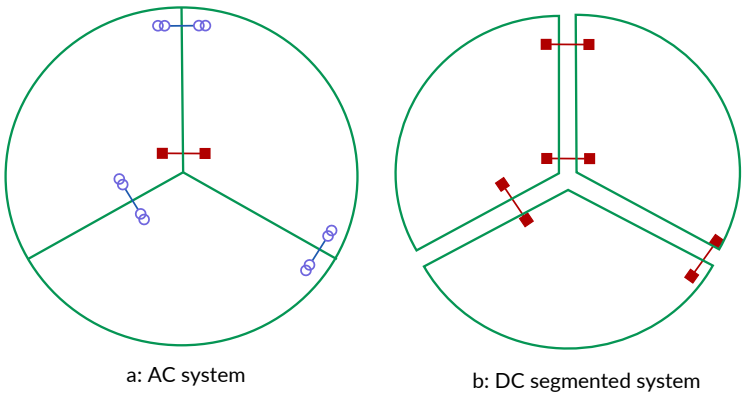


Figure 1.4: DC segmentation of a power system.

On the one hand, DC segmentation may seem to be going against the historical evolution of power systems as it consists in segmenting grids that have previously been linked together. However, it allows the exchange of power between regions while limiting the propagation of perturbations as the power through DC links is fully controllable. Thus, DC links can play the role of "grid shock absorber" as proposed by the Electric Power Research Institute (EPRI) [32] preventing large scale cascading outages.

On the other hand, DC segmentation can be seen as a natural evolution of power systems. Indeed, in some interconnections initially done by AC transmission lines, new DC links have been built and, in some places, they are progressively taking over the largest part of the total trans-border capacity. For example, the trans-border capacity between France and Spain is currently of 4 GW, half of it through 4 AC lines and half of it through a DC link [33]. However, a second 2 GW DC link is currently under consideration [34]. If the trend continues, one may ask why the AC transmission lines should be kept even if they transmit only a fraction of the power while limiting the degrees of freedom of the system (as they force the two regions to stay in synchronism permanently).

This situation has already occurred in southern China where five HVDC links carry a total of 26 GW from Yunnan to Guangdong. It has been found that a contingency of one of the DC links would have a chance of overloading the parallel inter-area AC lines. Since this risk has been estimated more important than the service offered by the parallel AC lines, it was decided to disconnect them in July 2016; leading to the first documented DC segmentation of a power system [35].

## 1.6 Main objectives of this PhD thesis

The scenario presented above, described a stressed power system operating closer to its stability limits and evolving towards a hybrid HVAC/HVDC power system with a growing share of HVDC transmission. Thus, while DC links are usually installed to increase the capacity of the system, it is of strong interest to study the potential of VSC-HVDC to improve the stability of stressed power systems. More specifically, this PhD thesis focuses on one use-case of VSC-HVDC, namely, *DC segmentation*.

This PhD thesis aims at providing technically sound and supported answers for the three following questions:

- Objective 1: What may be the effects of DC segmentation on the sta-

bility of a power system?

- Objective 2: How and where, to DC segment a power system in order to improve its stability?
- Objective 3: How to control a DC-segmented system in order to improve its stability?

In particular, this PhD will focus on the following power-system-stability phenomena:

- Angle stability under small disturbances (electromechanical oscillations).
- Angle stability under large disturbances (transient stability).
- Frequency stability.

As stated above, DC segmentation is a planning action requiring a significant investment. The tools presented in this PhD thesis are not for planning themselves, however, they can help the evaluation of DC segmentation when new grid developments are deemed necessary, taking into account technical aspects.

A review of previous work will be presented in Chapter 2 and the identified research niches will pinpoint more precisely the three objectives above.

## 1.7 Outline of this document

The manuscript is organised as follows:

- **Chapter 1** (this chapter) presents an introduction to the topic of the PhD thesis.
- **Chapter 2** presents a review of previous work on DC segmentation.
- **Chapter 3** presents the dynamic models used in this PhD and their implementation under Dymola and SSST. It details the electromechanical model of VSCs used both for dynamic simulations and small-signal analysis in the following chapters.
- **Chapter 4** investigates the impact of DC segmentation on the stability of power systems. To do so, two variations of the commonly used

Kundur two-area test system are compared: the usual AC one and a DC-segmented one (with the AC transmission line replaced by a DC link). The comparison is done by means of small signal analysis and dynamic simulations.

- **Chapter 5** studies the concept of dominant electromechanical-oscillation paths and their automatic identification. It discusses the use of various indicators, namely bus-voltage and frequency observability factors, to identify oscillation-propagation paths. It then proposes a fully automated algorithm for the identification of these paths and validates the proposed algorithm by applying it to the Nordic 44 test system.

- **Chapter 6** proposes an algorithm for the DC segmentation of power systems to mitigate electromechanical oscillations. This algorithm suppresses a selected inter-area electromechanical mode by DC-segmenting the system at the centre of the dominant paths of the target mode. Thus, this algorithm relies on the one proposed in Chapter 5. The algorithm is then applied and validated using the Nordic 44 test system.

- **Chapter 7** investigates whether the stability of a DC-segmented system can be further improved by additional controllers of the DC link. One frequency-support control based on active power is proposed to limit the deterioration of frequency stability due to the DC segmentation. Two POD-Q control strategies are proposed to damp the local modes of the system, one using only local measurement and one using the frequency of the centre of inertia of each region.

- **Chapter 8** concludes the PhD thesis by summarising its contributions, discussing its results and proposing potential novel lines of research to extend its results.

- **Appendices A, B and C** contain the details of the test systems used in previous chapters, namely the Kundur 2-area test system, the proposed 6-generator test system and the Nordic-44 test system.

# Chapter 2

# Review of previous work and identification of gaps for research

## 2.1 Introduction

This chapter presents a review of previous work on the main aspects of this PhD, namely, DC segmentation and supplementary controllers in VSC-HVDC systems. The chapter also identifies the open gaps for research addressed in this PhD thesis and it links them with the objectives defined in Section 1.6 of Chapter 1.

This chapter is organised has follows. Section 2.2 presents a full review of previous work on DC segmentation. Section 2.3 presents a review of previous work on the supplementary controllers used in VSC-HVDC systems to improve power system stability. Section 2.4 identifies the open research gaps addressed in this PhD thesis and Section 2.5 summarises them.

## 2.2 DC segmentation of power systems

As stated in Section 1.5, DC segmentation is a new promising application of VSC-HVDC technology and constitutes the main focus of this PhD thesis. For the sake of clarity, the review of previous work on DC segmentation is divided in 3 parts aligned with the three following key questions:

- What are the effects of DC segmentation on AC/DC power systems?

- How and where, to DC segment a power system?
- How to control the VSC-HVDC links of a DC-segmented system?

### 2.2.1 The effects of DC segmentation on AC/DC power systems

#### Mitigation of disturbance propagation

One of the most extensively documented effects of DC segmentation is its ability to limit the propagation of perturbations across the different resulting clusters [32, 36, 37]. For example, [32] describes the HVDC links as "Grid Shock Absorbers". Indeed, when controlled with constant power references, HVDC links are capable of preventing fluctuations in power or voltage from propagating between different AC clusters, effectively serving as an electrical firewall.

#### Limitation of cascading outages and black-outs

In contrast to AC lines, HVDC links offer full controllability which can play a significant role in limiting cascading outages and blackouts. Indeed, HVDC links can be controlled in order to always respect their thermal and stability limits, thus preventing unplanned tripping issues that might occur with AC lines during over-current situations. Likewise, HVDC links can be controlled to limit their power flow to levels that are safe for the providing cluster. This could strongly limit the risk of cascading failures and blackouts [30].

This effect has been confirmed in [38] with DC links controlled with frequency support and in [39] with DC links modelled as AC lines with controllable impedance. Both papers show that DC segmentation significantly reduces the risk of large-scale blackouts.

#### Increase of net transfer capacity

According to [30], DC segmentation increases the net transfer capacity between clusters. The main reason is that no line capacity needs to be held in reserve for uncontrolled power flows that can result from disturbances. Additionally, DC segmentation can be the occasion to upgrade existing lines from HVAC to HVDC which greatly increase their net transfer capacity as stated in Section 1.3.

#### Improvement of market operation

Thanks to the increase of controllability, market operation could become more efficient in a DC-segmented system, mainly if the segmentation boundaries correspond to different market sectors [32]. For this purpose, [40] proposes a method to segment a power network in order to improve its market operation.

#### Impact on power system stability

It is well known that AC power systems are planned to be meshed and large (when feasible) to improve their reliability and resiliency. However, in some cases involving stressed large-scale power systems, stability issues may introduce technical limitations that DC-segmentation could mitigate. Of course, this does not mean that all AC power systems should be DC-segmented.

In terms of the impact of DC segmentation on power system stability, two main aspects, have been reported in the literature:

- Impact on rotor angle stability: DC segmentation can increase the angle stability margin of the system [41]. Indeed, generators from different clusters are not bond to stay in synchronism with one another: DC segmentation suppresses the synchronisation constraint between the AC clusters. Moreover, since it decouples different parts of a power systems, DC segmentation can cut the dynamic paths associated to angle stability.

- Impact on frequency stability: DC segmentation can jeopardise the frequency stability of the resulting asynchronous clusters (since each of the resulting cluster will have a smaller inertia and weaker frequency support than the original system). Indeed, when controlled with constant active power references, HVDC links "prevent the propagation of perturbations but stop inertia sharing" [36].

### 2.2.2 Where and how to DC-segment a power system?

Once the advantages of DC segmentation reported in the literature have been understood, the problem of how to select the DC segmentation scheme for a given power system rises. To the best of the author's knowledge, the only previous work in this matter is the patent in [40] that proposes to follow

the market boundaries without consideration of power system stability aspects, and [42] that compares different segmentation schemes to limit the commutation failure of the LCC-HVDC converters of the system but without justifying the initial selection of the segmentation candidates. Thus, no previous work has addressed the problem of how to select the optimal DC segmentation scheme for a given power system based on technical aspects.

One possibility to maximise the stability advantage of DC segmentation would be to place the DC links in order to cut the propagation of the dominant inter-area oscillation dynamic paths associated to angle stability. Reference [43] proposes a method for the identification of dominant inter-area oscillation paths, and this method could be used in the context of DC segmentation. Finally, [44] proposes a list of principles to operate a grid of grids of DC and AC sub-grids interconnected by power converters. Since a DC-segmented system is a particular example of those grids, it seems important to follow these rules for selecting the segmentation boundaries and to develop the appropriate control.

### 2.2.3 How to control the VSC-HVDC links of a DC-segmented system?

The control of HVDC links between asynchronous areas is a well studied subject. For example, as stated in Section 2.3.3, numerous papers propose the use of some kind of frequency control for VSC-HVDC links between two asynchronous regions. In [44], the authors propose some principles to operate a "grid of grids", i.e., a system composed of numerous asynchronous AC grids connected by a large number of DC systems. Reference [45] proposes to optimise the role (GFM or GFL) of the VSC of such grid of grids to limit steady-state deviations, and improve small-signal stability.

The work in [46] analysed electromechanical oscillations in an AC power system segmented with LCC-HVDC links. The paper shows that an increase of the load in the DC-segmented system reduces the damping ratio of some electromechanical modes and the work proposes an operating-point adjustment of the active-power flow of the LCC-HVDC segments to counteract that reduction. The work in [47] also analyses a DC-segmented system with LCC-HVDC links and its impact on electromechanical oscillations. It proposes two control strategies for the LCC-HVDC segments to improve the overall stability of the system, in terms of electromechanical oscillations. The control strategies consist in adding a supplementary set-point term to the DC-current reference of the rectifier station and a supplementary set-point term to the

DC-voltage reference of the inverter station, which lead to an active-power modulation in the LCC-HVDC segments. The first supplementary controller (named GSC1) aims at isolating the electromechanical oscillations within each asynchronous area. The second control strategy (named GSC2) allows the propagation of electromechanical oscillations among the asynchronous AC areas of the DC-segmented system, but aiming at improving small-signal angle stability of the overall system. Supplementary controllers in the LCC-HVDC segments are designed using Linear-Quadratic-Gaussian (LQR) techniques.

However, there are few references studying the control of HVDC systems in the context of DC segmentation. Papers [30, 32, 37, 41, 42] all study DC-segmented systems with DC links controlled with strategies such as "fix power set points" or alternatives for "frequency control" but they do not compare control alternatives. Only [36] compares DC segmentation with fix active power set point versus an active-power control strategy using the inter-regional frequency difference. The work in [46] and in [47] proposed active-power set-point adjustment and supplementary controllers to damp electromechanical oscillations in the DC-segmented system, however, both papers analyse LCC-HVDC systems and not VSC-HVDC systems.

## 2.3 Supplementary controllers in VSC-HVDC systems to improve power system stability

Supplementary controllers in VSC-HVDC systems can be used to improve power system stability. This section presents a review of previous work of supplementary controllers in VSC-HVDC systems (a) to damp electromechanical oscillations (power oscillation damping), (b) to improve transient stability and (c) to improve frequency stability. These types of controllers could be useful when applied to DC-segmented power systems.

### 2.3.1 Power-Oscillation-Damping controllers

Traditionally, the most cost-effective solution to damp electromechanical oscillations in power systems has been the use of supplementary controllers attached to different devices of the power system. The most extended solution is the implementation of Power System Stabilisers (PSS) in synchronous machines [48]. Nevertheless, supplementary Power-Oscillation-Damping (POD) controllers in converter-interfaced renewable power plants [15, 49], Energy

Storage Systems (ESS) [50], Flexible Alternating Current Transmission Systems (FACTS) [25, 51], LCC-HVDC systems [52, 53], and VSC-HVDC systems [27, 54] systems have also proved to be effective solutions.

This PhD thesis focuses on DC segmentation of power systems with VSC-HVDC links. Hence, POD controllers attached to these installations will be the ones of interest. A comprehensive review of previous work on POD controllers in VSC-HVDC systems can be found in [27] and [54]. In VSC-HVDC systems, POD controllers can be applied to the active-power injections of the VSC stations (POD-P, for short), to the reactive-power injections of the VSC stations (POD-Q, for short) or to both (POD-PQ, for short). POD controllers have been applied to point-to-point VSC-HVDC systems and to multi-terminal VSC-HVDC systems (VSC-MTDC).

The work in [55] proposed POD-P controllers in point-to-point VSC-HVDC systems embedded in HVAC systems, using the frequency difference between the AC terminals of the link, as input signal. The work in [56–58] proposed the use of remote signals in POD-PQ controllers using a Wide Area Measurement System (WAMS) for the input signals. The work in [59] studied the use of remote signals for the inputs of a POD-P controller, which uses the difference of speed deviation of two remote synchronous machines, as input signal. The work in [60] proposed POD-PQ controllers using robust Linear Matrix Inequality (LMI) optimisation approach. The work also presented a comparison of different POD controllers. Ref. [61] proposed adaptive WAMS-based POD-PQ controllers with adjustable observation signal, actuator and parameters. An example of a VSC-HVDC equipped with POD-PQ controllers is the INELFE-1 France-Spain 2x1000 MW VSC-HVDC interconnector [62]. The work in [63] presented field tests of the POD-P controller of INELFE-1 VSC-HVDC inter-connector, where the gain of the POD-P was re-tuned and additional adjustments were made in order to make the POD-P controller compatible with the operation of the link in Angle Difference Control (ADC).

The work in [64] proposed POD-P controllers in VSC-MTDC systems embedded in HVAC systems using a WAMS for the input signals. Besides, the work in [65] proposed POD-P controllers using local measurements: every VSC of the VSC-MTDC system added a term to the DC-voltage set point for the DC-voltage droop (the so-called, DC-voltage loop shaping) using local measurements of the frequency deviation at the AC connection point. The work in [66] proposed POD-PQ controllers using, as input signal, the deviation between the frequency measured at the AC connection point of each VSC and a frequency set point. This frequency set point was calculated as

the weighted average frequency of the VSC-MTDC system. POD-PQ controllers were designed using a coordinated design method based on eigenvalue sensitivities, in order to damp a set of electromechanical modes.

All references discussed above addressed POD controllers in VSC-HVDC embedded into HVAC systems. In the context of VSC-HVDC connecting asynchronous AC systems, some additional precautions must be taken into account when designing POD controllers. POD-Q controllers could be used to damp electromechanical oscillations in each asynchronous AC grid, due to the independent reactive-power control of VSC converters. However, the case of POD-P controllers is different, since if the VSC-HVDC system could contribute to the damping of electromechanical oscillation of one of the AC areas by means of P modulation, it will necessarily cause a perturbation in some other AC areas. References [67] and [68] proposed POD-P controllers in offshore wind farms connected to the main AC grid through VSC-MTDC systems. The work in [69] proposed POD-P controllers in VSC-HVDC systems interconnecting asynchronous AC systems, where the energy storage of the MMC valves was used to provide damping capability to the two asynchronous AC grids connected to the VSC stations. Notice that this work, presented a preliminary study and the potential of the proposed solution needs further investigation, since the energy stored in the MMC vales is limited. Ref. [70] proposed a POD-P controller in VSC-HVDC systems interconnecting asynchronous AC systems, based on the concept of *virtual friction* proposed by the authors, in which a supplementary P set point proportional to the difference of the frequencies of both AC terminals of the VSC-HVDC systems is used. Since the effect of the POD-P controller in damping electromechanical oscillations of one of the AC areas produce a perturbation in the other one, a trade off in the design of the POD-P controller gain was proposed.

### 2.3.2 Transient-stability-tailored controllers

Previous work has shown that supplementary controllers in P and Q injections at the converter stations of VSC-HVDC systems embedded in HVAC systems can be used to improve power system transient stability.

The work in [71] proposed a P-based supplementary controller in a point-to-point VSC-HVDC system to improve transient stability, using as input signal a non-linear function of the difference between the angle of the voltage of the two ends of the VSC-HVDC system. The work in [72] proposed a control strategy for P injections in VSC-HVDC links, in which the supplementary P set point was calculated as a function of the frequency difference

of the two ends of the VSC-HVDC link. Ref. [73] proposed control strategies for P/Q injections of the VSC stations based on Model Predictive Control (MPC) and global measurements. The work in [74] analysed the impact of VSC-HVDC systems on transient stability, using P and Q control strategies. In active-power control strategies, the approach of [72] was used, while in reactive-power control strategies, Q injections in each VSC station were modulated comparing the frequency at the connection point with the average of the frequencies of both AC terminals of the VSC-HVDC link.

References [75] and [76] proposed control strategies for P injections of the converter stations of VSC-MTDC systems embedded in HVAC systems to improve transient stability using global measurements collected by a WAMS. In [75], P injections of VSC stations were modulated according to a bang-bang-type controller and using global measurements of the speed deviations of the synchronous generators of the systems with respect to the speed of the Centre Of Inertia (COI) of the system. In [76], a sliding-mode control law for P injections of the converter stations was used, requiring measurements of the speed of the COI and of the mechanical power and electrical power injection of synchronous generators. In the work of [77,78], transient-stability-tailored supplementary controllers in VSC-MTDC were proposed using global-but-practical measurements of the frequencies at the AC side of the converter stations of the VSC-MTDC systems. In the proposed control laws, the input signal of the supplementary controller of each VSC station is the error between a frequency set point and the frequency measured at the connection point of each VSC station. The frequency set point was calculated as the average of the frequencies of the converter stations of the VSC-MTDC system (Weighted Average Frequency, WAF). P and Q injections were modulated using this error input signal to improve transient stability (in [77] and [78], respectively). The work in [79] proposed a Q-based control strategy similar to the one in [78], but using local measurements, only. The work in [80] proposed P-based supplementary controllers in VSC-MTDC systems to improve transient stability also using global measurements of the converter stations of the VSC-MTDC system. In this case, the input signals of the P controllers is calculated from the angles and frequencies measured at the connection points of the VSCs. Reference [81] proposed WAMS-based P/Q supplementary controllers in VSC-MTDC systems containing offshore wind farms and connected to different points of the AC system to improve transient stability. Reference [82] also explored the improvement of angle stability under large and small disturbances by means of set-point adjustments in the converter stations of a VSC-MTDC system embedded in an HVAC system.

### 2.3.3 Frequency controllers

Frequency Controllers (FC) can be implemented in VSC-HVDC systems interconnecting asynchronous AC grids, to provide frequency support among them. FCs in VSC-HVDC are linked to active-power control of the VSC stations.

The work in [83,84] analysed frequency and inertial support provided with offshore wind farms connected to the AC systems through VSC-MTDC systems. References [85–87] addressed the problem of frequency support among asynchronous AC grids connected through VSC-HVDC systems using local FCs. The work in [88] proposed FCs based on cooperative control, in which every VSC station used information of some other VSCs to calculate the active-power set point value of its own FC control law. Ref. [88] proposed a FC for VSC-MTDC systems interconnecting asynchronous AC grids, in which the frequency set point for all VSCs was calculated as the average frequency of the VSC-MTDC stations, and the strategy was useful to reduce DC-voltage fluctuations. The work in [16] addressed the problem of frequency support of a large and high-inertia AC grid to a low-inertia AC grid though a VSC-HVDC link, in which the converter station connected to the latter is controlled with grid forming control. The work in [89] analysed the impact of frequency controllers in VSC-HVDC on electromechanical-oscillation damping, concluding that certain values of the FC controller gain could reduce the damping ratio of some electromechanical oscillations in the power system.

## 2.4 Identification of research gaps

DC segmentation is a promising solution, in particular for the improvement of the angle stability and prevent disturbance from propagating in bulk power systems. However, it is still a recent subject and many gaps for research exist. Based on the review of previous work presented in this chapter, scientific gaps have been identified and are described in the next subsections.

### 2.4.1 Impact of DC segmentation on power system stability

As illustrated in [41], DC segmentation of power systems can improve angle stability under small disturbances (electromechanical oscillations). Although the analysis of [41] presents some time-domain simulation results, it does not provide a detailed analysis. Furthermore, the DC segmentation of [41] was realised with LCC-HVDC systems, and not with VSC-HVDC technology,

which presents higher control flexibility. One could also conclude indirectly that DC segmentation may improve angle stability under large disturbances (transient stability), by suppressing the synchronism constraint between the different areas of an AC power system. However, this has not been analysed explicitly in previous work. Besides, since DC segmentation divides the system into asynchronous AC areas (coupled by HVDC links), each of them will have a lower amount of inertia and frequency support capability (frequency controllers and reserves). Hence, one could also conclude that DC segmentation may jeopardise frequency stability of the overall power system. However, this aspect has not been analysed in detail in previous work, either.

Therefore, a detailed analysis and full understanding of the impact of DC segmentation of power systems via VSC-HVDC links on electromechanical oscillations, transient stability and frequency stability has been identified as an open research gap. Chapter 4 addresses this research gap.

### 2.4.2 Where and how to segment a power system with DC?

Subsection 2.2.2 discussed previous work on determining architectures for DC segmentation of a power system for different applications. However, the problem of where to DC-segment an AC power system for the specific application of the mitigation of electromechanical oscillations in an AC system has not been addressed in previous work and it is a complex problem. This was, an open research gap and it is addressed in Chapter 6.

### 2.4.3 How to control the VSC-HVDC links of a DC-segmented system?

Subsection 2.2.3 discussed previous publications dealing with the control approaches in hybrid AC/DC systems involving asynchronous AC grids connected via HVDC systems. Furthermore, Subsection 2.3 presented a comprehensive review of previous work on supplementary controllers in VSC-HVDC systems to improve power system stability. Assuming that a large AC power system has been segmented with VSC-HVDC links to mitigate inter-area oscillations and to improve transient stability, one may conclude that some stability issues may still be present in the resulting DC-segmented system, for example, (a) intra-area electromechanical oscillations in the asynchronous AC grids and (b) frequency stability issues (due to the reduction of inertia and frequency support capability of each asynchronous AC grid). Intra-area oscillations may be damped with POD-Q controllers in the VSC-HVDC sys-

tems (with controllers similar to the ones described in Subsection 2.3.1), while frequency stability of the overall system may be improved by means of P-based frequency controllers in the VSC-HVDC systems (with controllers similar the ones described in Subsection 2.3.3). The use of POD-Q controllers to damp intra-area oscillations in a DC-segmented system may be more practical than the use of POD-P controllers since they may participate in the propagation of perturbations among the asynchronous AC areas. Although POD and frequency controllers in VSC-HVDC systems are a well studied subject (see Subsection 2.3), their use for this particular application of DC segmentation has not received attention in previous work.

Therefore, determining suitable supplementary controllers in DC-segmented systems via VSC-HVDC links to damp intra-area oscillations and to improve frequency stability of the overall system has been identified as an open research gap and is addressed in Chapter 7.

### 2.4.4 Electromechanical oscillation paths

In order to determine the most appropriate placement for DC segmentation of a given power system to mitigate electromechanical oscillations (research gap identified in Subsection 2.2.2), it is essential to characterise the propagation path of the target electromechanical oscillation through the power system, which may be a complex problem in meshed AC systems. As discussed in Subsection 2.2.2, the work in [43] proposed a method for the identification of dominant inter-area oscillation paths. Although the proposed method provided a very useful insight into the propagation of electromechanical oscillations through the different paths of a meshed power system, the method cannot be implemented in a fully-automatic way, and it requires further analysis by a user. The automatic application of this procedure is, definitely, a very desirable feature which has not been addressed in previous work.

Therefore, identifying the dominant electromechanical-oscillation paths in a certain meshed AC power system in an automatic way has been identified as an open research gap and is addressed in Chapter 5.

## 2.5 Summary of scientific gaps addressed in this work

Along the lines described in previous sections, the scientific gaps addressed in this PhD thesis can be summarised as follows:

- Analysis and full understanding of the impact of DC segmentation of power systems via VSC-HVDC links on electromechanical oscillations, transient stability and frequency stability.
- A methodology to automatically determine the most appropriate placement for DC segmentation in power systems via VSC-HVDC links to mitigate electromechanical oscillations. This achievement relies on the automatic identification of the dominant electromechanical-oscillation paths in a given meshed AC power system, which was addressed in the first place.
- Proposals for suitable supplementary controllers in DC-segmented systems via VSC-HVDC links to damp intra-area oscillations and to improve frequency stability of the overall system.

# Chapter 3

# Modelling and control of VSC-HVDC systems

## 3.1 Introduction

This chapter presents the modelling of hybrid HVAC/HVDC power systems with VSC-HVDC links as studied in this PhD thesis. Indeed, a number of simulations have been carried out in this PhD thesis and they require adapted models for the various components of hybrid HVAC/HVDC power systems for both time domain simulations and small-signal stability analysis. While the models of AC components are well known, the models for VSC-HVDC links are more diverse in the literature and thus the modelling method selected here requires an explanation.

This chapter is organised has follows. Section 3.2 presents the Root-Mean-Square (RMS) type models used in this PhD thesis for the elements of hybrid HVAC/HVDC systems. Section 3.3 presents the dynamic model of VSC-HVDC systems used in this PhD thesis. Section 3.4 presents the implementations of these models under the simulations tools selected, namely, Dymola and SSST. Finally, Section 3.5 concludes the chapter.

## 3.2 Power system modelling and simulation

Dynamic simulation of power systems can be categorised into two types [90]:

- Electromechanical simulation (also known as Root-Mean-Square (RMS)), that overlooks some fast dynamics and thus is appropriate for large power systems using standard levels of computer resources.

- Electromagnetic transient (EMT) simulation, that uses more detailed models to study fast transients and test control systems of devices. The application of this type of simulation in large power system would require often-unavailable computer resources.

Since this work focuses on slow electromechanical dynamics in power systems (angle and frequency stability), the following types of dynamic models will be used:

- RMS-type linearised models for small-signal stability analysis.
- RMS-type non-linear models for time-domain simulation.

Dynamic RMS models of hybrid HVAC/HVDC systems, as the ones studied in this PhD thesis, will consist of:

- HVAC system
  - Synchronous generators, turbine + speed regulators (governors), excitation systems + automatic voltage regulators (AVR) and power system stabilisers (PSS).
  - Non-synchronous generators, induction machines and FACTS.
  - Network components (lines, transformers and shunt elements).
  - Loads: Quasi-static models (constant impedance, constant current, constant power or combination of them).
- VSC-HVDC systems
  - VSC stations and their controllers.
  - HVDC grid.

In RMS simulation, time constants of interest range from 0.01 s to 10 s. In these models, AC branches are assumed to be quasi static while the slow dynamics of synchronous machines, their controllers and other devices, are taken into account. RMS models of HVAC systems are well known [24]. In particular, the ones used in this PhD thesis are the usual RMS models as such as the ones implemented in the OpenIPSL library[1] [91,92] that is used in this work. Note that the dynamic models used in this work have already been validated in previous work: [2,93,94] for the VSC-HVDC models and [91,92] for the HVAC models. Key aspects of RMS models of VSC-HVDC systems will be described in the next sections.

[1] OpenIPSL is a library of power system component models written in the Modelica language that can be used for power system dynamic analysis.

## 3.3 VSC-HVDC system modelling

The modelling approach used for VSC-HVDC systems under phasor approximations (for RMS simulation) follows the guidelines and practices described in [2,95–100]. This section presents the dynamic model of a VSC-HVDC system, divided into two main components: the VSC-station model and HVDC line model.

### 3.3.1 VSC-station model

#### The physical layer

The adopted model of the VSC station is the type-6 model defined in [101], which is suitable for large AC/DC grids simulations. It has been implemented in the phasor domain following the guidelines in [95–97].

The physical layer of the VSC station following this approach is depicted in Fig. 3.1.

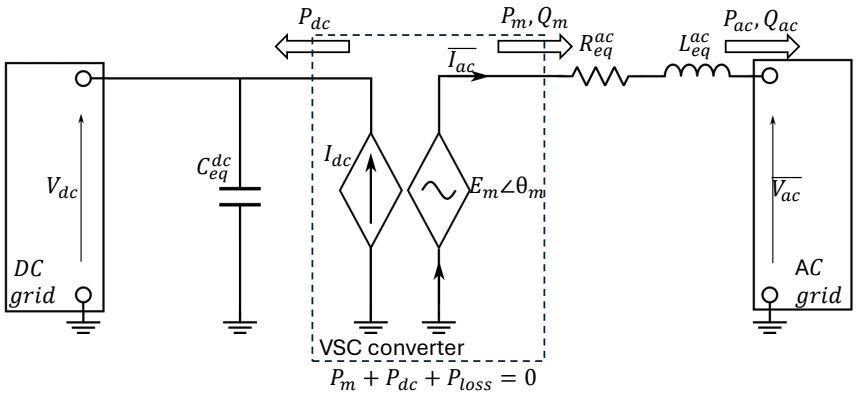


Figure 3.1: RMS model of a VSC-HVDC station in the common reference frame.

On the AC side, the converter is represented by a controllable voltage source, with voltage $\bar{E}_m = E_m \angle \theta_m$ (the angle is expressed with respect to a common reference frame of the phasor-time domain simulation), connected to the grid via the station's equivalent inductance $L_{eq}^{ac}$ and resistance $R_{eq}^{ac}$. The AC grid voltage is named $\bar{V}_{ac} = V_{ac} \angle \theta_{ac}$. Conversely, on the DC side, the converter is represented as a controllable current source, injecting a current $I_{dc}$. This current source is connected to the DC grid via the equivalent

capacitor $C_{eq}^{dc}$ which represents the total equivalent capacitance of the DC-bus of the VSC. $C_{eq}^{dc}$ includes both the equivalent capacitance of the VSC ($C_{eq}^{VSC}$) and the contributions of the capacitance of the DC lines connected to the DC side ($C_{cc}$ in Fig. 3.4). The AC voltage source and the DC current source are coupled by the principle of power conservation: the sum of the power flowing to the DC grid $P_{dc}$, the power flowing to the AC grid $P_{ac}$, and the equivalent converter losses $P_{loss}$ must equal zero. In the simulations conducted in this work, the equivalent converter losses $P_{loss}$ were neglected.

It is important to note that the main converter technology for HVDC applications is the Modular Multilevel Converter (MMC). The modelling of MMCs is significantly more complex than that of the 2-level VSC due to their intricate structure. Previous work has shown that the analysis of some interactions need the use of detailed EMT models of MMCs [102, 103]. However, [104] shows that if an MMC is controlled following a non-energy-based strategy (where the internal energy stored in the sub-module capacitors is not explicitly controlled), the RMS models of the MMC and the 2-level VSC can be considered equivalent. This equivalence simplifies the analysis and simulation of MMCs in large-system studies. Therefore, in this work, the presented model of the 2-level VSC will be used.

### The control system

The overall structure of the implemented control system is depicted in Fig. 3.2.

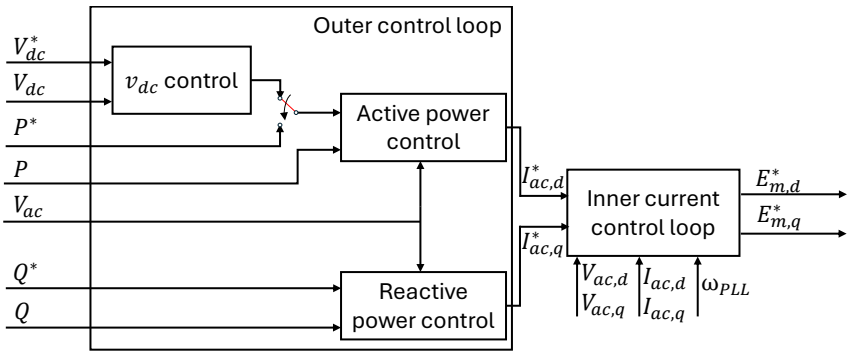


Figure 3.2: Outer and inner control loops implemented in the VSC.

The adopted control strategy follows a classical grid-following approach, implemented through cascaded control loops (outer and inner control loops)

in a dq reference frame. The dq frame chosen is a reference frame in which the d-axis is aligned with the grid voltage. To achieve this alignment, a Phase-Locked Loop (PLL) is used to track the grid voltage angle $\theta_{ac}$ at the point of connection. In RMS simulation, since the AC quantities are expressed in the phasor domain, the angle $\theta_{ac}$ can also be directly obtained without the need of a PLL. In the models implemented in this work, a PLL using a PI controller (with a closed-loop time response of 5ms), as shown in [105], has been employed.

Since the d-axis of the dq frame in which the control is applied is aligned with the grid voltage $V_{ac}$, the grid voltage projected onto the q-axis is zero. Therefore, the expressions of active (current injections in phase with the grid voltage, thus in the d-axis) and reactive power(current injections with a 90-degree phase shift relative to the voltage, thus aligned with the q-axis) can be expressed as:

$$\begin{aligned} P_{ac} &= V_{ac} I_{ac,d} \\ Q_{ac} &= -V_{ac} I_{ac,q} \end{aligned} \tag{3.1}$$

It is evident that active and reactive power can be controlled, by defining the injected currents in the d-axis and the q-axis. This is achieved via the inner current loop control depicted in Fig 3.3.

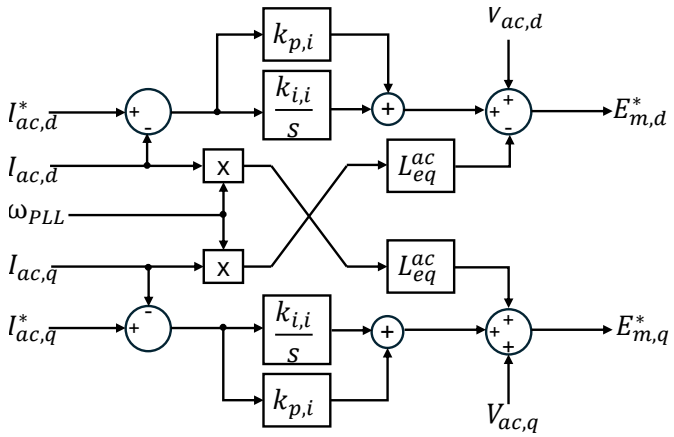


Figure 3.3: Inner current control loop implemented in VSCs.

The Current control loop consists of two PI controllers with a decoupling action, for the independent control of currents $I_{ac,d}$ and $I_{ac,q}$, and thus the independent control of active and reactive power. The current control calcu-

lates the voltage to be applied by the converter in the local dq frame ($E_{m,d}$ and $E_{m,q}$), which is then transformed into the common reference frame of the time domain simulation. For the simulations to be described later on, the PI controllers were designed so that the closed-loop time response of the inner current loop was between 1-10 ms. Controlling the currents has the advantage that the converter can naturally limit the injected current (to a value $I_{ac}^{max}$), which is especially useful in case of faults on the AC grid. Note that for RMS studies, a common practice is also to approximate the closed-loop inner control loop by current injections in the d-q frame with a desired time constant as described in [99, 100].

The outer loops include the active and reactive power control. These blocks provide the current references $I_{ac,d}^*$ and $I_{ac,q}^*$ based on the desired active and reactive power set points ($P^*$ and $Q^*$ respectively). From (3.1), the necessary current set points to obtain the desired active and reactive power values are derived as follows:

$$\begin{aligned} I_{ac,d}^* &= P^*/V_{ac} \\ I_{ac,q}^* &= -Q^*/V_{ac} \end{aligned} \tag{3.2}$$

Moreover, it is often beneficial to use PI controllers to control active and reactive power in order to avoid zero steady-state errors and to avoid dividing by the measured grid voltage module which can go to zero when there is a fault on the AC grid. For simplicity in our implementation, the open-loop control strategy in Eq. 3.2 is adopted.

Finally, the $v_{dc}$ control block is a PI controller that allows the DC voltage $V_{dc}$ to track the set point $V_{dc}^*$. As shown in Fig. 3.2, the converter control can be set to track either the active power set point (referred to as $p$ mode) or the DC voltage set point (referred to as $V_{dc}$ mode). Indeed, when operating a VSC-HVDC link, one converter is in $V_{dc}$ mode while the other converter is in $p$ mode. To protect the HVDC link from DC over-voltages in the event of an AC fault, which can lead to low AC voltage levels and hinder the converter in $V_{dc}$ mode from injecting or absorbing power into/from the AC grid, the converter in $p$ mode is switched to $V_{dc}$ mode when the DC voltage exceed the required limits.

### 3.3.2 Initialisation of the model

Normally, the initial steady-state operating point of the dynamic model of the power system is obtained through a power-flow algorithm. During the past years, power-flow calculations in hybrid HVAC/HVDC has been studied

extensively. Mainly, there are two extended approaches: (a) unified methods and (b) sequential methods. In the unified methods [106–109], power-flow equations of the HVAC and and HVDC systems are solved together. On the contrary, in the sequential methods [110–112], power-flow calculation of the HVAC and HVDC parts are solved sequentially within an iterative algorithm. Furthermore, linear approximations for AC/DC power flows have also been proposed in previous work [113].

In this work, a simple approach for the initialisation of the hybrid HVAC/ HVDC system is used. The initial operating point of the HVAC system is obtained with a conventional AC power flow, where the converter stations of the VSC-HVDC systems have been modelled as AC loads. The initial values of the VSC-HVDC systems are calculated separately. Then, the HVAC and HVDC systems are put together. Notice that this approach is an approximation and it could lead to some inaccuracies in comparison with more complete methods as the ones described above, but the accuracy obtained was enough for the scope of this work, which is related to power system stability.

### 3.3.3 HVDC line model

Following the modelling approach of [95], in this work, DC conductors will be represented by $\pi$-sections as shown in Fig. 3.4.

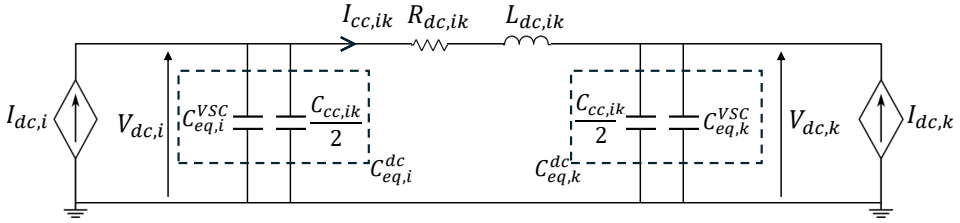


Figure 3.4: RL model of the HVDC line connected to two VSCs.

In Fig. 3.4, subscripts $i$ and $k$ correspond to buses $i$ and $k$ to which the line's terminals are connected. $V_{dc,i}$ and $V_{dc,k}$ are the voltages at DC buses $i$ and $k$, respectively, while $I_{cc,ik}$ is the current flow through the series part of the DC branch. Parameters $R_{dc,ik}$ and $L_{dc,ik}$ are the series resistance and series inductance, respectively. $C_{cc,ik}$ is the shunt capacitance of the DC line. Note that the shunt capacitance of the line is included in the equivalent capacitance of the VSC, therefore the equivalent capacitance at DC bus $i$

reads:

$$C_{eq,i}^{dc} = C_{eq,i}^{VSC} + \frac{C_{cc,i}}{2} \tag{3.3}$$

Current injections $I_{dc,i}$ and $I_{dc,k}$ represent the VSC stations seen from the DC side.

## 3.4 Simulation tools

In this PhD thesis, two modelling and simulations tools have been used: Dymola and SSST. Dymola has been used for all the non-linear simulations and most of the linear analysis. SSST has been used solely for the detailed linear analysis necessary for the algorithms of Chapters 5 and 6. Both tools will be presented in the following Subsections.

### 3.4.1 Implementation in Dymola

The models used in this PhD thesis were simulated using Dymola [114], a modelling and simulation environment based on the open Modelica modelling language. Modelica is an object-oriented, equation-based language suitable for modelling complex multiphysical systems using (hybrid) differential & algebraic equations (DAEs) [115]. This language is particularly effective for modelling large AC/DC power systems, especially when using phasor approximations. Dymola offers the capability of numerically linearising the models implemented. Consequently, Dymola was employed not only for all time-domain non-linear simulations but also for conducting some of the small-signal stability analysis presented in this work. Fig. 3.5 illustrates the Dymola software interface with the Nordic 44 (N44) test system used in this work and developed in [91, 92].

Regarding the modelling of the different grid components, the AC components used are those included in the Open IPSL library [91, 92], while the VSC-HVDC system models used are part of an internal library at SuperGrid Institute. This internal library was developed to be compatible with the IPSL library, with the purpose of simulating AC/DC transmission systems including multi-terminal HVDC (MTDC) systems. This library includes the VSC models presented in Section 3.3 and used in this thesis, models of MMCs (following the modelling approach of [93]) with grid-forming control (as reported in [94]), as well as examples of AC/DC systems with MTDC grids (as in [116, 117]).

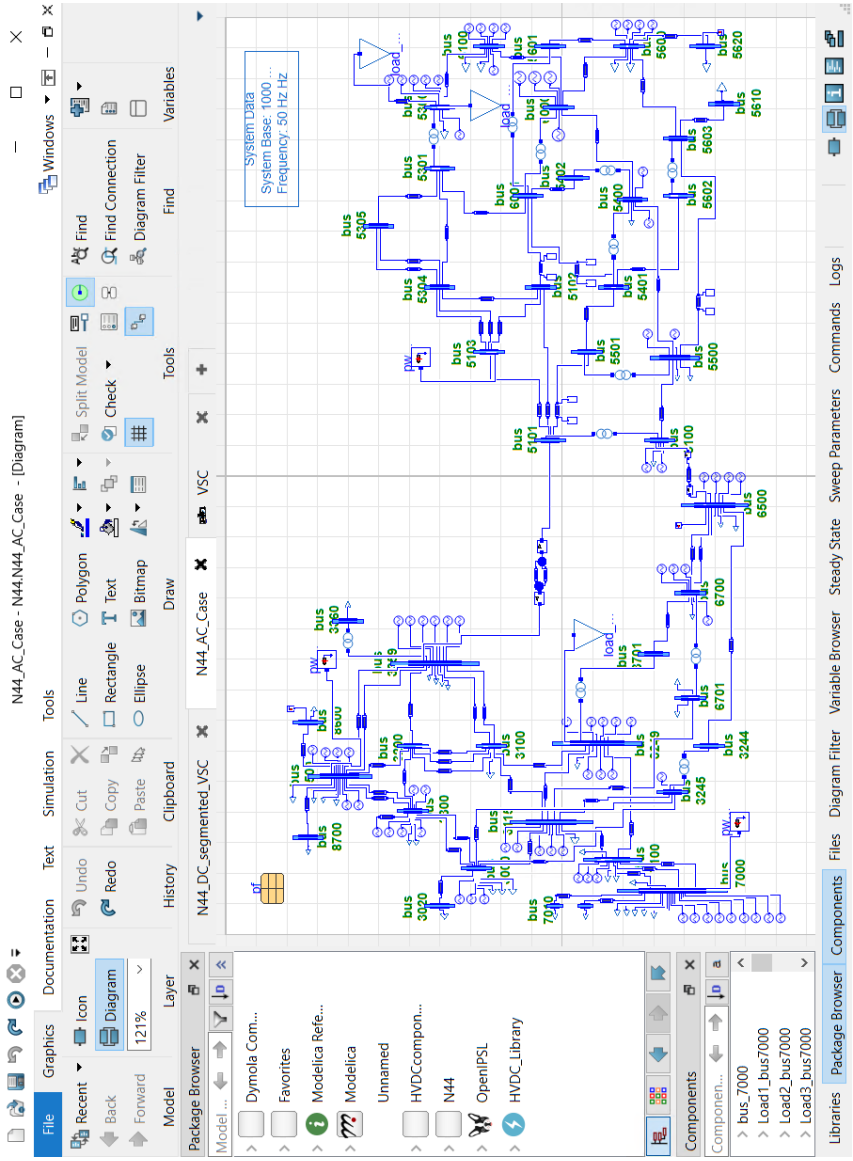


Figure 3.5: The Nordic 44 (N44) test system in Dymola.

### 3.4.2 Implementation in SSST

Small-signal stability analysis is a crucial step for the contributions of this PhD thesis. SSST is a commercial MATLAB-based tool designed for the small-signal stability analysis of large power systems [118]. It is based on SMAS3, a FORTRAN-based tool developed for the same purpose [119]. Both tools have been developed by the IIT of Comillas Pontifical University.

In SSST, the linearized equations of all grid components are directly written in the code. This increases calculation speed and accuracy of results compared to tools that rely on numerical linearization. Additionally, SSST implements many routines for calculating important indicators in small-signal analysis, such as mode shapes, bus frequency observability factors, and branch current observability factors. These indicators cannot be directly obtained from the numerical linear analysis in Dymola. As explained in Chapter 5 and 6, the proposed algorithms for identifying electromechanical paths and deciding the cutting edges of these paths to achieve DC-segmentation rely on these indicators. Therefore, SSST was considered the most suitable tool for the small-signal analysis necessary for the proposed algorithms.

To illustrate its use, Figure 3.6 shows some results from the eigenvalue analysis of the N44 test system obtained with SSST software.

Recently, the work in [120] upgraded SSST by including models of VSC-HVDC systems, allowing for the linear analysis of AC/DC systems. However, in this work, only the AC-version of SSST was used.

## 3.5 Summary and Conclusion

This chapter can be summarised as follow:

- Key aspects of modelling of VSC-HVDC systems have been discussed, including relevant references on the topic.
- The models used for the modelling of hybrid HVAC-HVDC systems have been presented: AC components, VSC-HVDC systems (VSC stations and DC lines).
- The two software environments used for simulation and analysis, namely, Dymola and SSST, have been presented.

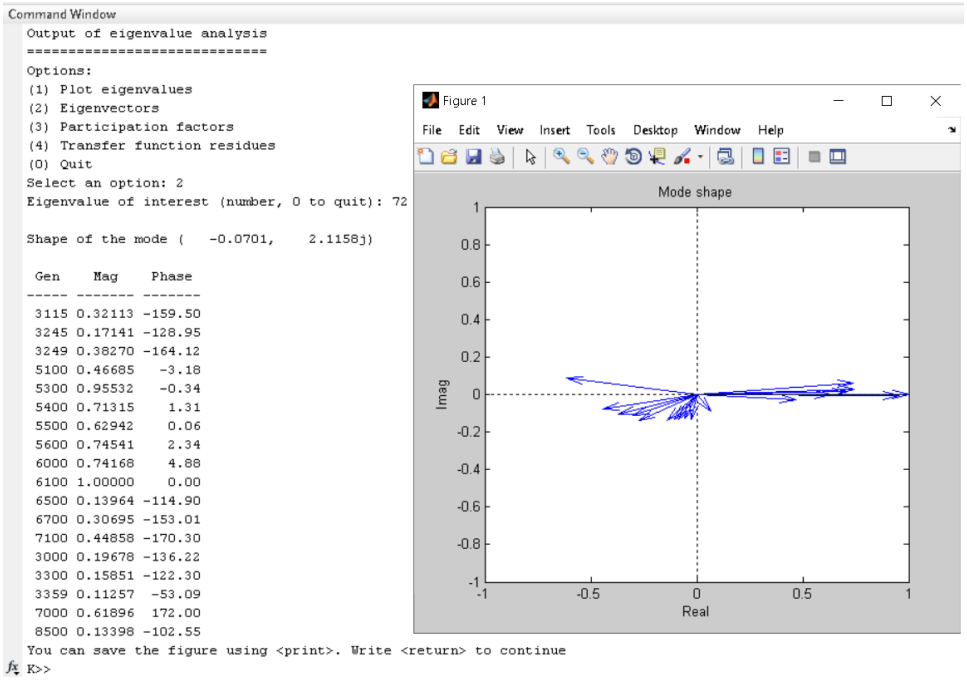


Figure 3.6: Eigenvalue analysis of the main inte-area mode of the N44 test system in SSST.

# Chapter 4

# Analysis of the potential of DC segmentation to improve angle stability

## 4.1 Introduction

This chapter investigates the effects of DC segmentation (with VSC-HVDC links) on power system stability. More precisely, the chapter analyses:

- Angle stability under small disturbances (electromechanical oscillations).
- Angle stability under large disturbances (transient stability).
- Frequency stability.

In order to segregate the effects of DC segmentation from the ones of the control of the VSC-HVDC links (DC segments), this chapter will consider VSC-HVDC links controlled with fixed power set points, only. In this chapter small signal analysis and dynamic simulations are applied to a simple two-area test system before and after DC segmentation.

As described in Chapter 2, DC segmentation has been used to improve different aspects of power system stability and operation [30, 32, 37, 41, 42]. However, a comprehensive analysis of the impact of DC segmentation on angle stability (under small and large disturbances) and on frequency stability has not been carried out before. This analysis is very relevant to fully understand the advantages and disadvantages of DC segmentation regarding such

important aspects of complex power systems. This chapter and the following ones of this thesis aim at occupying this existing niche.

This chapter is organised as follows. Section 4.2 presents the two-area test system used in this chapter. A small-signal stability analysis of the system is carried out in Section 4.3, while Section 4.4 presents the dynamic simulations applied to this system. Finally, Section 4.5 concludes the chapter.

## 4.2 Description of the case study

The system studied in this chapter is a simple four generator two-area system as presented in [24]. Two variations of the test system are compared:

- The AC base case: A two-area system with an AC interconnection as seen in Fig. 4.1.
- The DC-segmented case: A two-area system with a VSC-HVDC interconnection as seen in Fig. 4.2.

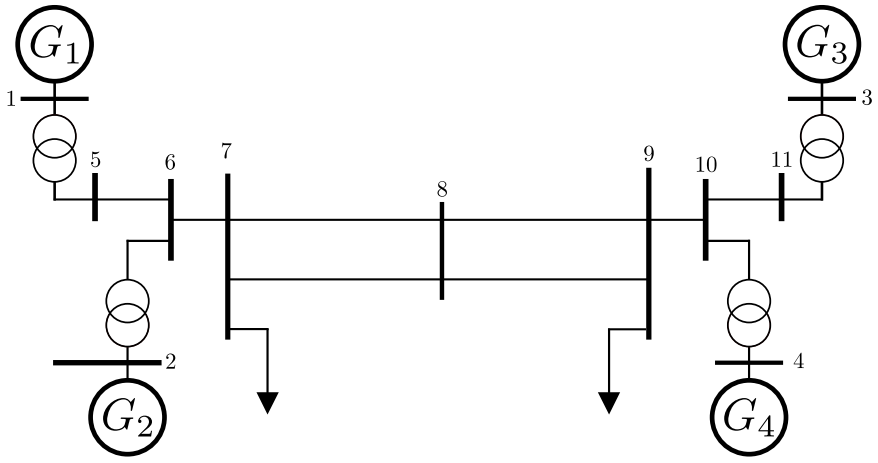


Figure 4.1: AC base case: Two-area system with an AC interconnection.

Thus, the DC-segmented case corresponds to the AC case where the two parallel lines between buses 7 and 9 have been substituted by an VSC-HVDC link. For simplicity, the left-hand side of the system (generators 1 and 2) will be referred to as region 1 and the right-hand side (generators 3 and 4) will be referred to as region 2.

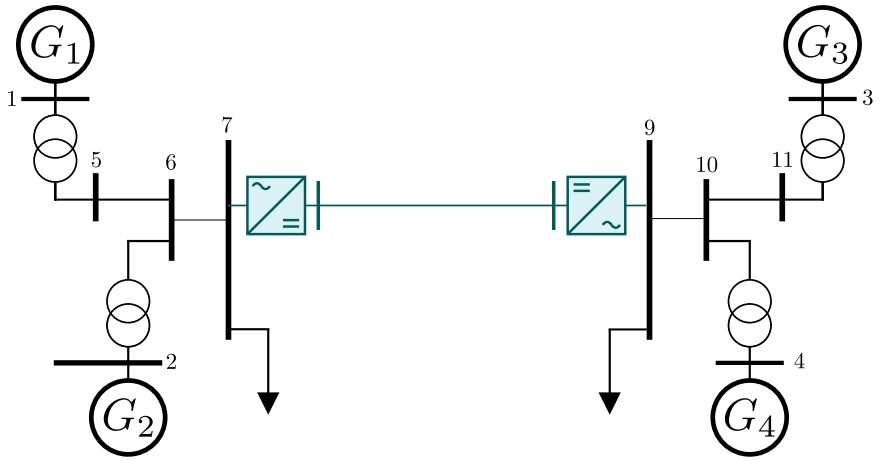


Figure 4.2: DC-segmented case: Two-area system with a VSC-HVDC interconnection.

In the DC-segmented case, VSC of bus 7 was set in p-control mode while VSC of bus 9 was set in $V_{dc}$-control mode. The active power and reactive injections of the VSC of bus 7 and 9 was respectively: -418 MW/100 MVAr and 400 MW/-100 MVAr.

The effects of the DC-segmentation proposed were investigated using Dymola [114]. VSC-HVDC links were modelled as proposed in Section 3.3 and models were implemented in Modelica language to be tested in combination with the OpenIPSL library [92]. Details of the two case systems can be found in Section A.1 and A.2 of the Appendix.

## 4.3 Small-signal stability analysis

Fig. 4.3 and Table 4.1 show the electromechanical modes of the system obtained for the AC-base case and for the DC-segmented case. Notice that the power system stabilisers (PSSs) of the generators have been removed for this case to have a case with poorly damped electromechanical oscillations. Regions of the electromechanical modes can be identified by means of participation-factor analysis [121, 122].

Results show an inter-area mode in the AC base case (mode 1 of Table 4.1, with damping of -0.38% and frequency of 0.57 Hz). This mode has been suppressed by the DC segmentation. Meanwhile, the frequency and damping ratios of the two other (local) electromechanical modes do not

present significant differences between the two cases.

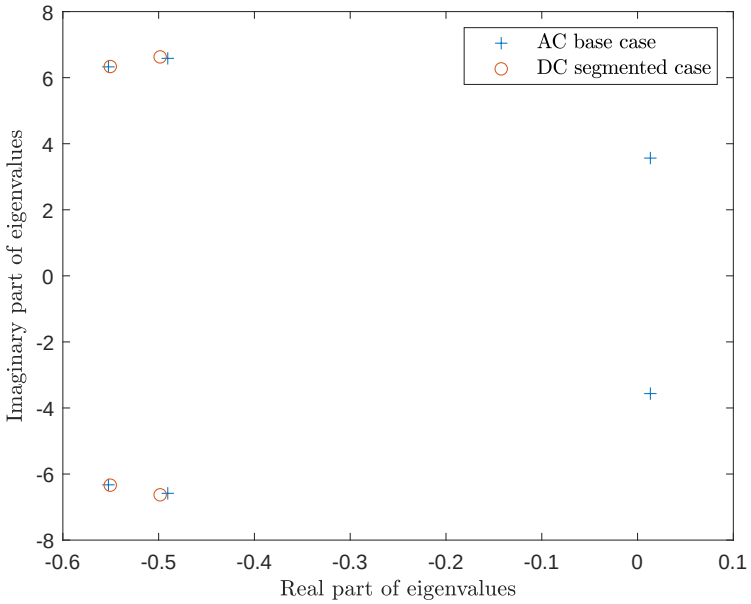


Figure 4.3: Weakly damped electromechanical modes of the two-area system with AC or DC interconnection.

Table 4.1: Weakly damped electromechanical modes of the two-area system with AC or DC interconnection

| N0. | AC base case | | DC-segmented case | | Region of the mode |
|---|---|---|---|---|---|
| | $\zeta$ (%) | Freq (Hz) | $\zeta$ (%) | Freq (Hz) | |
| 1 | -0.38 | 0.57 | - | - | inter-area |
| 2 | 7.43 | 1.05 | 7.50 | 1.06 | region 2 |
| 3 | 8.70 | 1.01 | 8.65 | 1.01 | region 1 |

## 4.4 Non-linear time-domain simulation

### 4.4.1 Electromechanical oscillations

In order to evaluate the effect of DC segmentation on the electromechanical oscillations of the two-area test system, a three-phase-to-ground short circuit

was applied at bus 6, with a clearing time of 100ms. This event triggers the electromechanical oscillations of interest. As mentioned before, the power system stabilisers (PSSs) of the generators have been removed for this case to emphasise poorly damped electromechanical oscillations.

Fig. 4.4 shows the frequency of the generators. In the all-AC case (Fig. 4.4a), all generators are affected by the fault. Additionally, an inter-area mode with negative damping ratio is present (mode 1 of Table 4.1). However, in the DC-segmented case (Fig. 4.4b), generators of the non-faulty region (i.e., generators 3 and 4) are hardly affected by the fault. The DC link strongly mitigated the propagation of the fault. But more importantly, the inter-area oscillation is fully suppressed in the DC-segmented case as shown in Section 4.3.

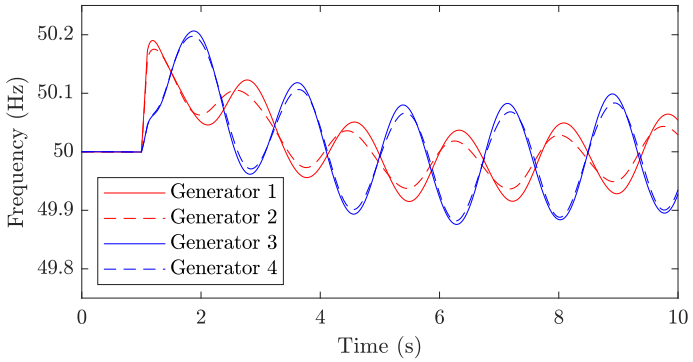


(a) AC base case

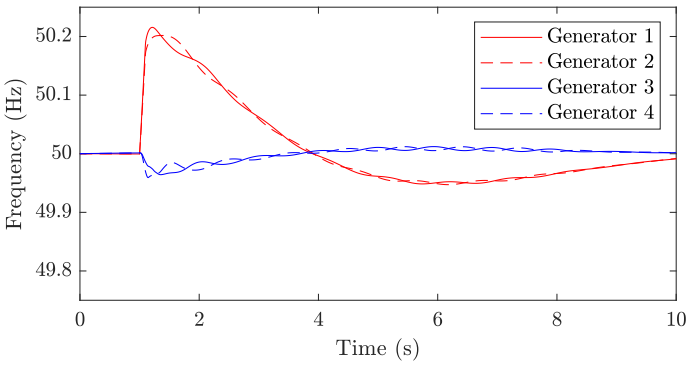


(b) DC-segmented case

Figure 4.4: Frequency of the generators after a 100ms short circuit at bus 6.

Fig. 4.5 shows the angle difference of the generators of each sector. The intra-area oscillations (local modes of each area) observed in the DC-segmented case present a reasonable damping ratio. In the AC-interconnected case, intra-area oscillations cannot be observed clearly because of the effect of the undamped inter-area mode.

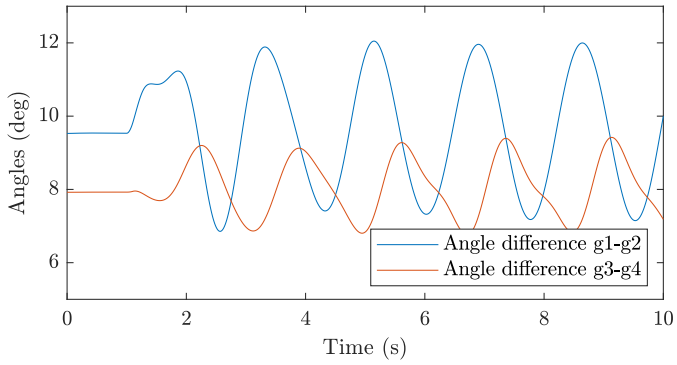


(a) AC base case

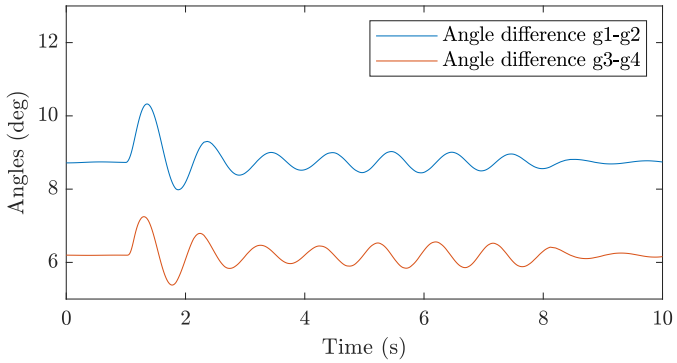


(b) DC-segmented case

Figure 4.5: Intra-area angle differences after a 100ms short circuit at bus 6.

These results confirm the ones of Section 4.3: DC segmentation with constant power reference improves the small-signal angle stability of the AC-interconnected system by removing the inter-area oscillations, while it does not affect the damping of the local modes.

### 4.4.2 Transient stability

In order to evaluate the impact of DC segmentation on the transient stability of our two-area test system, a three-phase-to-ground short circuit was applied to bus 6, with a clearing time of 500ms.

Fig. 4.6 shows the inter-area angle difference (more precisely the angle difference between generator 1 and 3), Fig. 4.7 the active power exchange between the two regions of the system (more precisely the AC active power injected at bus 9 by the two parallel lines 8-9 in the AC base case (Fig. 4.7a) or the DC link in the DC-segmented case (Fig. 4.7b)). The improvement in the latter case is noticeable. Finally, Fig. 4.8 shows the intra-area angle difference (i.e., the difference of angle between the generators of the same region). For the sake of clarity, the same scales are used for the AC base case and the DC-segmented case.

In the AC base case, the event caused the angle of the two sectors to diverge (Fig. 4.6a): the generators 1 and 3 have lost their synchronism. Since they are in the same AC system, this means the system has lost its stability. This is confirmed by the fact that the active power exchanged between the two regions is non consistent anymore (Fig. 4.7a) and that the angle difference between the generators of the same region are not stable (Fig. 4.8a).

On the other hand, the divergence in angle between the generator 1 and 3 in the DC-segmented case (Fig. 4.6b) does not represent a loss of synchronism, indeed thanks to the DC segmentation of the system, these two generators do not have to be synchronous since they are located in two AC asynchronous areas. Additionally, the power exchanged between the regions is stable (Fig. 4.7b) and the generators of one given region stay in synchronism with one another (Fig. 4.8b), thus the DC-segmented case stayed stable.

Additional simulations have been carried out to evaluate the critical clearing time (CCT) of the fault for both cases. The CCT is the maximum duration that a fault can last before being removed without producing loss of synchronism. It is an indicator of the transient-stability margin. Table 4.2 shows the CCTs for a three-phase-to-ground short circuit at bus 6 obtained in the AC base case and the DC-segmented case. For the calculation of the CCT, a precision of 10 ms and a maximum value of 2 s were used. Results show that the AC base case has a CCT of 420 ms and the DC segmented case a CCT of more than 2 s. Therefore, DC segmentation significantly increased the fault critical clearing time.

These results show that DC segmentation with constant power reference

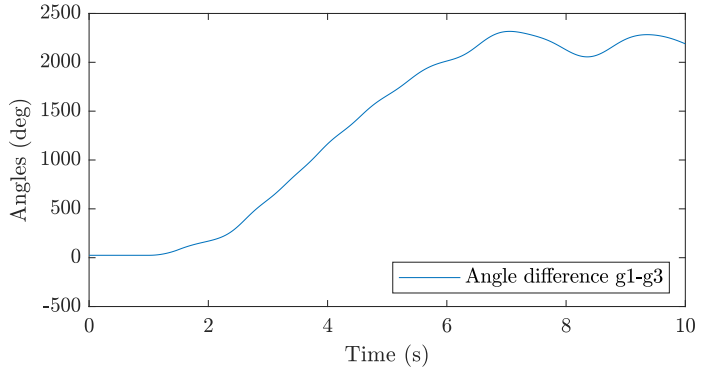


(a) AC base case: the synchronism is lost at time t=2s.

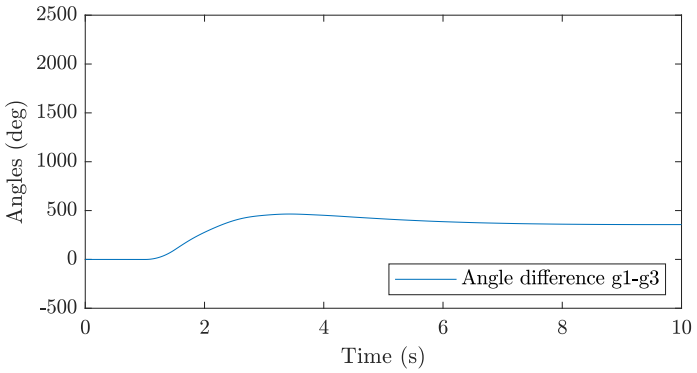


(b) DC-segmented case: g1 and g3 are in asynchronous regions, thus their big angle difference does not mean a loss of synchronism.

Figure 4.6: Inter-area angle difference after a 500ms short circuit at bus 6.

Table 4.2: CCTs of the two-area system with AC or DC interconnection for a fault at bus 6.

| | AC base case | DC-segmented case |
|---|---|---|
| CCT | 420 ms | above 2 s |

improves transient stability of the overall system by suppressing the inter-area synchronism constraint.

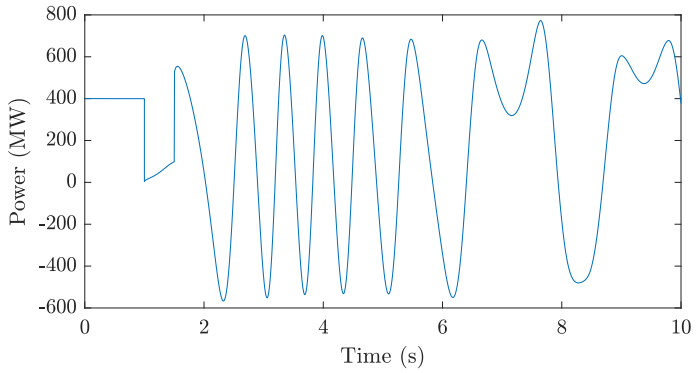


(a) AC base case

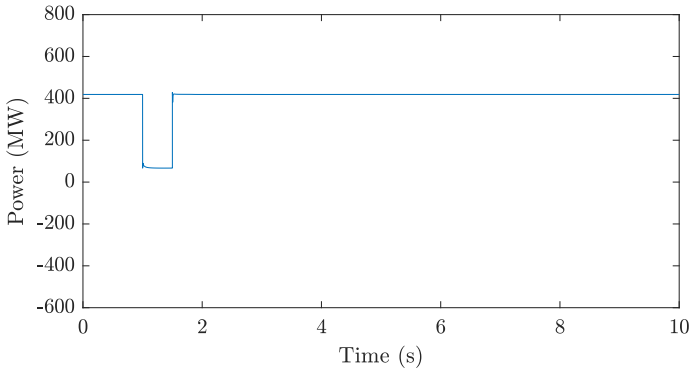


(b) DC-segmented case

Figure 4.7: Active power exchange from region 1 to region 2 after a 500ms short circuit at bus 6.

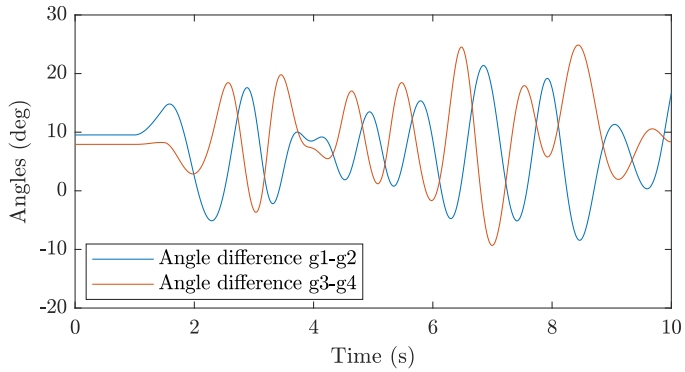


(a) AC base case

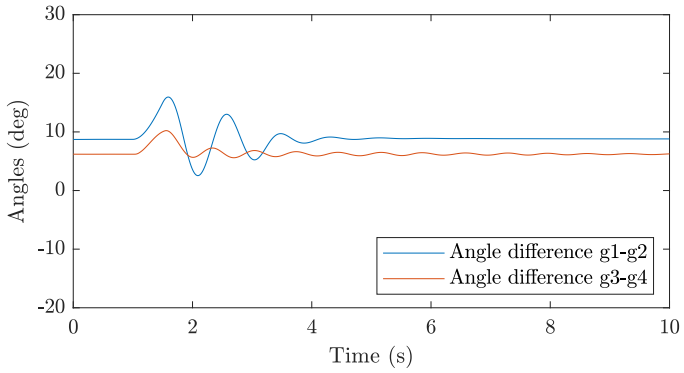


(b) DC-segmented case

Figure 4.8: Intra-area angle difference after a 500ms short circuit at bus 6.

### 4.4.3 Frequency stability

In order to evaluate the effect of DC segmentation on the frequency stability of our two-area test system, the connection of a 200MW load at bus 2 at 1s was simulated. Fig. 4.9 shows the frequency variation of the generators and Fig. 4.10 the active power exchange between the two regions of the system.

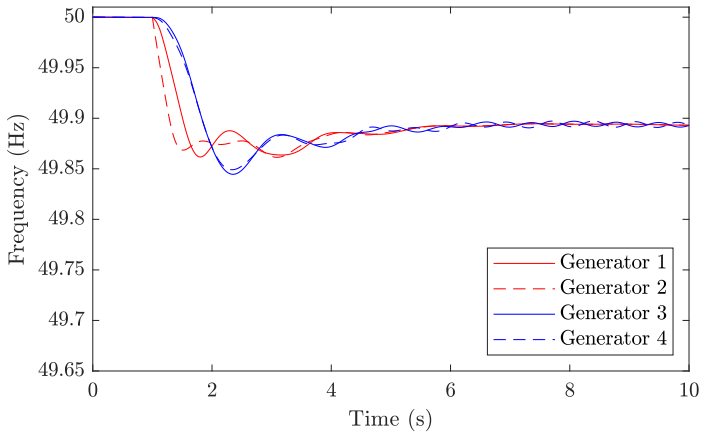


(a) AC base case

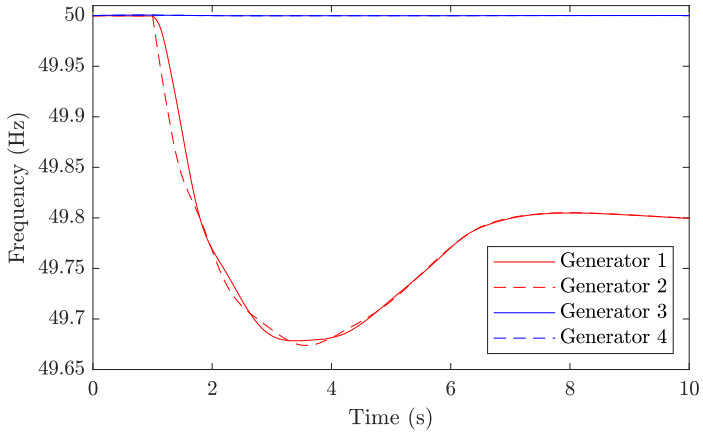


(b) DC-segmented case

Figure 4.9: Generators frequency after the connection of a load at bus 2.

In the AC-interconnected system, all generators see a similar frequency drop of around 0.15Hz before stabilising at around -0.1Hz (Fig. 4.9a). How-

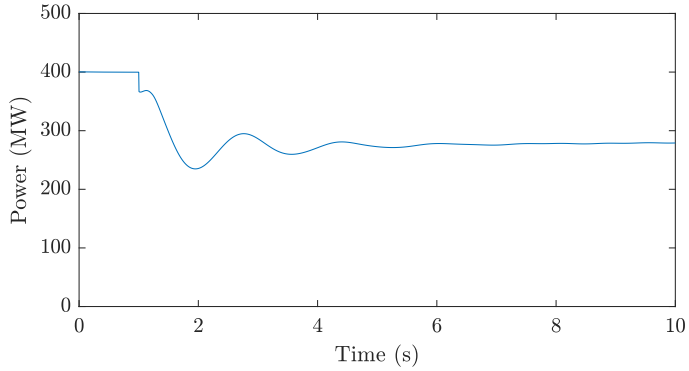


(a) AC base case

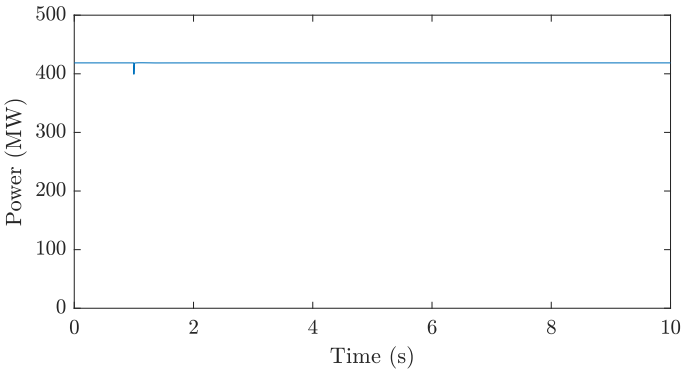


(b) DC-segmented case

Figure 4.10: Active power exchange from region 1 to region 2 after the connection of a load at bus 2.

ever, in the DC-segmented system, generators of region 1 (i.e., generators 1 and 2) initially see a frequency drop of 0.32Hz before stabilising at -0.2Hz (Fig. 4.9b), while generators of region 2 (i.e., generators 3 and 4) do not have any frequency variation. The frequency deviation of generators 1 and 2 in the DC-segmented case is twice as big as in the other case. This happens because the generators of region 2 did not contribute to the frequency support (with their primary frequency controller and their inertia constants). Clearly, with a constant-power set point in the VSC-HVDC link, the power exchange between the areas could not change during the event (Fig. 4.10b).

This result illustrates the fact that DC segmentation with constant-power

set point jeopardises the frequency stability of the overall system.

## 4.5 Summary and Conclusion

This chapter analysed the impact of the DC segmentation of power systems on electromechanical oscillations, transient stability and frequency stability. Small-signal analysis and time-domain dynamic simulations have been carried out to show the effect of DC segmentation with fix power control on the stability of a simple test system. The response of a single interconnected AC system has been compared with the response of a DC segmented system composed of two AC areas linked by a VSC-HVDC link.

The following conclusions have been obtained from the results presented in this chapter:

- DC segmentation improves small-signal angle stability of the system (electromechanical oscillations) by removing the inter-area oscillations without affecting the damping of the local modes.
- DC segmentation also improves angle stability under large disturbances (transient stability) of the overall system by removing the inter-area synchronism constrain by decoupling the two areas.
- However, it jeopardises the frequency stability of the overall system. This problem should be mitigated by implementing suitable control strategies for primary frequency support through the VSC-HVDC system (i.e., through the DC links see Chapter 7).

# Chapter 5

# Dominant electromechanical-oscillation paths

## 5.1 Introduction

The literature survey reported in Chapter 2 has not found any proposal for the selection of DC-segmentation boundaries for a given AC system. Chapter 6 will tackle this gap. More precisely, it proposes an algorithm for the DC segmentation of power system with the purpose of mitigating electromechanical oscillations. This algorithm relies on the study and identification of inter-area oscillation paths. Thus, the present chapter presents a study of those paths and an algorithm for their automatic identification.

The definition of dominant inter-area oscillation paths was proposed in [43] alongside with an algorithm to identify them. However, the work presented in this chapter goes further by discussing the use of various observability factors to be used for the definition and identification of these paths and by proposing a fully automated algorithm for the determination of these paths. This algorithm constitutes the first step towards the DC segmentation of a power system and must be followed by the procedure detailed in Chapter 6.

This chapter is organised as follows. Section 5.2 presents some necessary theoretical background. The concept of dominant inter-area oscillation path is presented in Section 5.3. Section 5.4 discussed the use of different observability factors for the identification of the path. The algorithm proposed to

determine the path is detailed in Section 5.5, and is applied on the Nordic 44 test system in Section 5.6. Results are validated in Section 5.7. Finally, Section 5.8 concludes the chapter.

## 5.2 Theoretical background

The electromechanical behaviour of a power system can be described by a set of non-linear algebraic-differential equations (also known as electromechanical-type or Root-Mean-Square (RMS)-type model) [24]. In addition, the dynamic behaviour of a power system when subject to small disturbances can be analysed using a linearised model of the system around the steady-state operating points [24]. For example, the free response of the system can be written as:

$$\boldsymbol{\Delta \dot{x}} = \boldsymbol{A \Delta x},\ \boldsymbol{\Delta x} = [\boldsymbol{\Delta \delta},\ \boldsymbol{\Delta \omega},\ \boldsymbol{\Delta z}]^T \tag{5.1}$$

$$\boldsymbol{\Delta y} = \boldsymbol{C \Delta x} \tag{5.2}$$

where $\boldsymbol{\Delta x} \in \mathbb{R}^{n_x \times 1}$ is the state vector (increments with respect to the operating point), $\boldsymbol{\Delta y}$ is the output vector and $\boldsymbol{A} \in \mathbb{R}^{n_x \times n_x}$ is the state matrix of the system. The state vector contains, explicitly, the rotor angles ($\boldsymbol{\Delta \delta}$) and speeds of the generators ($\boldsymbol{\Delta \omega}$), and the rest of the state variables ($\boldsymbol{\Delta z}$), to analyse electromechanical oscillations [43].

In addition, if $\lambda_k$ is an eigenvalue of matrix $\boldsymbol{A}$ and $\boldsymbol{v_k}$ is its associated right eigenvector (i.e., $\lambda_k \boldsymbol{v_k} = \boldsymbol{A v_k}$), [24] shows that:

$$\boldsymbol{\Delta x} = \sum_{k=1}^{n_x} \left( \boldsymbol{v_k} z_k(0) e^{\lambda_k t} \right) \tag{5.3}$$

where each $z_k(0)$ is a linear combination of the initial conditions of the state variables.

Therefore, right eigenvector $\boldsymbol{v_k}$ "shapes" how a system mode (eigenvalue) affects the time response of each of the state variables. For example, if the elements of vector $\boldsymbol{v_k}$ are complex numbers, the phases of those numbers affect the relative phases of the oscillatory response of the state variables due to $\lambda_k$ and its complex conjugate. This is why right eigenvectors are also known as "mode shapes". If two elements of mode shape $\boldsymbol{v_k}$ (e.g., $\boldsymbol{v_k}(i)$ and $\boldsymbol{v_k}(j)$) have similar phases, these two variables are said to be oscillating together while if their phases differ in almost $180^o$, they are said to oscillate against each other. Using this property, mode shapes of the modes associated

to generator speeds have been remarkably useful to analyse generator speed oscillations in power systems [24, 48, 123]. Modes related to generator speeds can be identified looking at participation factors [121, 122, 124].

Matrix $\boldsymbol{C}$ in (5.1) can be further detailed to highlight the way in which state variables affect the time response of the output variables. For example, if bus-voltages, bus-frequencies and branch-current flows are selected as outputs, one can write:

$$\begin{bmatrix} \boldsymbol{\Delta V} \\ \boldsymbol{\Delta f} \\ \boldsymbol{\Delta I_f} \end{bmatrix} = \boldsymbol{C\Delta x} = \begin{bmatrix} \boldsymbol{C_V} \\ \boldsymbol{C_f} \\ \boldsymbol{C_{I_f}} \end{bmatrix} \begin{bmatrix} \boldsymbol{\Delta \delta} \\ \boldsymbol{\Delta \omega} \\ \boldsymbol{\Delta z} \end{bmatrix} \tag{5.4}$$

where

$$\begin{aligned} \boldsymbol{C_V} &= \begin{bmatrix} \boldsymbol{C_{V\delta}} & \boldsymbol{C_{V\omega}} & \boldsymbol{C_{Vz}} \end{bmatrix} \\ \boldsymbol{C_f} &= \begin{bmatrix} \boldsymbol{C_{f\delta}} & \boldsymbol{C_{f\omega}} & \boldsymbol{C_{fz}} \end{bmatrix} \\ \boldsymbol{C_{I_f}} &= \begin{bmatrix} \boldsymbol{C_{I_f\delta}} & \boldsymbol{C_{I_f\omega}} & \boldsymbol{C_{I_fz}} \end{bmatrix} \end{aligned} \tag{5.5}$$

and $\boldsymbol{C_V}$, $\boldsymbol{C_f}$, $\boldsymbol{C_{I_f}}$ are defined in [125] as Network sensitivity matrices of bus-voltages, bus-frequencies and branch-current flows, respectively.

Given a set of system outputs, observability factors of a system mode $\lambda_k$ are defined as the product of the output-variables network sensitivity matrix by the right eigenvector associated to $\lambda_k$ [43, 125]. For example, given the output partition in (5.4), the corresponding observability factors would be:

$$\boldsymbol{\phi_{V,k}} = \boldsymbol{C_V v_k}, \;\; \boldsymbol{\phi_{f,k}} = \boldsymbol{C_f v_k}, \;\; \boldsymbol{\phi_{I_f,k}} = \boldsymbol{C_{I_f} v_k} \tag{5.6}$$

Very much like with mode shapes, the phases of two complex elements of an observability factor will tell which output variables oscillate together and which ones oscillate against each other when a system mode is excited.

The work in [125] uses the term *network mode shape* to refer to vectors in (5.6), although the more popular term observability factor will be used in this work, as in [24].

## 5.3 Dominant inter-area oscillation path

The work in [43] proposed the concept of dominant inter-area oscillation path which can be illustrated using the two-area 6-generator system shown in Figure 5.1 (test system 1) with the data reported in Appendix B .

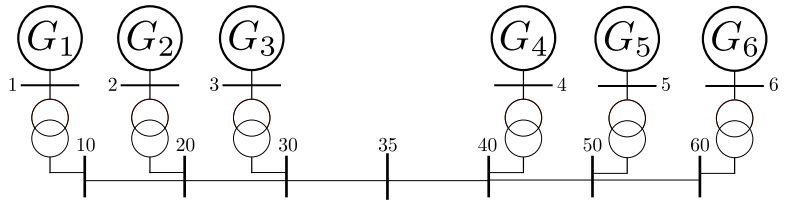


Figure 5.1: Test system 1: Conceptual 6-generator system.

The small-signal analysis of the system in Fig. 5.1 reveals that it has an inter-area mode with a damping coefficient of 5.5% and a frequency of 0.83 Hz (all system modes are included in Table 5.1). The generator-speed mode shapes of this mode have been drawn in Fig. 5.2 which shows that generators G1, G2 and G3 oscillate against generators G4, G5 and G6. Fig. 5.2 also shows that the generators further away from the centre of the system (G1 and G6) are subject to the largest oscillations (the moduli of their mode shapes are the two largest ones) and they are called "edges" of the inter-area mode. This mode also affects G2, G3, G4 and G5 whose mode shapes are placed between the two extremes G1 and G6. The buses between 1 and 6 constitute the dominant oscillation path of the inter-area mode 1 since they form the only possible path between the two "edges" of the path.

Table 5.1: Test system 1: Electromechanical modes.

| Mode | Real | Imag | $\zeta$ (%) | Freq. (Hz) | Oscillation |
|---|---|---|---|---|---|
| 1 | -0.29 | 5.23 | 5.5 | 0.83 | G1,G2,G3//G4,G5,G6 |
| 2 | -1.17 | 6.35 | 18.1 | 1.03 | G4,G3//G6,G1 |
| 3 | -1.22 | 6.48 | 18.5 | 1.05 | G3,G6//G1,G4,G5 |
| 4 | -1.25 | 6.60 | 18.6 | 1.07 | G2//G1 |
| 5 | -1.27 | 6.51 | 19.2 | 1.06 | G5//G4,G6 |

Figs. 5.3, 5.4 and 5.5 show the bus-frequency, bus-voltage and branch-current observability factors along the dominant inter-area oscillation path, respectively. The main characteristics of the dominant oscillation path are as follows [43]:

- The bus with lowest value of $|\phi_{f_i}|$ (Fig. 5.3a) determines the centre of the path, and it is called the inter-area pivot (or pivot bus, for short) [43] (bus 35, in this example).
- The pivot bus divides the path into two groups with opposite phases

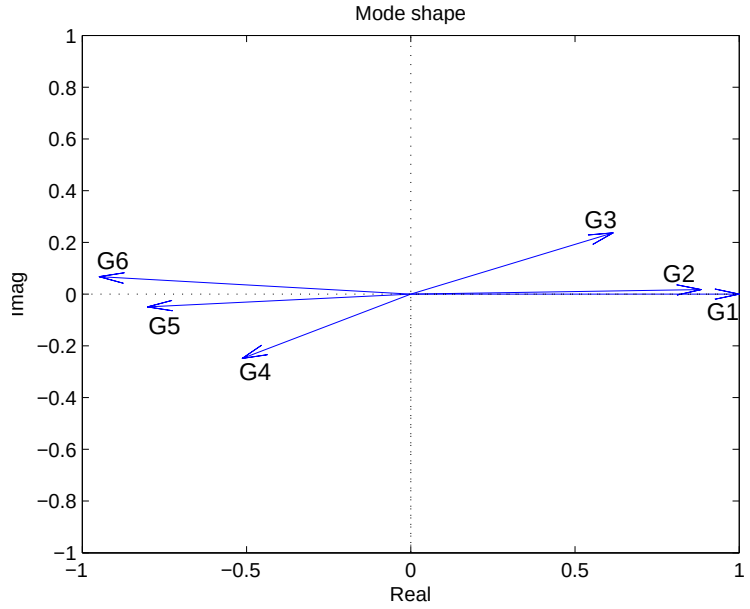


Figure 5.2: Test system 1: Graphical representation of the mode shape of inter-area mode 1.

of $\phi_{f_i}$ (Fig. 5.3b).

- The edges of the path have the highest value of $|\phi_{f_i}|$ (Figure 5.3a), this confirm that the oscillations are stronger at the edges of the path. In this example, buses 1 and 6 are confirmed as the edges of the path of inter-area mode 1 (see also Fig. 5.2.)

- When going from the pivot bus to one of the edges, $|\phi_{f_i}|$ see a continuous increase and thus form a V-shape (Figure 5.3a).

- In test system 1, buses close to the centre of the path have larger values of $|\phi_{V_i}|$ than those of buses at the edges of the path, as shown in [43]. Buses close to the centre of the path of this test system also present low values of the phase of bus-voltage observability factors. This point will deserve further discussion in the next Section.

- The higher the value of $|\phi_{I_{ij}}|$ (Fig. 5.5a) is in a branch, the more the oscillation propagates through that branch. Branches with high $|\phi_{I_{ij}}|$ are usually those close to the pivot bus.

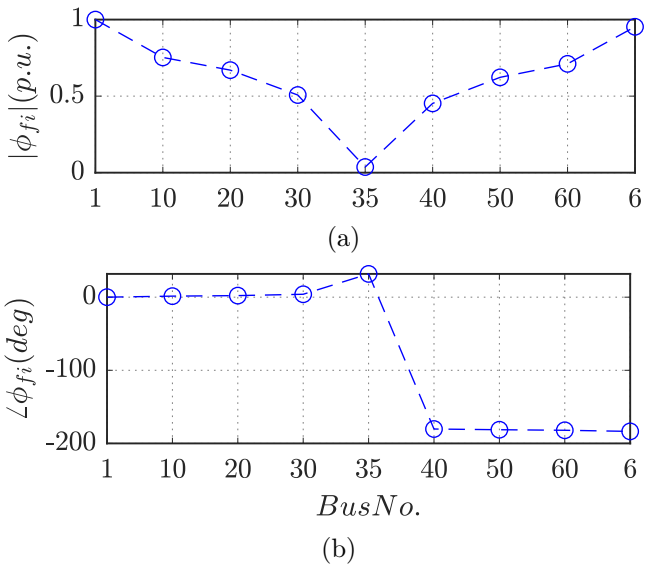


Figure 5.3: Test system 1: Bus-frequency observability factors along the dominant oscillation path of inter-area mode 1: (a) magnitudes, (b) phases.

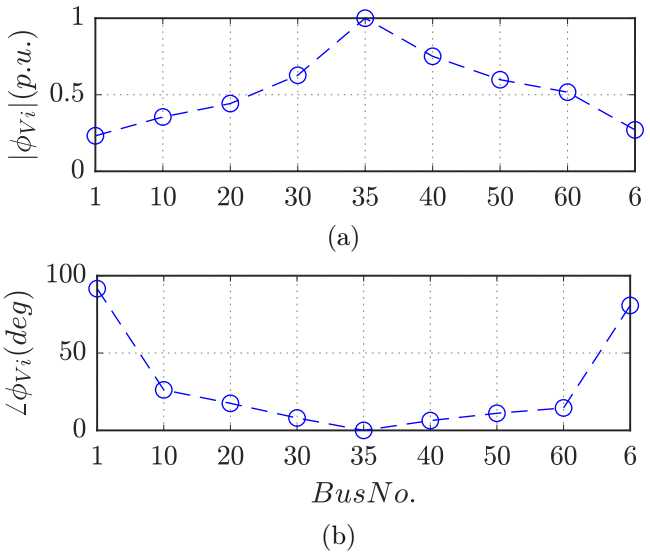


Figure 5.4: Test system 1: Bus-voltage observability factors along the dominant oscillation path of inter-area mode 1: (a) magnitudes, (b) phases.

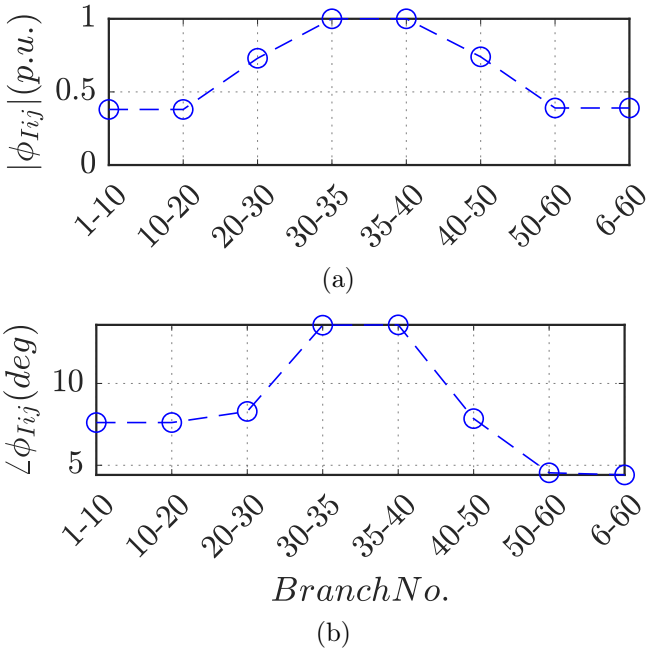


Figure 5.5: Test system 1: Branch-current observability factors along the dominant oscillation path of the inter-area mode 1: (a) magnitudes, (b) phases.

- In test system 1, there is no clear pattern in the phases of $\phi_{I_{ij}}$ (Fig. 5.5b). They were not analysed in [43], probably because they were not very useful to characterise inter-area oscillation paths.

## 5.4 Characterising dominant inter-area oscillation paths: bus-frequency vs. bus-voltage observability factors

Let us consider the system in Fig. 5.6 (test system 2), it is the same system as the one of Fig. 5.1 but with a load in bus 35 that consumes the power supplied by the generators. The data of this new situation are in Section B.2 of the Appendix.

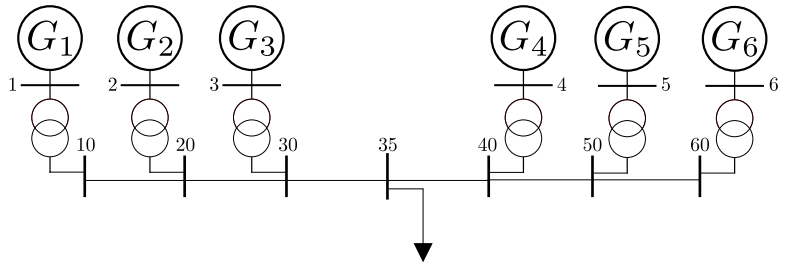


Figure 5.6: Test system 2: Conceptual 6-generator system with one load.

The small-signal stability analysis of test system 2 shows that this additional load does not strongly impact the main electromechanical characteristics of the system. This system still has a lightly-damped inter-area electromechanical mode (damping coefficient of 11.8 % and frequency of 0.80 Hz) associated to generators G1, G2 and G3 oscillating against G4, G5 and G6. As for test system 2 (Section 5.3), the largest oscillations are seen at the edges of the two areas (G1 and G6) and the oscillation path includes buses 1, 10, 20, 30, 35, 40, 50, 60 and 6. Mode shapes for test system 2 are plotted in Fig. 5.7.

Table 5.2: Test system 2: Electromechanical modes.

| Mode | Real | Imag | $\zeta$ (%) | Freq. (Hz) | Oscillation |
|---|---|---|---|---|---|
| 1 | -0.59 | 4.98 | 11.8 | 0.80 | G1,G2,G3//G4,G5,G6 |
| 2 | -1.25 | 6.58 | 18.7 | 1.07 | G2//G1,G3 |
| 3 | -1.22 | 6.43 | 18.7 | 1.04 | G3,G6//G1,G2,G4 |
| 4 | -1.24 | 6.36 | 19.2 | 1.03 | G4,G3//G1,G2,G6 |
| 5 | -1.30 | 6.56 | 19.5 | 1.06 | G5//G4,G6 |

Figs. 5.8, 5.9 and 5.10 show the bus-frequency, bus-voltage and branch-current observability factors along the dominant inter-area oscillation path in test system 2, respectively.

Results show that:

- The conclusions related to the bus-frequency observability factors, $\phi_{f_i}$, are the same as those obtained for test system 1. This confirms that bus-frequency observability factors are a robust tool to characterise dominant inter-area oscillation paths and they will be used in this study.

- The conclusions related to the bus-voltage observability factors, $\phi_{V_i}$,

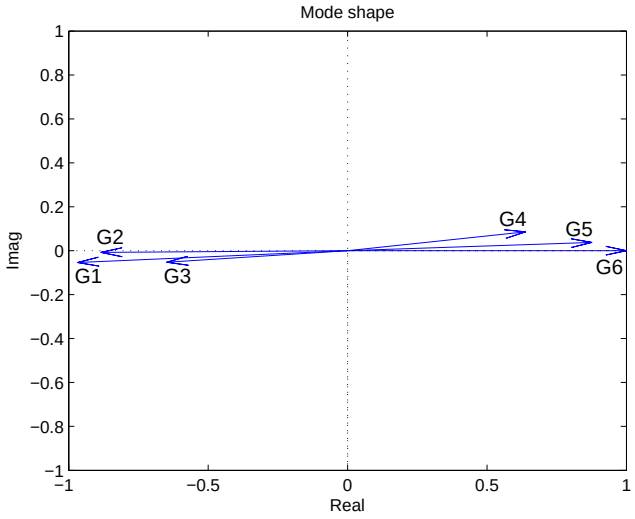


Figure 5.7: Test system 2: Graphical representation of the mode shape of inter-area mode 1.

are different from those obtained for test system 1. Results strongly depend on the topology and power flows of the system as mentioned without further discussion in [126]. Hence, bus-voltage observability factors are not considered a robust tool to characterise dominant inter-area oscillation paths.

- The conclusions related to the magnitude of the branch-current observability factors, $|\phi_{I_{ij}}|$, are the same as those for test system 1 confirming that branch-current observability factors are a robust tool to characterise dominant inter-area oscillation paths and they will be used in this study.

- Finally, the conclusions related to the phase of the branch-current observability factors, $\angle\phi_{I_{ij}}$, are different from the ones obtained for test system 1: the presence of the load affects the pattern of the phases of the branch-current observability factors. In fact, they would depend on the direction of the current flows. Hence, the angles of branch-current observability factors are not considered a robust tool to characterise

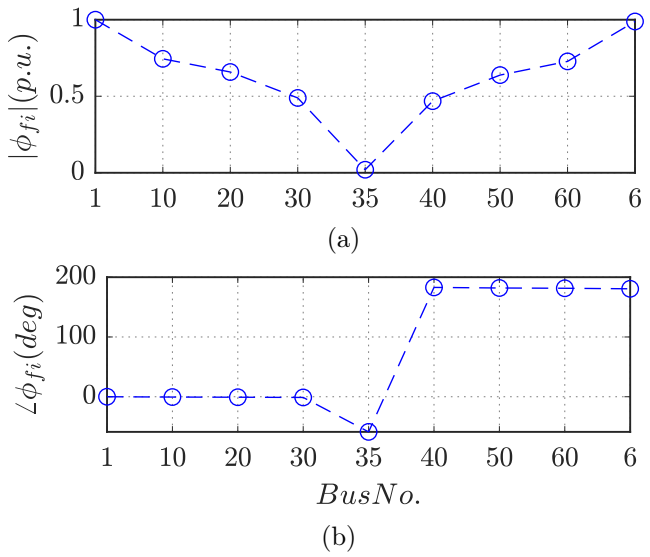


Figure 5.8: Test system 2: Bus-frequency observability factors along the dominant oscillation path of inter-area mode 1: (a) magnitudes, (b) phases.

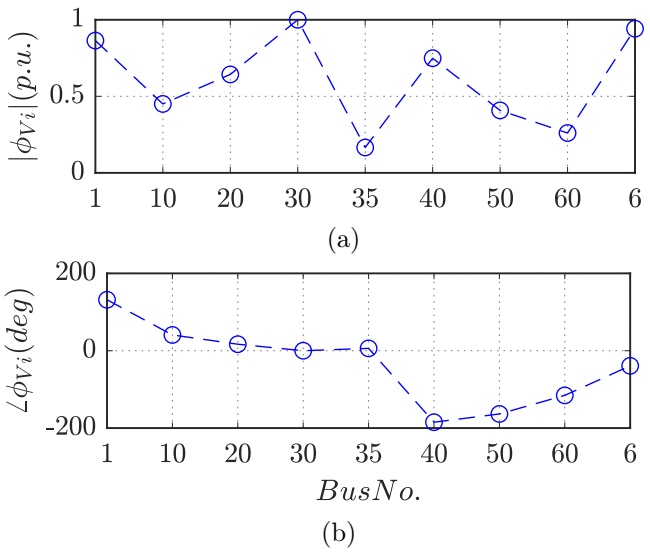


Figure 5.9: Test system 2: Bus-voltage observability factors along the dominant oscillation path of inter-area mode 1: (a) magnitudes, (b) phases.

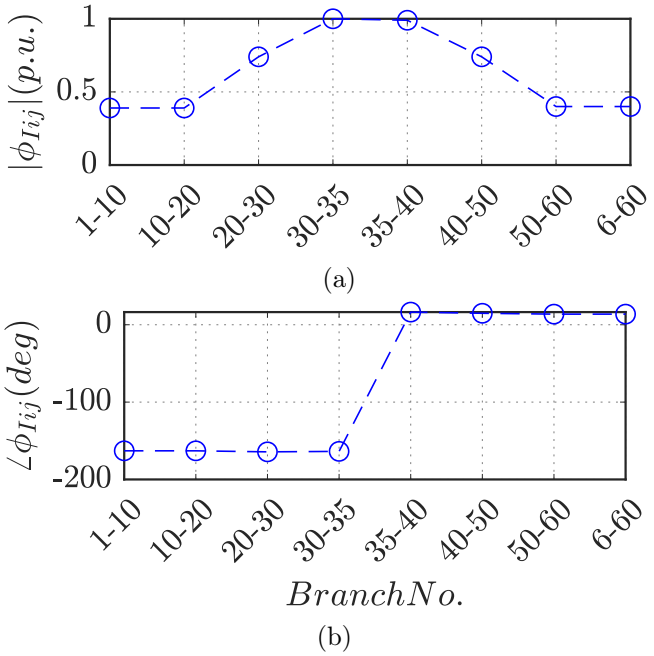


Figure 5.10: Test system 2: Branch-current observability factors along the dominant oscillation path of the inter-area mode 1: (a) magnitudes, (b) phases.

dominant inter-area oscillation paths.

## 5.5 Proposed algorithm for the identification of the dominant inter-area oscillation path

A meshed AC power system with an inter-area mode of interest (typically a mode with low damping ratio) will be now considered. The objective of the proposed algorithm is to systematically find the main inter-area oscillation path of this mode. Notice that the concept of dominant path can be used to characterise electromechanical oscillations in general(i.e, in general it will be called *dominant electromechanical-oscillation path*), although the inter-area ones are often the most critical ones in large power systems.

A linearised small-signal model of the power system is used to identify the inter-area mode of interest ($\lambda_{k_{crit}}$). The proposed algorithm for the identification of the dominant inter-area oscillation path consists of two steps:

- **Step 1**: Identification of the edges of inter-area oscillation path.
- **Step 2**: Identification of the dominant inter-area oscillation path between the two edges.

The algorithm uses the information provided by the modal analysis of the linearised model of the power system:

- Mode shapes of the target inter-area mode participating in the speeds of the generators ($v_{i,k_{crit}}$).
- Frequency observability factors of the target inter-area mode of all buses ($\phi_{f_{i,k_{crit}}}$).
- Magnitude ($|\phi_{I_{ij},k_{crit}}|$) of the current observability factors of the target inter-area mode of all branches ($\phi_{I_{ij},k_{crit}}$).

For the sake of clarity, the subscript of the target inter-area mode will be removed from the indicators above in the future (i.e., $\phi_{f_i}$ will be used instead of $\phi_{f_{i,k_{crit}}}$). Table 5.3 presents a summary of the notations used in the algorithm. Figure 5.11 depicts a flowchart of the algorithm.

Table 5.3: Notations used in the algorithm.

| Notation | Variable |
|---|---|
| $\lambda_{k_{crit}}$ | Inter-area mode of interest |
| $v_i$ | Mode shape associated to the speeds of generator i |
| $\phi_{f_i}$ | Bus frequency observability factor of bus $i$ |
| $\phi_{I_{ij}}$ | Branch current observability factor of $L_{ij}$ |
| $En$ | Bus of the n (with n=1 or 2) edge of the path |
| $GEn$ | Synchronous generator connected at bus $En$ |
| path-$ip$ | Path being identified |
| bus $i$ | Bus i |
| $L_{ij}$ | Branch ij |
| $B_{path,ip}$ | Set of buses of the system ($i$) that belong to path-$ip$ |
| $A_{path,ip}$ | Set of branches of the system ($L_{ij}$) that belong to path-$ip$ |
| $A_{EX,ip}$ | Set of branches of the system ($L_{ij}$) that are excluded from path-$ip$ |
| $A^C$ | Complement of set $A$ |
| $A_{L,i}$ | Set of branches connected to a certain bus $i$ |
| PB | Pivot bus |
| bus $A$ | first bus of the ascending sub-path |

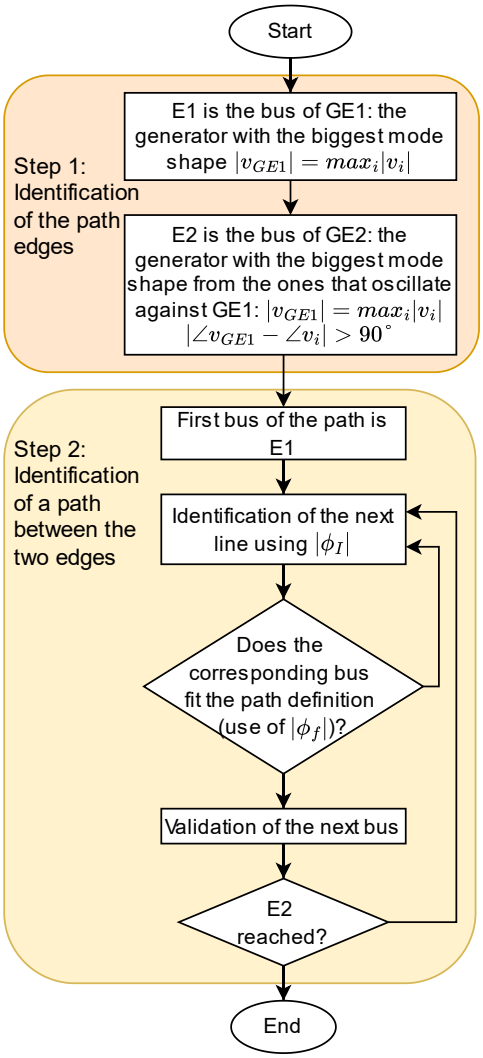


Figure 5.11: Flowchart of the proposed algorithm for the identification of the dominant inter-area oscillation path

### 5.5.1 Step 1: Identification of the edges of inter-area oscillation path

The bus of the first edge of the path will be called $E1$ and it contains a synchronous generator ($GE1$). The bus of the other edge will be called $E2$ and it contains another synchronous generator ($GE2$). The edges of the path are obtained as follows:

- The bus with the generator with the largest magnitude of inter-area mode shape ($|v_{GE1}| = \max_i |v_i|$) will be designated as "the first edge" ($E1$ and $GE1$).
- The bus with the generator with the largest magnitude of inter-area mode shape among those oscillating with a phase greater than 90° with respect to generator $GE1$, will be designated as "the second edge" ($E2$ and $GE2$). In other words, generator $GE2$ is the one that satisfies $|v_{GE2}| = \max_i |v_i|$, among those that satisfy $|\angle v_{GE1} - \angle v_i| > 90°$.
- All generators $i$ with $|v_i| > 0.1$ pu and $|\angle v_{GE1} - \angle v_i| < 45°$ will belong to the coherent group of generators associated with edge $E1$.
- All generators $i$ with $|v_i| > 0.1$ pu and $|\angle v_{GE2} - \angle v_i| < 45°$ will belong to the coherent group of generators associated with edge $E2$.

Notice that there could be inter-area modes with more than two coherent groups of generators. This algorithm will focus only on the first two groups.

### 5.5.2 Step 2: Identification of the dominant inter-area oscillation path between the two edges

The algorithm presented here revisits the idea presented in [43] but includes some additions needed to fully automate the process. The main additions are highlighted in Section 5.5.4.

The target inter-area oscillation path will go from $E1$ to $E2$. To tackle meshed systems, where more than one propagation path is possible for the target inter-area mode, let us add the following definitions:

- $A_{path,ip}$ is the set of branches of the system ($L_{ij}$) that belong to path-$ip$.
- $B_{path,ip}$ is the set of buses of the system ($i$) that belong to path-$ip$.
- $A_{EX,ip}$ is the set of branches of the system ($L_{ij}$) that are excluded from path-$ip$ at each iteration.

- $A_{L,i}$ is the set of branches connected to a certain bus $i$.

Sets $A_{path,ip}$, $B_{path,ip}$ and $A_{EX,ip}$ are empty at the beginning of Step 2. Notice that all inter-area oscillation paths will start at edge $E1$ and will end at edge $E2$.

Recalling the definition of "pivot bus" ($PB$) in Section 5.3 ($PB$ is the bus of the path with the minimum value of the magnitude of the bus-frequency observability factor: $|\phi_{f_{PB}}| = \min_{i \in B_{path,jp}} |\phi_{f_i}|$), the dominant inter-area oscillation path-$ip$ can be split into two parts:

- Descending sub-path: From $E1$ to $PB$.
- Ascending sub-path: From $PB$ to $E2$.

The descending sub-path will move along the branches with the highest current observability factor linking buses with a decreasing frequency observability factor. The ascending sub-path will move along the branches with the highest current observability factor linking buses with increasing frequency observability factor. The end of the descending sub-path will be established by detecting the PB which splits the path into two parts with opposite phases in the frequency observability factors (Section 5.3).

When moving along the descending sub-path, if the magnitude of bus frequency observability factor increases, it means that:

- either that the ascent has started,i.e., the first bus of the ascent ($A$, for short) has been reached;
- or the line selected is going "backwards",i.e., in the direction of E1. In this case, this line must be suppressed from the sub-path.

If the ascent has been reached, the pivot bus has been passed. Thus, bus $A$ is the first bus of the path that satisfies:

$$|\angle\phi_{f_A} - \angle\phi_{f_{E1}}| > 90^\circ \tag{5.7}$$

Although bus $A$ is part of the ascending sub-path, it will actually be identified during the descending sub-path.

Figure 5.12 depicts a simplified flowchart of step 2 of the algorithm. Only the most important steps are included (steps b of both sub-paths are nor represented).

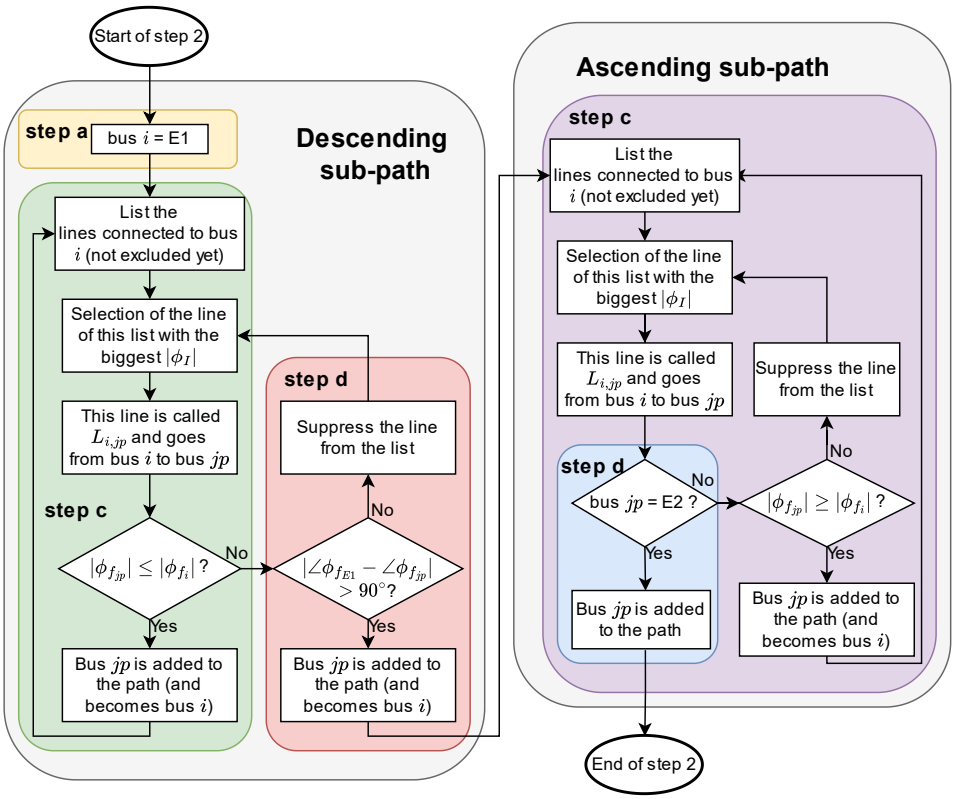


Figure 5.12: Flowchart of step 2: identification of the dominant inter-area oscillation path between the two edges

### Descending sub-path

The descending sub-path is determined as follows:

**Step a**: It starts at the first edge of the inter-area oscillation path (bus $i = E1$).
**Step b**: Feasibility check: Consider all branches $L_{ij}$ connected to bus $i$: $L_{ij} \in A_{L,i}$. Check if those branches have not been excluded to be selected as the next line of the path ($L_{ij} \in A_{EX,ip}$).

**if** there are no feasible candidates ($A_{L,i} \cap A^C_{EX,ip} = \emptyset$), **then**
Exclude the last branch of the path, go back to the previous bus of the path (i.e., include $L_{i-1,i}$ in set $A_{EX,ip}$ and put $i = i - 1$) and

repeat **Step b**
**else**
Continue
**end if**
The feasibility check has two purposes: excluding branches that are already part of the path, and excluding branches that belong to a radial part of the system that has already been broken by a previous DC segment.
**Step c**: Consider all the feasible branches $L_{ij}$ connected to bus $i$: $L_{ij} \in A_{L,i} \cap A^{C}_{EX,ip}$ and choose the one with the largest magnitude of the branch-current observability factor $|\phi_{I_{ij}}|$. The next bus selected will be called $jp$ and thus the selected line will be called $L_{i,jp}$.
**if** in $L_{i,jp}$ the bus-frequency observability factor decreases (i.e., $|\phi_{f_{jp}}| < |\phi_{f_i}|$), **then**
we are still on the descent, branch $L_{i,jp}$ and bus $jp$ can be added to the path and $L_{i,jp}$ is included into $A_{path,ip}$ and bus $jp$ is included into $B_{path,ip}$. At this point, branch $L_{i,jp}$ is part of path-$ip$ and cannot be selected any more. Hence, it is included into the set of excluded lines $A_{EX,ip}$. Finally, put $i = jp$ and return to **Step b**.
**else**
Go to **Step d**
**end if**
**Step d**: Check if bus jp is part of the ascending sub-path.
**if** If $|\angle\phi_{f_{E1}} - \angle\phi_{f_{jp}}| > 90°$ **then**
bus $jp$ is the first one of the ascent: $A = jp$. Branch $L_{i,jp}$ and bus $jp$ can be added to the path. The descending sub-path can be exited and the ascending sub-path started.
**else**
Bus $jp$ correspond to a dead end, exclude branch $L_{i,jp}$ of the path, go back to the previous bus of the path, and repeat **Step b**.
**end if**

### Ascending sub-path

The ascending sub-path is determined as follows:
**Step a**: It starts at the bus $A$ identified during the descending sub-path.
**Step b**: Feasibility check:
**if** there are feasible branches $L_{ij}$ connected to bus $i$ **then**
Continue
**else**

(i.e. $A_{L,i} \cap A^C_{EX,ip} = \emptyset$), include branch $L_{i-1,i}$ into set $A_{EX,ip}$, put $i = i - 1$ and repeat **Step b.**

**end if**

**Step c**: Consider all the feasible branches $L_{ij}$ connected to bus $i$ (i.e., $L_{ij} \in A_{L,i} \cap A^C_{EX,ip}$). From those branches, choose the one with largest magnitude of the branch-current observability factor $|\phi_{I_{ij}}|$. The next bus selected will be called $jp$.

**if** in this branch the magnitude of the bus-frequency observability factor increases (i.e., $|\phi_{f_{jp}}| > |\phi_{f_i}|$), **then**

bus $jp$ will the next bus of the path. Branch $L_{i,jp}$ is included into $A_{path,ip}$ and $A_{EX,ip}$, and $jp$ is included into $B_{path,ip}$.

**else**

$L_{i,jp}$ correspond to a dead end, exclude it from the path, go back to the previous bus of the path, and repeat **Step b**.

**end if**

**Step d**: Check if the second edge of the path has been reached

**if** $jp = E2$, **then**

stop.

**else**

put $i = jp$ and return to **Step b**.

**end if**

### 5.5.3 Illustrative example

The proposed algorithm will now be illustrated in the 6-generator system of Fig. 5.1 (test system 1). Although it is a simple power system with radial configuration, it is useful to help to understand the proposed algorithm. The algorithm has been implemented in Matlab [127] and linked with a tool box for small-signal stability analysis (SSST) [118, 120].

The results of the algorithm when applied to test system 1 (Fig. 5.1) can be summarised as follows:

1. **Step 1**: (see Fig. 5.2) The first edge of the inter-area oscillation path is bus 1 ($E1 = 1$). The coherent generators of this group are generators G1, G2 and G3. The second edge of the inter-area oscillation path is bus 6 ($E2 = 6$). The coherent generators of this group are generators G4, G5 and G6.

2. **Step 2**: (see Fig. 5.3)

- The descending sub-path is 1-10-20-30-35.
  Bus 40 has been identified as the first bus of the ascending sub-path ($A = 40$).
  Bus 35 has been identified as the pivot bus of the path ($PB = 35$).
- The ascending sub-path is 40-50-60-6.

Hence, the propagation path is 1-10-20-30-35-40-50-60-6.

### 5.5.4 Beyond the state-of-the-art contributions of the algorithm for the identification of the inter-area oscillation path

The main characteristics of the algorithm to identify the inter-area oscillation path proposed in [43] can be summarised as follows:

- It uses small-signal stability analysis and bus-angle, bus-voltage and branch-current observability factors.
- Branches with high values of the current observability factors $|\phi_{I_{ij}}|$ are included in the inter-area oscillation path.
- Eventually, the user analyses the single-line-diagram of the system, the branches initially included in the path and the information provided by the observability factors, and makes a decision on the inter-area oscillation path.

The proposed algorithm to identify the inter-area oscillation path (Step 2 of the main algorithm, see Section 6.3.2), can be summarised as follows:

- It uses small-signal stability analysis, generator-speed mode shapes, bus-frequency and branch-current observability factors.
- The algorithm proposed in this work is incremental: starting from the first edge of the path (E1), it gradually finds all the branches and buses of the path, one by one, until the second edge of the path (E2) is reached.
- The path is found using not only branch-current observability factors, but also bus-frequency observability factors.
- The inter-area oscillation path is fully determined by the algorithm, without additional analysis.

- Since the determination of the path is fully automatised by the algorithm, it can be applied to systems of any size and arbitrary topology (and, thus, level of complexity).

## 5.6 Application of the path identification algorithm to the Nordic 44 test system

The proposed algorithm has been applied to the Nordic 44 test system (Fig. 5.13) which is a representation of the interconnected grids of Norway, Sweden and Finland. The information about the model and the scenario considered is provided in Section C.1 of the Appendix.

The result of the algorithm applied to the Nordic 44 system is depicted in Fig. 5.14. All generators, buses and lines of interest for the discussion that follows are highlighted in colours (namely pink and yellow).

Table 5.4 shows the poorly damped electromechanical modes of Nordic 44 test system, (damping ration under 20%). They have been obtained with OpenIPSL. Mode 1 (damping of 1.85% and frequency of 0.39 Hz) is selected as the target inter-area mode for the DC-segmentation algorithm because it has the lowest damping ratio. Regarding inter-area mode 1, generators of the South of Norway (named group 1 in Fig. 5.14) are oscillating against most of the remaining generators of the system.

Table 5.4: Electromechanical modes of Nordic 44 system with low damping ratio.

| | AC base case | |
|---|---|---|
| N0. | $\zeta$ (%) | Freq. (Hz) |
| 1 | 1.85 | 0.39 |
| 2 | 5.45 | 0.83 |
| 3 | 12.22 | 0.54 |
| 4 | 12.11 | 0.75 |
| 5 | 11.68 | 0.88 |
| 6 | 13.12 | 0.98 |
| 7 | 12.12 | 1.07 |
| 8 | 13.57 | 1.23 |
| 9 | 15.69 | 1.10 |
| 10 | 15.17 | 1.88 |
| 11 | 16.69 | 1.77 |

The proposed algorithm is implemented in Matlab+SSST. This tool is used, because the information needed for the implementation of the algorithm

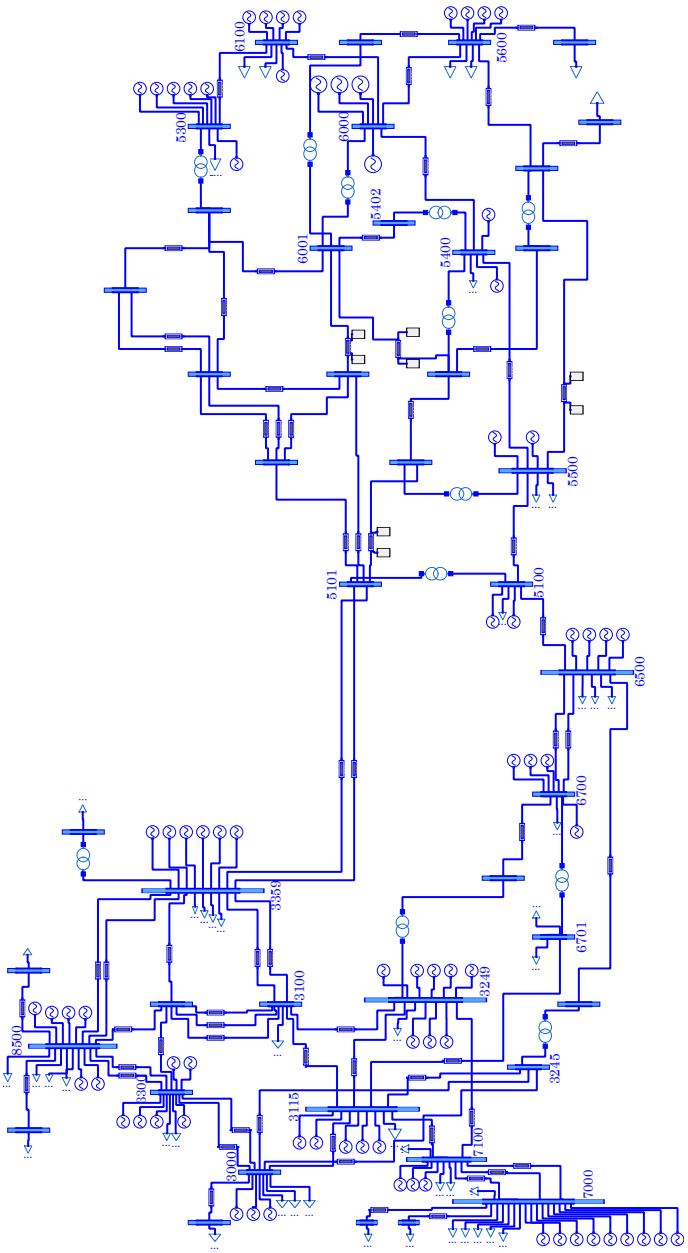


Figure 5.13: Nordic 44 test system under Dymola.

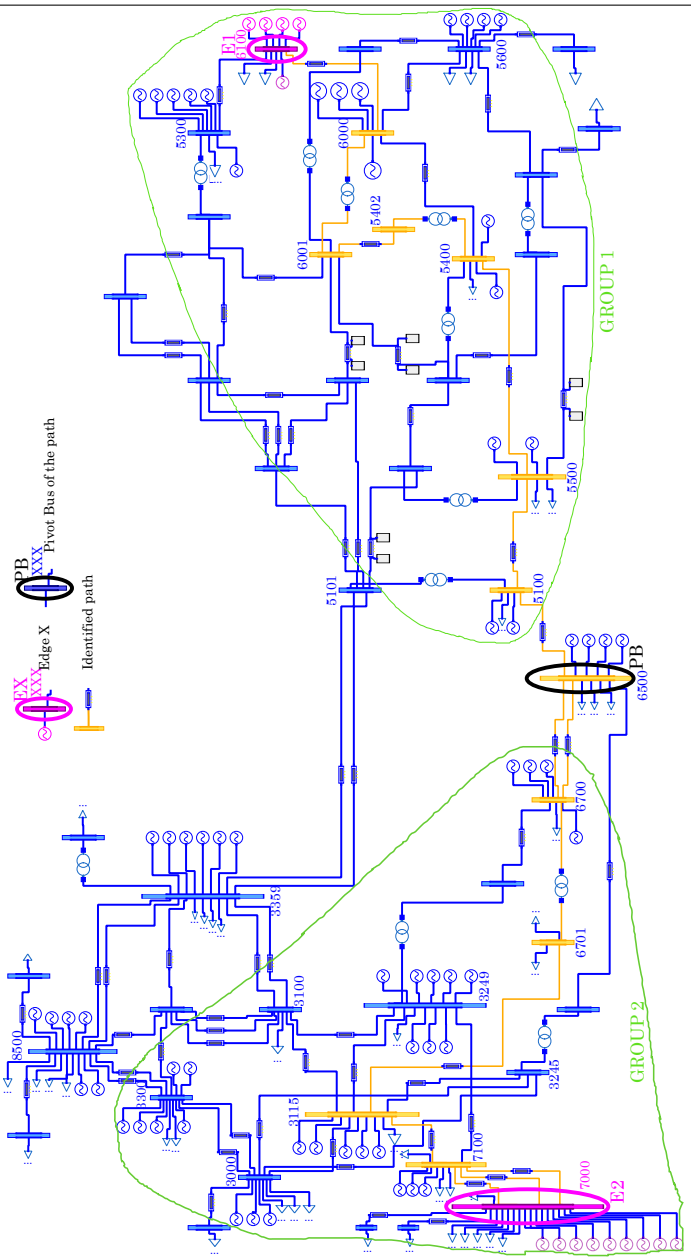


Figure 5.14: Nordic 44 test system under Dymola with the identified inter-area electromechanical oscillation path.

(e.g., mode shapes and observability factors) is not provided by the linearised model of OpenIPSL.

Since the toolbox SSST does not accept more than one generator connected to a bus, generators on the same bus in the original system have been aggregated into a single unit. Likewise, if a pair of buses were connected by more than one circuit (e.g. buses 7100 and 7000 of Fig. 5.13), this circuits were aggregated into a single line, before running the algorithm.

**Step 1: Identification of the path edges**

Fig. 5.15 shows the generator mode shapes of the system.

The first edge of the inter-area-oscillation path is bus 6100 (E1=6100). The coherent generators of this group are 6100, 5300, 5600, 6000, 5400, 5500 and 5100. The second edge of the inter-area-oscillation path is bus 7000 (E2=7000). The coherent generators of this group are 7000, 7100, 3249, 3115, 6700, 3000, 3245 and 3300.

Note that generators 6500, 8500 and 3359 have not been identified as being in one of the two groups.

In Fig. 5.14, generators 3359 and 7000 (the path edges) are coloured in pink, the groups of generators are encircled in green.

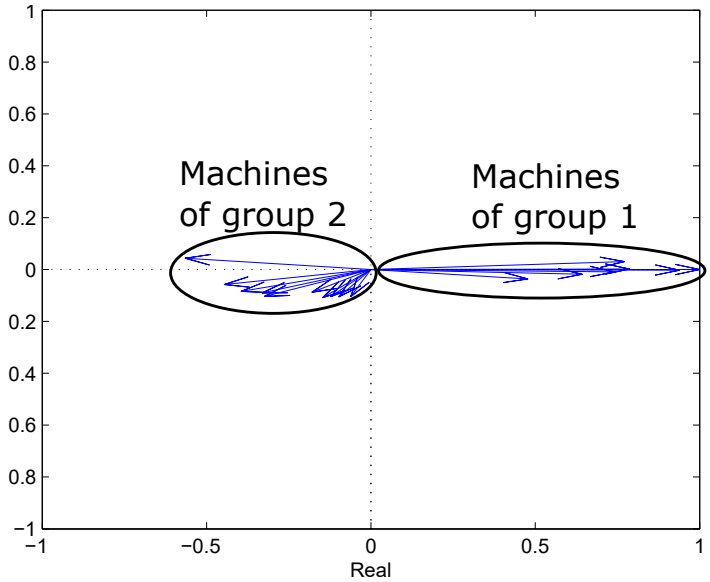


Figure 5.15: Mode shape of the Nordic 44 test system in mode 1.

**Step 2: Identification of the dominant inter-area oscillation path between the two edges**

The identified path (coloured in orange in Fig. 5.14) consists of buses 6100 (E1), 6000, 6001, 5402, 5400, 5500, 5100, 6500, 6700, 6701, 3115, 7100, 7000 (E2).

Bus 6500 was identified as the pivot bus of the oscillation path ($PB = 35$) and bus 6700 was identified as the first bus of the ascending sub-path ($A = 40$).

Fig. 5.16 and Table 5.5 show the bus-frequency observability factors along this oscillation path and confirms the observations made in the Section 5.3. Fig. 5.17 and Table 5.6 shows the branch-current observability factors along this path.

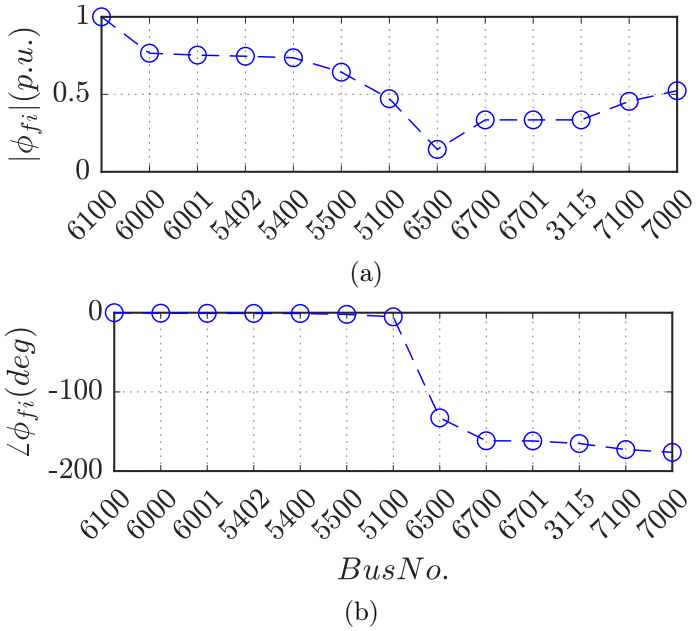


Figure 5.16: Bus-frequency observability factor along the dominant oscillation path in the Nordic 44 test system: (a) magnitude and (b) phase.

Table 5.5: Bus-frequency observability factor along the dominant oscillation path in the Nordic 44 test system.

| Bus No. | $\lvert\phi_{fi}\rvert(p.u.)$ | $\angle\phi_{fi}(deg)$ |
|---|---|---|
| 6100 | 1.00 | 0.0 |
| 6000 | 0.77 | -0.6 |
| 6001 | 0.75 | -0.8 |
| 5402 | 0.75 | -0.9 |
| 5400 | 0.74 | -1.0 |
| 5500 | 0.64 | -2.1 |
| 5100 | 0.47 | -5.2 |
| 6500 | 0.14 | -132.8 |
| 6700 | 0.33 | -161.7 |
| 6701 | 0.33 | -161.9 |
| 3115 | 0.33 | -165.2 |
| 7100 | 0.45 | -172.8 |
| 7000 | 0.52 | -176.3 |

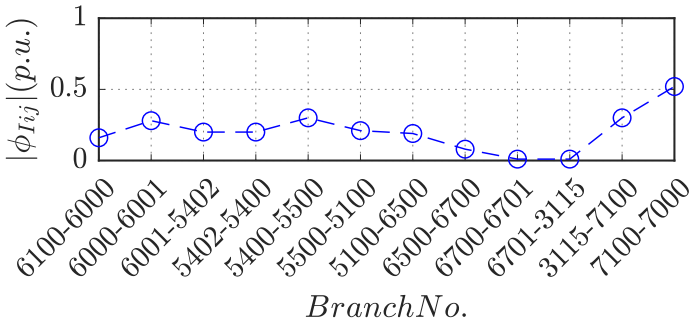


Figure 5.17: Magnitude of branch-current observability factor along the dominant oscillation path in the Nordic 44 test system.

Table 5.6: Branch-current observability factor along the dominant oscillation path in the Nordic 44 test system.

| From Bus | To Bus | $\lvert\phi_{Iij}\rvert(p.u.)$ | $\angle\phi_{Sij}(deg)$ |
|---|---|---|---|
| 6000 | 6100 | 0.16 | -33.5 |
| 6000 | 6001 | 0.28 | -27.6 |
| 5402 | 6001 | 0.20 | -29.1 |
| 5400 | 5402 | 0.20 | -29.1 |
| 5400 | 5500 | 0.30 | -29.6 |
| 5100 | 5500 | 0.21 | -29.6 |
| 5100 | 6500 | 0.19 | -29.8 |
| 6500 | 6700 | 0.08 | 144.6 |
| 6700 | 6701 | 0.01 | 60.4 |
| 3115 | 6701 | 0.01 | 60.6 |
| 3115 | 7100 | 0.30 | 132.3 |
| 7000 | 7100 | 0.52 | 124.8 |

## 5.7 Validation of the algorithm

The path given by the algorithm fully corresponds to the definition of Section 5.3. However, it cannot be said that this path is "the main path" of the oscillation. In fact, the definition does not provide any metric to say whether a given dominant oscillation path is better than any other dominant oscillation path. Thus, we propose to validate it by dynamic simulation (Section 5.7.1) and by showing that the path identified by the algorithm is a better choice than an oscillation path selected arbitrarily (Section 5.7.2).

### 5.7.1 Dynamic simulation

In order to validate the inter-area oscillation path identified by the algorithm, we simulated the loss of line 3249-7100. The fault occurs at $t = 1$ s.

Fig. 5.18 shows the frequency of representative generators along the path (the generators edges, the pivot bus and two generators in between) after the fault.

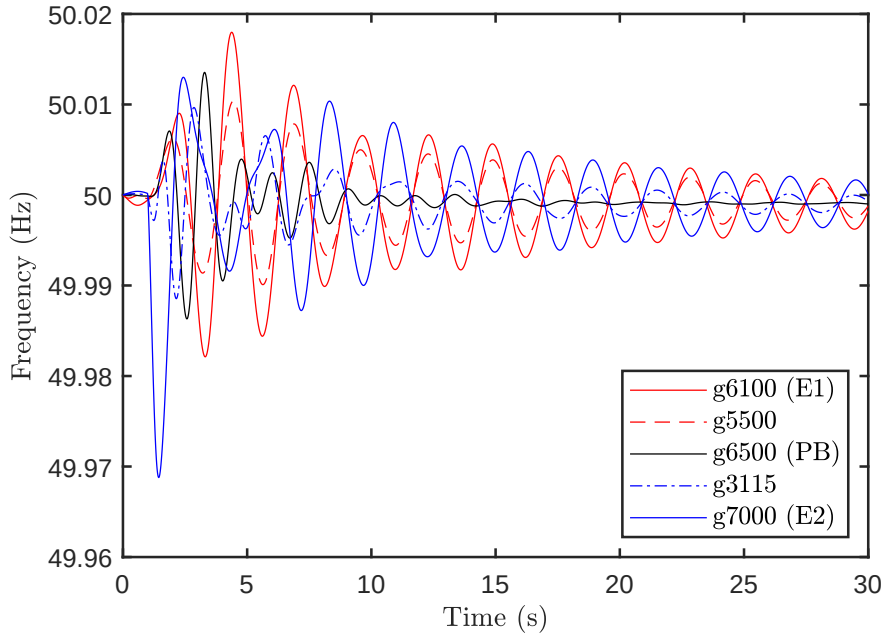


Figure 5.18: Frequency of representative generators along the identified path after the loss of line 3249-7100.

As the information on the magnitude of bus-frequency observability factor suggested (Fig. 5.16a), the generators with the largest oscillations are those at the edges of the path (generators 6100 and 7000) while the pivot bus barely oscillates (generator 6500) and the other generators have an intermediate oscillation.

Additionally, as the information on the phase of bus-frequency observability factor suggested (Fig. 5.16b), the generators at the two sides of the pivot bus oscillate against each others (generators 6100 and 5500 against generators 3115 and 7000).

### 5.7.2 Arbitrary path

We propose to compare the path given by the algorithm to a path chosen arbitrarily. To be a dominant path of the oscillation it must naturally link the two edges: buses 6100 and 7000. The selected arbitrary path consist of buses: 6100, 5300, 5301, 5304, 5103, 5102, 6001, 6000, 5600, 5603, 5500, 5100, 6500, 3244, 3245, 3000, 3300, 3200, 3359, 3100, 3115, 7100, 7000 (E2). This path has been highlighted in green in Fig. 5.19.

Fig. 5.20 and Table 5.7 show the bus-frequency observability factors along this path. The information present in the figure and the table can be summarised as follows:

- Bus 3359 is the one with the bus-frequency observability factor $|\phi_{f_i}|$ of the smallest magnitude (Fig. 5.20a), and thus is the pivot bus of the path.
- However, it does not divide the path into two groups with opposite phases in the bus-frequency observability factors $\phi_{f_i}$ (Fig. 5.20b).
- Additionally, $|\phi_{f_i}|$ does not show a constant increase between bus 3359 and bus 6100 (E1).

Thus it can be said that this path is not a dominant oscillation path as it does not fit to the definition of Section 5.3.

Fig. 5.21 and Table 5.8 show the branch-current observability factors along this path. The average of the magnitude of the branch-current observability factor $|\phi_{I_{ij}}|$ for the arbitrarily selected case (0.19 pu) is smaller than for the path found by the algorithm (0.21 pu). This shows that the algorithm proposed makes a better choice and, overall, maximises the value of $|\phi_{I_{ij}}|$ across the path selected.

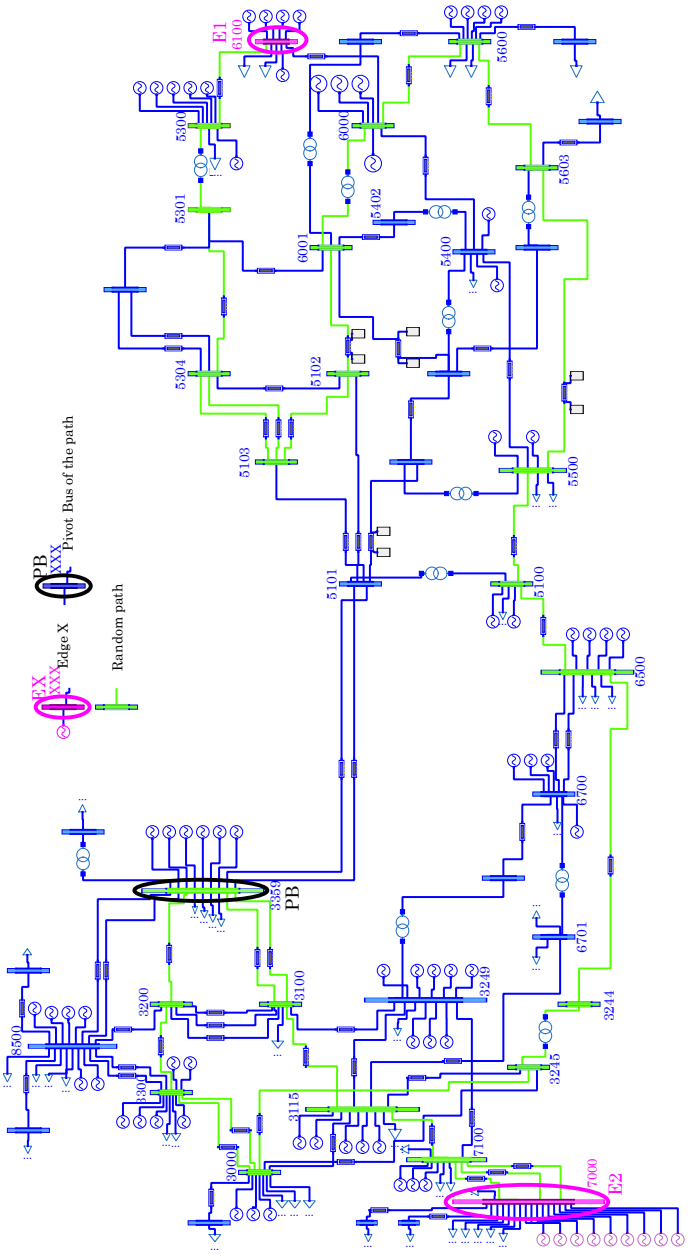


Figure 5.19: Nordic 44 test system under Dymola with the selected arbitrary inter-area electromechanical oscillation path.

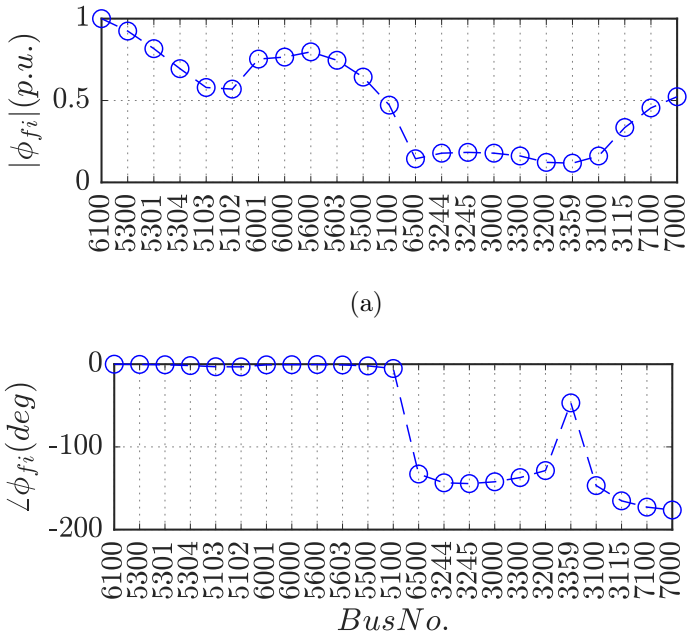


(a)




(b)

Figure 5.20: Bus-frequency observability factor along an arbitrary path in the Nordic 44 test system: (a) magnitude and (b) phase.

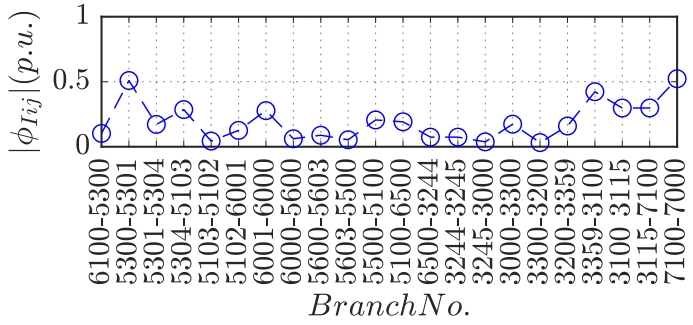


Figure 5.21: Magnitude of branch-current observability factor along an arbitrary path in the Nordic 44 test system.

Table 5.7: Bus-frequency observability factor along an arbitrary path in the Nordic 44 test system.

| Bus No. | $\|\phi_{fi}\|(p.u.)$ | $\angle\phi_{fi}(deg)$ |
|---|---|---|
| 6100 | 1.00 | 0.0 |
| 5300 | 0.92 | -0.3 |
| 5301 | 0.82 | -0.7 |
| 5304 | 0.69 | -1.7 |
| 5103 | 0.58 | -3.1 |
| 5102 | 0.57 | -3.2 |
| 6001 | 0.75 | -0.8 |
| 6000 | 0.77 | -0.6 |
| 5600 | 0.80 | -0.4 |
| 5603 | 0.75 | -0.9 |
| 5500 | 0.64 | -2.1 |
| 5100 | 0.47 | -5.2 |
| 6500 | 0.14 | -132.8 |
| 3244 | 0.18 | -143.4 |
| 3245 | 0.18 | -144.4 |
| 3000 | 0.18 | -142.2 |
| 3300 | 0.16 | -137.1 |
| 3200 | 0.12 | -128.6 |
| 3359 | 0.12 | -46.8 |
| 3100 | 0.16 | -146.8 |
| 3115 | 0.33 | -165.2 |
| 7100 | 0.45 | -172.8 |
| 7000 | 0.52 | -176.3 |

Table 5.8: Branch-current observability factor along an arbitrary path in the Nordic 44 test system.

| From Bus | To Bus | $\|\phi_{Iij}\|(p.u.)$ | $\angle\phi_{Sij}(deg)$ |
|---|---|---|---|
| 5300 | 6100 | 0.10 | -31.2 |
| 5300 | 5301 | 0.51 | -32.0 |
| 5301 | 5304 | 0.17 | -30.9 |
| 5103 | 5304 | 0.29 | -30.2 |
| 5102 | 5103 | 0.04 | -31.5 |
| 5102 | 6001 | 0.13 | -30.1 |
| 6000 | 6001 | 0.28 | -27.6 |
| 5600 | 6000 | 0.06 | 150.0 |
| 5600 | 5603 | 0.09 | 151.3 |
| 5500 | 5603 | 0.05 | -30.2 |
| 5100 | 5500 | 0.21 | -29.6 |
| 5100 | 6500 | 0.19 | -29.8 |
| 3244 | 6500 | 0.07 | 146.1 |
| 3244 | 3245 | 0.07 | 146.1 |
| 3000 | 3245 | 0.04 | -51.3 |
| 3000 | 3300 | 0.17 | -36.1 |
| 3200 | 3300 | 0.03 | 164.8 |
| 3200 | 3359 | 0.16 | 149.1 |
| 3100 | 3359 | 0.42 | 145.0 |
| 3100 | 3115 | 0.30 | 143.2 |
| 3115 | 7100 | 0.30 | 132.3 |
| 7000 | 7100 | 0.52 | 124.8 |

## 5.8 Summary and conclusions

In this chapter, the concept of dominant inter-area oscillation path in an AC power system has been defined and explained using a simple 6-generator test system. Furthermore, an algorithm for the identification of the dominant inter-area oscillation path has been proposed in this chapter.

The following conclusions have been obtained from the results presented in this chapter:

- The use of different observability factor (bus-frequency, bus-voltage and branch-current) has been discussed. Bus-frequency and branch-current observability factors proved to be useful to characterise the dominant inter-area oscillation path. However, the use of bus-voltage observability factor has been discarded since the information it contains is not consistent in relation to the dominant inter-area oscillation path.
- An algorithm for the detection of the dominant inter-area oscillation path has been proposed and explained in detail. Noticeably, the algorithm is fully automated and obtains the desired path systematically.
- The algorithm has been tested on the Nordic 44 test system. The resulting path does fit nicely the definition of the dominant oscillation path.
- The resulting path has been shown to be better than an arbitrary path between the two same edges since this arbitrary path does not fit the definition of the dominant inter-area oscillation path.
- The proposed algorithm for the identification of the dominant inter-area oscillation path will be used for DC segmentation (Chapter 6). Nevertheless, it should be highlighted that the algorithm proposed in this chapter could be used for other applications.

# Chapter 6

# Proposed algorithm for DC segmentation to mitigate electromechanical oscillations

## 6.1 Introduction

As discussed in Chapter 2, no work proposes a method to select adapted DC segmentation boundaries for a given system. This chapter aims at filling this void by proposing a systematic algorithm for DC segmentation of power systems to improve small-signal angle stability (electromechanical oscillations). Indeed, Chapter 4 has shown that DC segmentation structurally stops the electromechanical oscillations between different AC clusters of the system, thus a well selected DC segmentation could stop a targeted inter-area mode. More precisely, this chapter proposes an algorithm that, for a given AC power system, gives a DC-segmentation solution to improve electromechanical oscillation damping. The algorithm relies on separating the groups of generators oscillating against each other using the mode shapes of the system. The exact boundaries of the clusters are then identified using the concept of dominant inter-area oscillation path, presented in Chapter 5. Finally, the algorithm selects the AC lines to be replaced by VSC-HVDC links, leading to a DC-segmented system with asynchronous AC clusters. Notice that the necessary previous steps, i.e., the identification of the oscillating generators and of the dominant inter-area oscillation path were already discussed in Chapter 5.

This chapter is organised as follows. Section 6.2 studies different placements of DC segmentation on a simple 6-generator test system along its

dominant inter-area oscillation path. The algorithm for DC segmentation of power system is explained in Section 6.3. It is then applied to the Nordic 44 test system in Section 6.4 and the results are described in Section 6.5. Finally, Section 6.6 concludes the chapter.

## 6.2 DC-segmentation of the 6-generator system

Once the dominant inter-area oscillation path has been determined (see Chapter 5), the place where to break it with a DC segment (with VSC-HVDC technology), in order to suppress the critical inter-area mode needs to be investigated.

Let's consider again the two-area 6-generator system shown in Fig. 6.1 (test system 1). The study carried out in Chapter 5 has shown that:

- It has an inter-area mode with a damping coefficient of 5.5% and a frequency of 0.83 Hz (all system modes are included in Table 6.1).
- The first edge of the inter-area oscillation path is bus 1 (E1=1). The coherent generators of this group are generators G1, G2 and G3.
- The second edge of the inter-area oscillation path is bus 6 (E2=6). The coherent generators of this group are generators G4, G5 and G6.
- The propagation path is 1-10-20-30-35-40-50-60-6.
- Bus 35 is the pivot bus of the path ($PB = 35$).

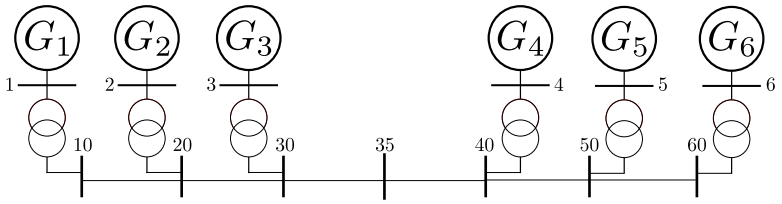


Figure 6.1: Test system 1: Conceptual 6-generator system.

Let us consider two DC segmentation alternatives of our system:

- DC-segmentation 1: Line 35-40 is replaced by a VSC-HVDC link (Fig. 6.2) with parameters as in Section B.3 of the Appendix.

Table 6.1: Test system 1: Electromechanical modes.

| Mode | Real | Imag | $\zeta$ (%) | Freq. (Hz) | Oscillation |
|---|---|---|---|---|---|
| 1 | -0.29 | 5.23 | 5.5 | 0.83 | G1,G2,G3//G4,G5,G6 |
| 2 | -1.17 | 6.35 | 18.1 | 1.03 | G4,G3//G6,G1 |
| 3 | -1.22 | 6.48 | 18.5 | 1.05 | G3,G6//G1,G4,G5 |
| 4 | -1.25 | 6.60 | 18.6 | 1.07 | G2//G1 |
| 5 | -1.27 | 6.51 | 19.2 | 1.06 | G5//G4,G6 |

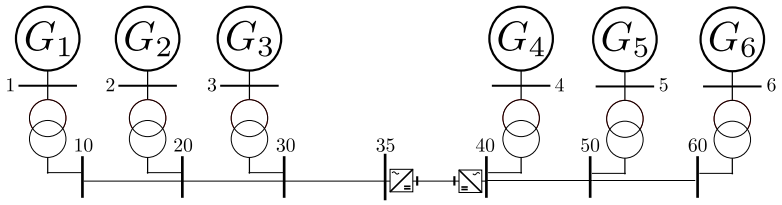


Figure 6.2: Test system 1-DC 1:6-generator system with DC segmentation 1.

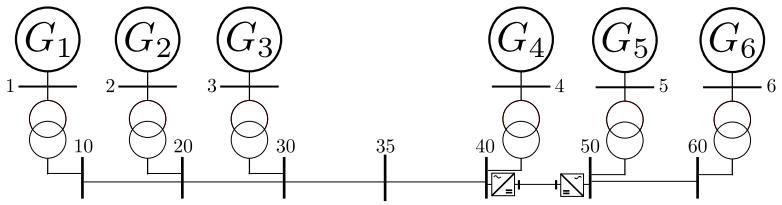


Figure 6.3: Test system 1-DC 2: 6-generator system with DC segmentation 2.

- DC-segmentation 2: Line 40-50 is replaced by a VSC-HVDC link (Fig. 6.3) with the same parameters as in the previous case.

Details of the models can be found in Appendix B of the Appendix.

A small-signal analysis of the system of Fig. 6.2 gives the electromechanical modes in Table 6.2(a). Results show that the critical inter-area mode has disappeared (compare with Table 5.1) while the remaining four electromechanical modes have similar damping ratios and frequencies to those of the AC case (Table 5.1). Hence, DC segmentation case 1 improves inter-area oscillation damping, significantly.

Table 6.2(b) shows the electromechanical modes DC segmentation case 2. This time, a lightly-damped inter-area mode 1 (G1, G2 and G3 oscillating against G4) is still present and, although its damping has improved with

respect to the most problematic one in Table 5.1, it is still worrying. The remaining three local modes have similar damping ratios and frequencies to those in the AC case (Table 5.1). This time the improvement with DC segmentation is not as noticeable as before due to the fact that the DC link has been moved away from the pivot bus of the dominant inter-area oscillation path.

Thus, a DC-segmentation closer to the pivot bus of the path will be more efficient to stop the targeted inter-area electromechanical oscillation.

Table 6.2: Electromechanical modes of the 6-generator system with DC segmentation

| (a) DC-segmented at line 35-40 | | | | | |
|---|---|---|---|---|---|
| Mode | Real | Imag | $\zeta$ (%) | Freq. (Hz) | Oscillation |
| 1 | -1.17 | 6.32 | 18.3 | 1.02 | G4//G6 |
| 2 | -1.21 | 6.43 | 18.5 | 1.04 | G3//G1 |
| 3 | -1.25 | 6.60 | 18.6 | 1.07 | G2//G1,G3 |
| 4 | -1.27 | 6.51 | 19.2 | 1.06 | G5//G4,G6 |
| (b) DC-segmented at line 40-50 | | | | | |
| Mode | Real | Imag | $\zeta$ (%) | Freq. (Hz) | Oscillation |
| 1 | -0.46 | 6.02 | 7.7 | 0.96 | G4//G1,G2,G3 |
| 2 | -1.20 | 6.47 | 18.3 | 1.05 | G3//G1,G4 |
| 3 | -1.24 | 6.58 | 18.5 | 1.07 | G1//G2 |
| 4 | -1.25 | 6.56 | 18.7 | 1.06 | G5//G6 |

## 6.3 Proposed algorithm for DC segmentation

The philosophy of the proposed algorithm is illustrated first with a very simple power system. Fig. 6.4-a shows a schematic diagram of an AC power system and Fig. 6.4-b shows the power system after DC segmentation, where the AC interconnection line has been replaced by a VSC-HVDC link, decoupling the two remaining AC systems. It is assumed that the original AC power system has a critical inter-area oscillation, involving AC areas 1 and 2. The objective is to segment the system with VSC-HVDC links and eliminate the critical inter-area oscillation, as was discussed in the previous section. However, in meshed AC power systems, the choices for DC segmentation for this purpose are not as simple as in the example of Fig. 6.4. Therefore, an algorithm for DC segmentation is needed, and is presented below.

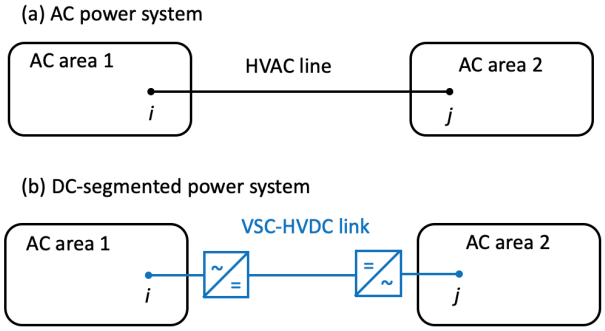


Figure 6.4: (a) AC power system and (b) DC-segmented power system.

A meshed AC power system with a critical inter-area mode (with low damping ratio) is considered. The objective of the proposed algorithm is to systematically find a DC segmentation configuration in order to suppress a critical inter-area mode.

A linearised small-signal model of the power system is used to identify the target inter-area mode ($\lambda_{k_{crit}}$) (i.e. the critical inter-area mode, with the lowest damping ratio). The proposed algorithm for DC segmentation consists of four steps:

- **Step 1**: Identification of the edges of the inter-area oscillation path.
- **Step 2**: Identification of the dominant inter-area oscillation path between the two edges.
- **Step 3**: Selection of the AC line to be converted into DC.
- **Step 4**: Check if the present configuration divides the original AC system into two asynchronous AC areas (one for each of the edges).

  (*) If this occurs, the algorithm stops. Otherwise, return to step 2.

  Once the algorithm stops, each AC line selected for DC segmentation will be replaced by a VSC-HVDC link.

Fig. 6.5 depicts a flowchart of the algorithm. Steps 1 and 2 constitute the algorithm for the identification of the inter-area oscillation path presented in Chapter 5.

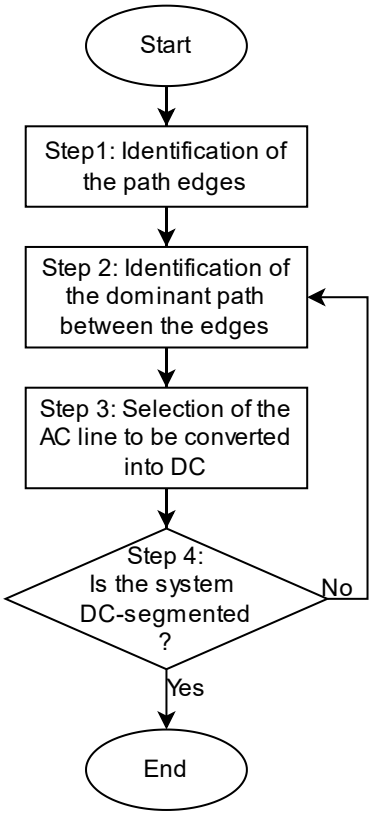


Figure 6.5: Flowchart of the algorithm for the DC segmentation of power systems.

The algorithm will use the information provided by the modal analysis of the linearised model of the power system which has to be executed only once at the beginning (it is not repeated at every iteration of the loop). Hence, the computational burden of the algorithm is low. The algorithm uses the following information:

- Mode shapes of the target inter-area mode participating in the speeds of the generators ($v_{i,k_{crit}}$).
- Frequency observability factors of the target inter-area mode of all buses ($\phi_{f_{i,k_{crit}}}$).

- Magnitude ($|\phi_{I_{ij},k_{crit}}|$) of the current observability factors of the target inter-area mode of all branches ($\phi_{I_{ij},k_{crit}}$).

For the sake of clarity, the sub-index of the target inter-area mode will be removed from the indicators above in the future (i.e., $\phi_{f_i}$ will be used instead of $\phi_{f_{i,k_{crit}}}$).

### 6.3.1 Step 1: Identification of the edges of inter-area oscillation path

This step has been described in the previous chapter in Section 5.5.1. It consists in finding the two edge buses of the path (i.e., $E1$ and $E2$).

### 6.3.2 Step 2: Identification of the dominant inter-area oscillation path between the two edges

This step has been described in the previous chapter in Section 5.5.2. It consists in finding the buses that form the oscillation path and thus link the two edges $E1$ and $E2$.

In order to take into account the lines selected for DC segmentation in a potential previous iteration of step 3, a new set must be defined:

- $A_{DC,segs}$ is the set of branches of the system ($L_{ij}$) that have been selected for DC segmentation during the execution of the algorithm. This set is empty when the algorithm starts.

Before starting step 2 as defined in Section 5.5.2, the AC branches that have been selected to be replaced by DC segments ($L_{ij} \in A_{DC,segs}$) must be included into the set of the branches excluded from path-$ip$ ($A_{EX,ip}$).

### 6.3.3 Step 3: Selection of the AC line to be converted into DC.

Once the dominant inter-area oscillation path has been identified, the next step is to select the AC line that will be replaced by a VSC-HVDC link, eventually. As discussed in Section 6.2, DC segmentation is more effective when placed close to the centre of the dominant inter-area oscillation path. Therefore, the two lines of the path connected to the $PB$ would be the ideal candidates for segmentation. Of this two lines, the one with the highest value of the magnitude of the branch-current observability factor is selected, since it is the one with the most intense inter-area oscillation. The selected AC line, is then included into set $A_{DC,segs}$.

### 6.3.4 Step 4: Is the system DC-segmented?

Each iteration of the algorithm (Steps 2 and 3) determines a path of the target inter-area oscillation (path $ip$) and the AC branch to be replaced by a DC segment. This does not guarantee dividing the system into two asynchronous areas, as the DC segments could contain parallel AC paths. Step 4 scans the grid looking for a continuous connection between E1 and E2 through an AC path. If an AC connection is found, the algorithm goes back to Step 2 and repeats the process until no such connection is found and the algorithm can be terminated.

Once the algorithm has stopped, each AC line selected for DC segmentation ($L_{ij} \in A_{DC,segs}$) is replaced with a VSC-HVDC link with the same nominal apparent power.

### 6.3.5 Illustrative example

The proposed algorithm is now illustrated in the 6-generator system of Fig. 6.1 (test system 1). Although it is a simple power system with radial configuration, it will help to understand the proposed algorithm. The algorithm has been implemented in Matlab and linked with a tool box for small-signal stability analysis (SSST) [118].

The results of the algorithm when applied to test system 1 (Fig. 6.1) can be summarised as follows:

1. **Step 1**: As stated in Section 5.5.3, the edges of the path are bus 1 (E1=1) and bus 6 (E2=6).

2. **Step 2**: As stated in Section 5.5.3, the propagation path is 1-10-20-30-35-40-50-60-6.

3. **Step 3**: AC line 35-40 is selected for DC segmentation.

4. **Step 4**: The system has been divided into two asynchronous areas and the segmentation algorithm stops.Finally, line 35-40 is replaced by a VSC-HVDC link with the same nominal apparent power as the AC line replaced.

Notice that the DC-segmentation obtained here is the one of Fig. 6.2 which succeeded in suppressing the critical inter-area mode, as shown in Section 6.2.

## 6.4 Application of DC-segmentation algorithm to the Nordic 44 test system

The proposed algorithm has also been applied to the Nordic 44 test system (Fig. 6.6) which is a representation of the interconnected grids of Norway, Sweden and Finland. The information about the model and the scenario considered is provided in Section C.1 of the Appendix.

The result of the algorithm applied to the Nordic 44 system is depicted in Fig. 6.7 (see Section C.1 of the Appendix). All generators, buses and lines of interest for the discussion that follows are presented in colours (namely pink, yellow and green).

Table 6.3 shows the poorly damped electromechanical modes of Nordic 44 test system, (damping ratio under 20%). They have been obtained with OpenIPSL. Mode 1 (damping of 1.85% and frequency of 0.39 Hz) is selected as the target inter-area mode for the DC-segmentation algorithm because it has the lowest damping ratio. Regarding inter-area mode 1, generators of the South of Norway (named region 1 in Fig. 6.7) are oscillating against most of the remaining generators of the system.

Table 6.3: Electromechanical modes of Nordic 44 system with low damping ratio.

| | AC base case | |
|---|---|---|
| N0. | $\zeta$ (%) | Freq. (Hz) |
| 1 | 1.85 | 0.39 |
| 2 | 5.45 | 0.83 |
| 3 | 12.22 | 0.54 |
| 4 | 12.11 | 0.75 |
| 5 | 11.68 | 0.88 |
| 6 | 13.12 | 0.98 |
| 7 | 12.12 | 1.07 |
| 8 | 13.57 | 1.23 |
| 9 | 15.69 | 1.10 |
| 10 | 15.17 | 1.88 |
| 11 | 16.69 | 1.77 |

The proposed algorithm was implemented in Matlab+SSST. This tool was used, because the information needed for the implementation of the algorithm (e.g., mode shapes and observability factors) is not provided by the linearised model of OpenIPSL.

Since the toolbox SSST does not accept more than one generator con-

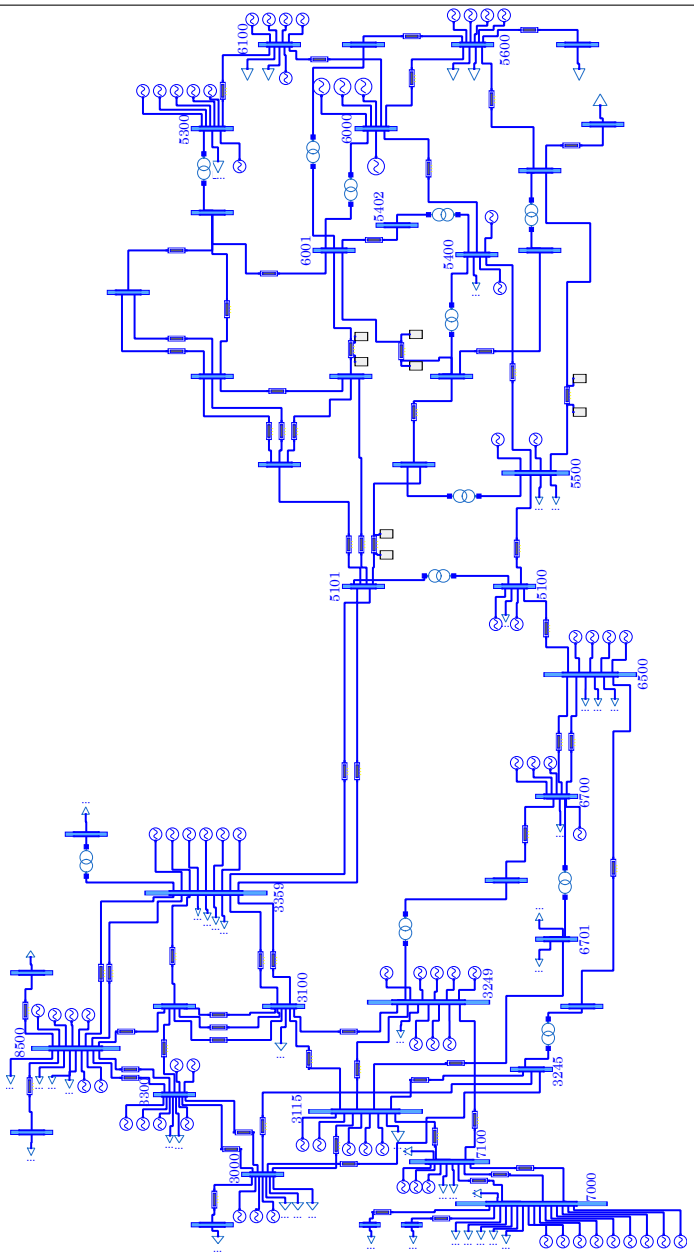


Figure 6.6: Nordic 44 test system under Dymola.

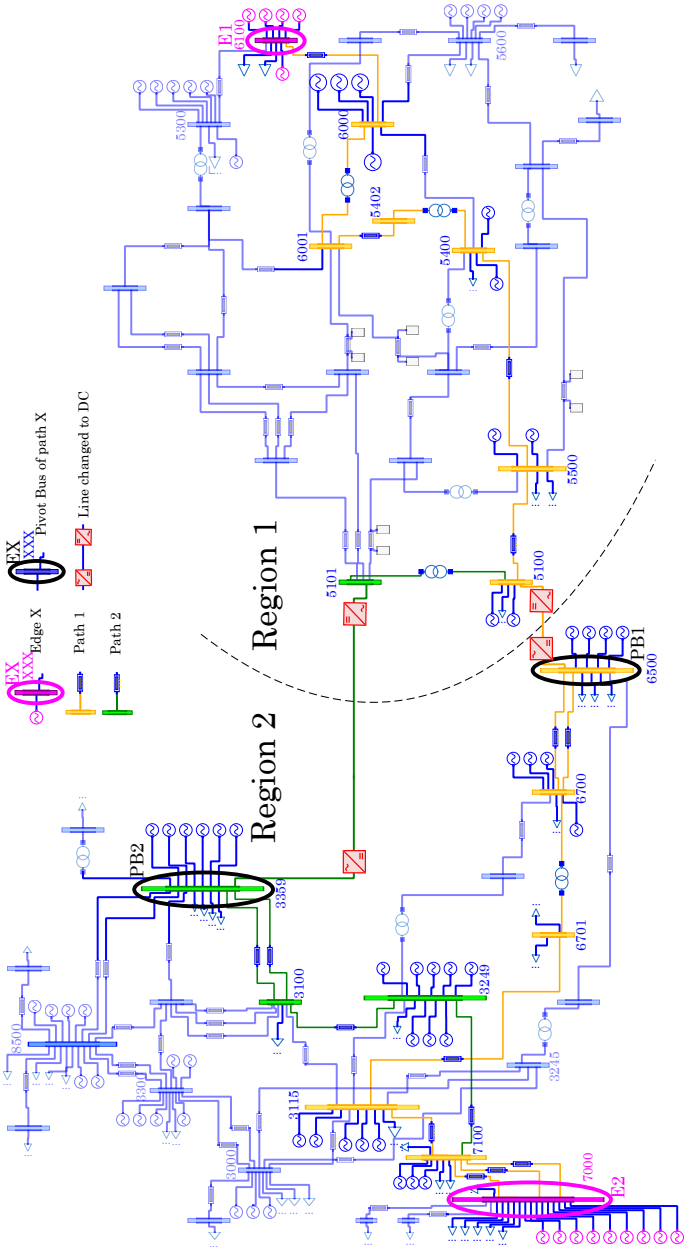


Figure 6.7: DC-segmented Nordic 44 test system under Dymola with identified path.

nected to a bus, generators on the same bus in the original system have been aggregated into a single unit. Likewise, if a pair of buses were connected by more than one circuit (e.g. buses 7100 and 7000 of Fig. 6.6), this circuits were aggregated into a single line, before running the algorithm.

**Step 1: Identification of the path edges**

As stated in Section 5.6:

- The first edge of the inter-area oscillation path is bus 6100 (E1=6100). The coherent generators of this group are 6100, 5300, 5600, 6000, 5400, 5500 and 5100.
- The second edge of the inter-area oscillation path is bus 7000 (E2=7000). The coherent generators of this group are 7000, 7100, 3249, 3115, 6700, 3000, 3245 and 3300.

In Fig. 6.7, generators 6100 and 7000 (the path edges) are coloured in pink, group 1 corresponds to the generators of region 1 while group 2 corresponds to the generators of region 2 (with the exception of generators 6500, 8500 and 3359 that are not in any of those groups).

**Step 2, 3 and 4 first iteration: identification and breaking of the first dominant inter-area path**

**Step 2**: As stated in Section 5.6, the identified path (coloured in orange in Fig. 6.7) consists of buses 6100 (E1), 6000, 6001, 5402, 5400, 5500, 5100, 6500, 6700, 6701, 3115, 7100, 7000 (E2).

Bus 6500 was identified as the pivot bus of the path ($PB = 6500$) and bus 6700 was identified as the first bus of the ascending sub-path ($A = 6700$).

Fig. 6.8 shows the bus frequency observability factors along this path. Fig. 6.9 shows the branch current observability factors along this path.

**Step 3**: Line 5100-6500 is selected for DC segmentation.

**Step 4**: With the first DC segment, the system is not divided into two asynchronous AC systems. Thus, the algorithm goes back to step 2.

**Step 2, 3 and 4 second iteration: identification and breaking of the second dominant inter-area path**

**Step 2**: The identified path comprises buses 6100 (E1), 6000, 6001, 5402, 5400, 5500, 5100, 5101, 3359, 3100, 3249, 7100, 7000 (E1). Several buses are

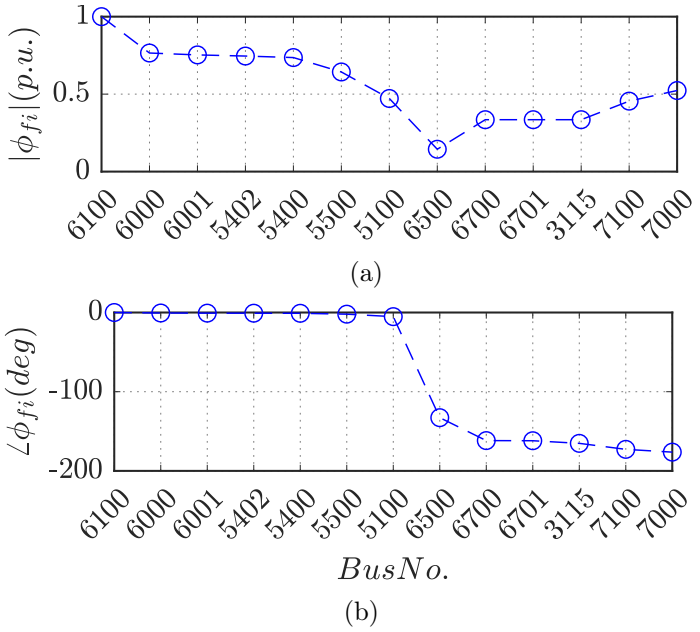


Figure 6.8: Bus frequency observability factor along the first dominant path (path 2) in the Nordic 44 test system: (a) magnitude and (b) phase.

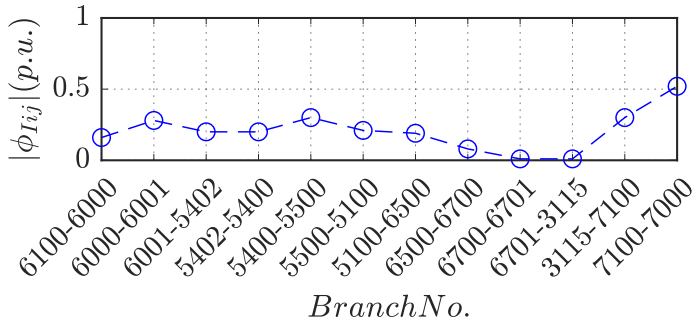


Figure 6.9: Magnitude of branch current observability factor along the first dominant path (path 1) in the Nordic 44 test system.

also in the previous path. In Fig. 6.7, the part of path 2 that differs from path 1 is coloured in green.

Bus 3359 was identified as the pivot bus of the path ($PB = 35$), and bus 3100 was identified as the first bus of the ascending sub-path ($A = 40$).

Fig. 6.10 shows the bus frequency observability factors along this path

and confirms the observations made in the Section 5.3. Fig. 6.11 shows the branch current observability factors along this path.

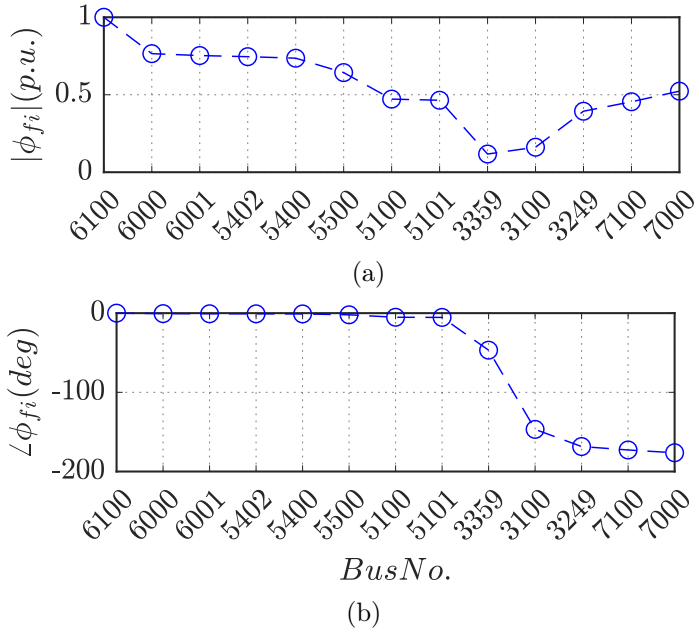


Figure 6.10: Bus frequency observability factor along the second dominant path (path 2) in the Nordic 44 test system: (a) magnitude and (b) phase.

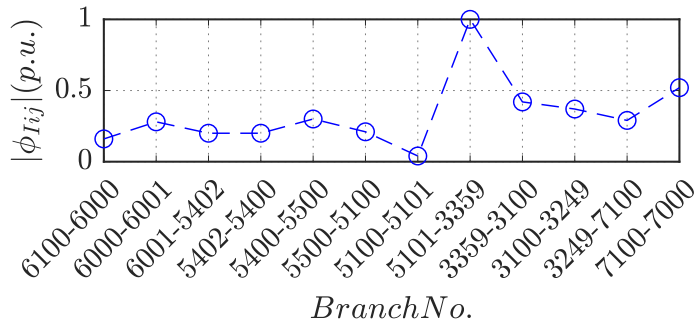


Figure 6.11: Magnitude of branch current observability factor along the second dominant path (path 2) in the Nordic 44 test system.

**Step 3**: Line 3359-5101 is selected for DC segmentation.
**Step 4**: The system has now been split into two AC areas.

#### Algorithm termination

Lines 5100-6500 and 3359-5101 were replaced by VSC-HVDCs links of the same capacity: 800 MVA (path 1) and 3500 MVA (path 2), to complete DC-segmentation.

The original AC system was split in two AC clusters, one with all the generators of group 1 and another one with all the generators of group 2 (regions 1 and 2, respectively, in Fig. 6.7).

## 6.5 Validation of the algorithm

The effects of the DC-segmentation proposed were investigated using Dymola [114]. VSC-HVDC links were modelled as proposed in Section 3.3 and models were implemented in Modelica language to be tested in combination with the OpenIPSL library [92]. Two cases were compared:

- AC-base case: The initial Nordic 44 system in Fig. 6.6.
- DC-segmented case: The DC-segmented system in Fig. 6.7 obtained with the proposed algorithm, where AC lines 5100-6500 and 3359-5101 were replaced by VSC-HVDC links.

Details of the two cases can be found in Section C.1 and C.2 of Appendix C.

For the DC-segmented case, the operating point considered of the VSC-HVDC links is when they transmit the same active-power as the AC lines in the AC-base case, while reactive power injections equal zero at both converter stations on both links:

- VSC-HVDC link A (VSC A1 at bus 5101, VSC A2 at bus 3359): Active power of 1548 MW from VSC A1 to VSC A2.
- VSC-HVDC link B (VSC B1 at bus 5100, VSC B2 at bus 6500): Active power of 447 MW from VSC B1 to VSC B2.

The two scenarios have been compared by means of:

- Small-signal stability analysis
- Non-linear time-domain simulation

**Small-signal analysis**

Fig. 6.12 and Table 6.4 show the electromechanical modes of the system with damping ratio under 20% obtained for the AC-base case and for the DC-segmented case. Results confirms that the critical inter-area mode (mode 1 of Table 6.4, with damping of 1.85% and frequency of 0.39 Hz) has been suppressed by the DC segmentation. Meanwhile, the damping ratios of the rest of the electromechanical modes do not present significant differences between the two cases.

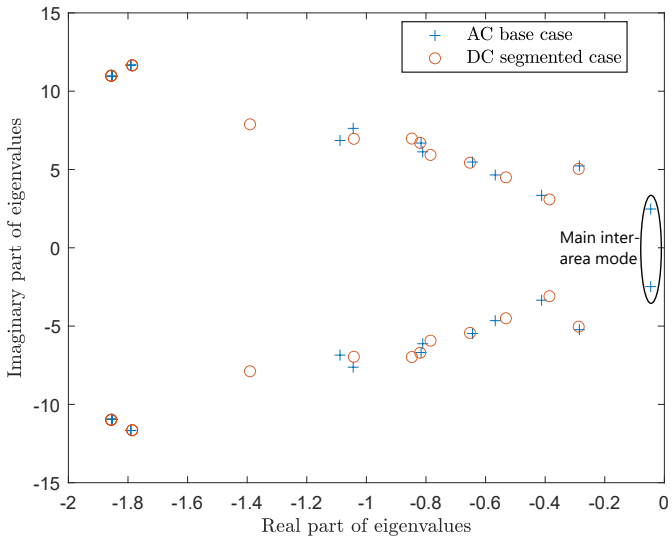


Figure 6.12: Weakly damped electromechanical modes of the two scenarios

Table 6.4: Weakly damped electromechanical modes of the two scenarios

| | AC base case | | DC-segmented case | |
|---|---|---|---|---|
| N0. | $\zeta$ (%) | Freq. (Hz) | $\zeta$ (%) | Freq. (Hz) |
| 1 | 1.85 | 0.39 | - | - |
| 2 | 5.45 | 0.83 | 5.70 | 0.80 |
| 3 | 12.22 | 0.54 | 12.38 | 0.50 |
| 4 | 12.11 | 0.75 | 11.73 | 0.72 |
| 5 | 11.68 | 0.88 | 11.92 | 0.87 |
| 6 | 13.12 | 0.98 | 13.12 | 0.95 |
| 7 | 12.12 | 1.07 | 12.14 | 1.07 |
| 12 | - | - | 12.06 | 1.12 |
| 8 | 13.57 | 1.23 | 14.81 | 1.12 |
| 9 | 15.69 | 1.10 | 17.37 | 1.27 |
| 10 | 15.17 | 1.88 | 15.15 | 1.88 |
| 11 | 16.69 | 1.77 | 16.66 | 1.77 |

**Non-linear time-domain simulation**

Two faults were simulated, one in each region of the Nordic 44 system (Fig. 6.6 and 6.7):

- Fault 1 (in region 1): Three-phase-to-ground short circuit at line 6001-5402 (close to bus 6001), cleared 200 ms later by disconnecting the line. The fault occurs at $t = 1$ s.

- Fault 2 (in region 2): Three-phase-to-ground short circuit at line 7000-7100 (close to bus 7000), cleared 200 ms later by disconnecting the three circuits of the line. The fault occurs at $t = 1$ s.

Fig. 6.13 shows the speed deviations of some generators of the system when Fault 1 occurs, for the AC-base case and for the DC-segmented case. The generators have been selected to be representative of the system: three generators are in region 1 (generators 5600, 5100 and 6100 represented in blue) and the other three are in region 2 (generators 7000, 8500 and 6500 represented in red).

In the AC base case (Fig. 6.13a), all the generators are affected by the fault and there is a poorly damped inter-area oscillation between the generators of the two regions corresponding to the targeted critical inter-area mode (mode 1 of Table 6.4).

In the DC-segmented case (Fig. 6.13b), generators 7000, 8500, 6500 are not affected by the fault because the VSC-HVDC links act as a firewall

between regions 1 and 2. Additionally, the critical inter-area oscillation is not present. Notice that some oscillations are still present due to the rest of electromechanical modes but they are not critical.

Fig. 6.14 shows the results of Fault 2. The speed deviations of the same generators as before are showed. Again, in the AC base case (Fig. 6.14a), the fault excites the speed of all generators and the critical inter-area oscillation is poorly damped. On the contrary, in the DC-segmented case (Fig. 6.14b), the fault does not propagate from region 2 to region 1 due to the VSC-HVDC segments, and the critical inter-area oscillation is not present.

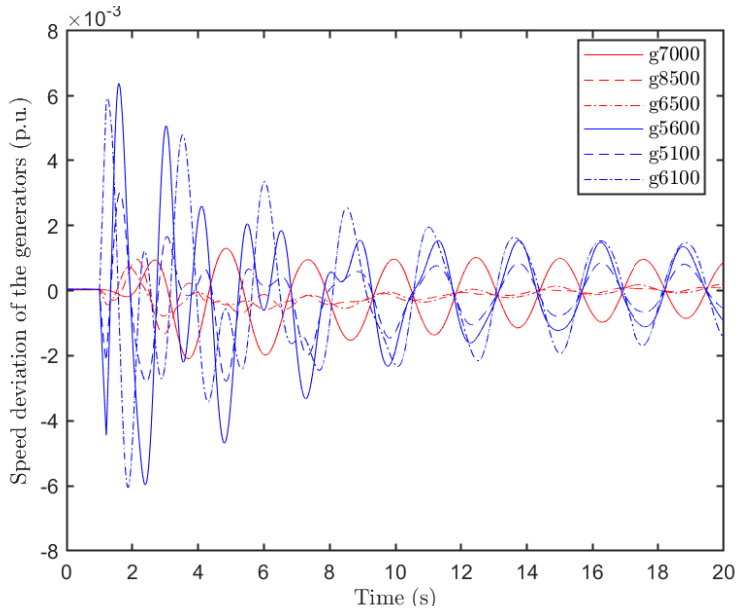


(a) AC base case

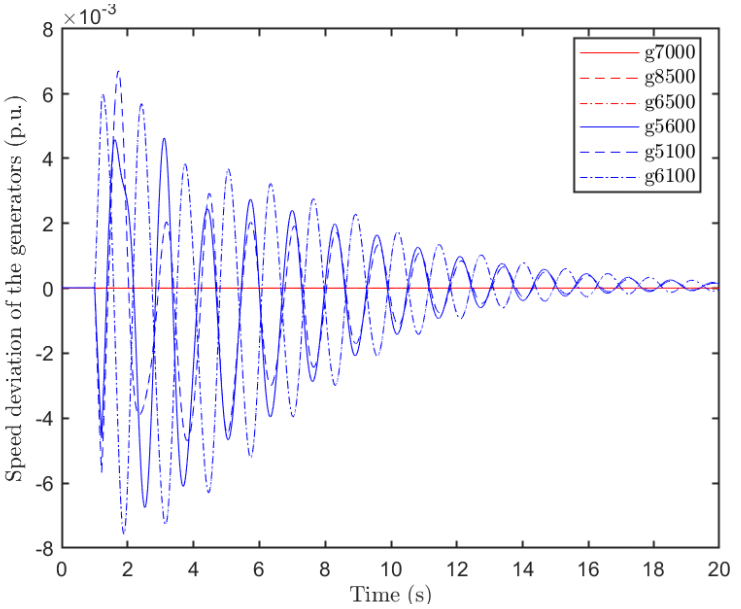


(b) DC-segmented case

Figure 6.13: Fault 1. Speed deviations of generators.

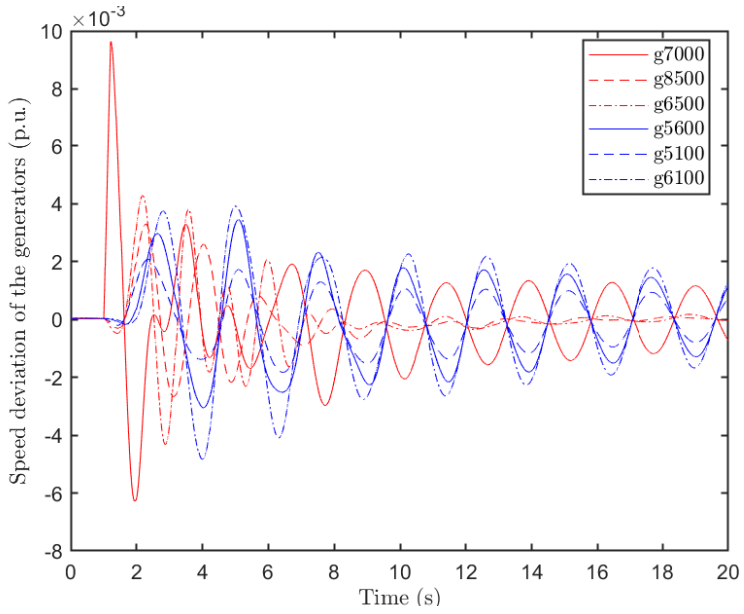


(a) AC base case

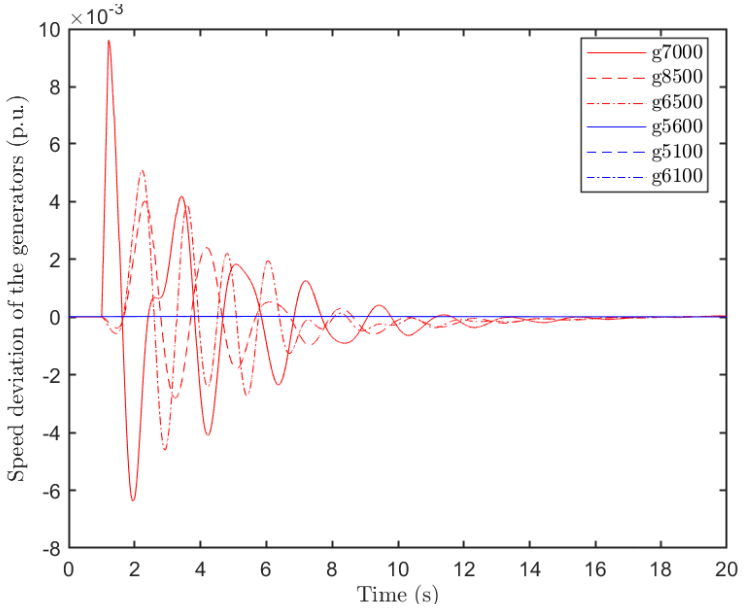


(b) DC-segmented case

Figure 6.14: Fault 2. Speed deviations of generators.

## 6.6 Summary and conclusions

This chapter proposed an algorithm for DC segmentation of AC power systems to mitigate electromechanical oscillations, using VSC-HVDC links. The objective of the proposed algorithm is to suppress the most critical inter-area oscillation of the initial AC power system. The proposed algorithm uses information of the small-signal stability analysis of the system and the concept of dominant inter-area oscillation paths. The proposed algorithm for the DC segmentation of power system uses the algorithm to identify electromechanical oscillation path proposed in Chapter 5 (as a part of the main algorithm). Small signal stability analysis and time domain simulation have been used to validate the effect of the DC segmentation proposed by the algorithm. The proposed algorithm has been illustrated on a basic 6-generator test system and then applied to the Nordic 44 test system.

The following conclusions have been obtained from the results presented in this chapter:

- The proposed algorithm obtains systematically a DC-segmentation scheme of the initial AC power system.
- In the resulting DC-segmented scheme, the critical inter-area oscillation of the initial AC power system is suppressed, without jeopardising the damping ratio of the intra-area modes.
- The concept of inter-area oscillation path is remarkably useful to determine where to segment the system with DC technology, at least when tackling electromechanical oscillations.

# 6 Proposed algorithm for DC segmentation to mitigate electromechanical oscillations

# Chapter 7

# DC segmentation and supplementary controllers to improve power system stability

## 7.1 Introduction

As discussed in Chapter 2, a good number of supplementary controllers for VSC-HVDC systems have been proposed in previous work. However, the application of supplementary controllers in VSC-HVDC systems in DC-segmented power systems is scarce in previous work. As shown in Chapter 4, DC segmentation with fixed power references improved the angle stability of power system (against small and large disturbances) while jeopardising its frequency stability. The present chapter investigates supplementary controllers adapted to a DC segmented power system: it will aim at obtaining further improvements in angle stability, while improving frequency stability in comparison with the initial AC power system.

More precisely a frequency control (FC) on the active power injections of the converter stations of the VSC-HVDC systems has been investigated to improve the frequency stability of DC-segmented power systems. Since the algorithm for DC segmentation proposed in Chapter 6 suppresses the inter-area oscillation mode without impacting the intra-area modes of the AC clusters, reactive power oscillation damping (POD-Q) controllers targeting the intra-area modes in the DC-segmented system have been implemented and analysed. Two variation of POD-Q controllers using either local or global measurements are proposed and compared.The local POD-Q controller is

based on previous proposals [50, 126], while the global POD-Q controller has been proposed in this work, for the first time.

All the controllers are tested on the DC segmented Nordic 44 test system of Chapter 6.

This chapter is organised as follows. Section 7.2 presents the FC (Section 7.2.1) and POD-Q control (Section 7.2.2) used in this chapter. In Section 7.3 the Nordic 44 test system is used to implement the supplementary controllers and study their effects. Finally, Section 7.4 concludes the chapter.

## 7.2 Supplementary controllers

Fig. 7.1-a depicts a schematic diagram of an AC power system and Fig. 7.1-b shows the power system after DC segmentation, where the AC interconnection line has been replaced by a VSC-HVDC link, decoupling the two remaining AC systems.

The following supplementary controllers in VSC-HVDC links of the DC-segmented case will be considered:

- Frequency Control (FC): The objective is to provide frequency support between the asynchronous AC areas through the VSC-HVDC links.
- Power Oscillation Damping (POD) controllers for the Q injections (POD-Q): The objective is to contribute to damp intra-area oscillations in the asynchronous AC areas by means of Q-modulation in the VSC stations of the DC segments.

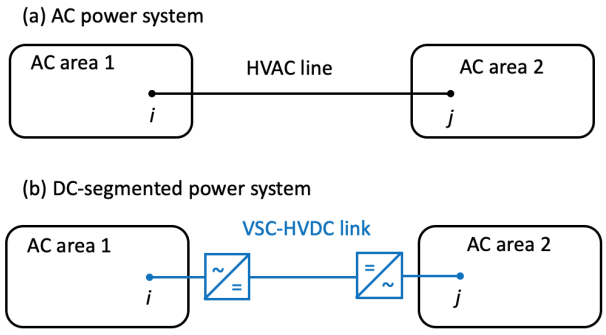


Figure 7.1: (a) AC power system and (b) DC-segmented power system.

### 7.2.1 Frequency Controllers (FC)

In FC, the P set point of the VSC station ($P^*_{ac,i}$) that controls the active power through each DC segment (VSC-$i$) is given by:

$$P^*_{ac,i} = P^0_{ac,i} + \Delta P^{ref,FC}_{ac,i} \tag{7.1}$$

where $P^0_{ac,i}$ is a constant P set-point value, and $\Delta P^{ref,FC}_{ac,i}$ is the supplementary P set-point value provided by the FC.

Fig. 7.2 shows the block diagram of the FC, based on strategy FC-WAF proposed in [128] for multi-terminal VSC-HVDC systems (VSC-MTDC), which uses the average frequency of the VSC-MTDC as set point ($\omega^* = \bar{\omega}$) for the frequency controller. The FC uses a proportional controller with gain $K_{FC,i}$, a low-pass filter with time constant $T_{FC,i}$, to filter out noise in the frequency difference, and a saturation parameter $\pm\Delta P^{max}_{ac,i}$. The frequency set point for the FC is given by:

$$\omega^* = \bar{\omega} = \frac{\omega_i + \omega_j}{2} \tag{7.2}$$

where $\omega_i$ and $\omega_j$ are the frequency measured at the two AC terminals of the VSC-HVDC link (in pu).

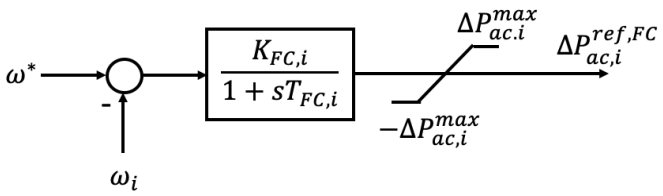


Figure 7.2: Frequency Controller (FC) using FC-WAF.

Notice that in point-to-point VSC-HVDC links, strategy FC-WAF [128] is equivalent to a FC controller proportional to the frequency difference between

the frequencies of each terminal of the link as long as $K'_{FC,i} = K_{FC,i}/2$:

$$\begin{aligned} \Delta P_{ac,i}^{ref,FC} &= \frac{K_{FC,i}}{1+sT_{FC,i}}(\bar{\omega}-\omega_i) \\ &= \frac{K_{FC,i}}{1+sT_{FC,i}}\big[\frac{\omega_i+\omega_j}{2}-\omega_i\big] \\ &= \frac{K_{FC,i}/2}{1+sT_{FC,i}}(\omega_j-\omega_i) = \frac{K'_{FC,i}}{1+sT_{FC,i}}(\omega_j-\omega_i). \end{aligned} \tag{7.3}$$

With the FC of Fig. 7.2, frequency support among the asynchronous AC areas through the VSC-HVDC links is achieved, independently of the location of the disturbance, since the FC uses frequency measurements at both ends of the VSC-HVDC links.

### 7.2.2 POD-Q controllers

Two POD controllers for the reactive-power injections of the VSC stations (POD-Q) will be analysed and compared in this work:

- POD-Q-LF: It modulates Q injections of each VSC using local measurement of the frequency at the AC connection point.
- POD-Q-FCOI: It modulates Q injection of the VSC using global measurements of the frequency of the Centre Of Inertia (COI) of the AC area at which the VSC is connected to.

The Q set point of each VSC-$i$ is given by ($Q^*_{ac,i}$):

$$Q^*_{ac,i} = Q^0_{ac,i} + \Delta Q^{ref,POD}_{ac,i} \tag{7.4}$$

where $Q^0_{ac,i}$ is a constant Q set-point value, and $\Delta Q^{ref,POD}_{ac,i}$ is the supplementary Q set-point value provided by the POD-Q controller.

The two POD-Q controllers above can be described as in Fig. 7.3. The input signal of the controller is the frequency error (in pu) between the frequency set point ($\omega^*_i$) and the frequency measured at the AC connection point of the VSC station ($\omega_i$). The POD-Q controller has a low-pass filter (with time constant $T_{Qf,i}$ usually between 0 and 1.2s) to filter out noise in the frequency difference, a wash-out filter (with time constant $T_{QW,i}$ usually between 1 and 20s), to prevent the controller from acting in steady state average, a lead/lag filter (with time constants $T_{Q1,i}$, $T_{Q2,i} = a_{Q,i}T_{Q1,i}$, filtering

ratio $a_{Q,i}$ and $N_{QS,i}$ lead/lag networks), that produce the necessary phase shift needed for the control action, a controller gain $K_{Q,i}$ and a saturation parameter $\pm\Delta Q_{ac,i}^{max}$.

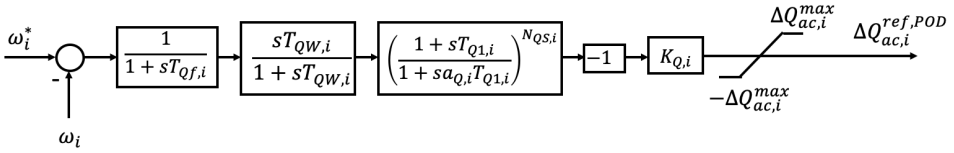


Figure 7.3: POD-Q controller.

**POD-Q-LF**

In POD-Q-LF controller, the frequency set point of Fig. 7.3 is the nominal frequency in pu: $\omega_i^* = \omega_0 = 1$ pu. Hence, it uses local measurements. This scheme of POD-Q controller is based on previous schemes proposed in [50, 126].

**POD-Q-FCOI**

In POD-Q-FCOI controller, proposed in this work, the frequency set point of Fig. 7.3 is calculated as the frequency of the COI (in pu) of the AC area which station VSC-$i$ is connected:

$$\omega_i^* = \omega_{COI,i} = \sum_{k \in A_i} \frac{H_k}{H_T} \omega_k, \; H_T = \sum_{j \in A_i} H_j. \tag{7.5}$$

With $H_k$ the inertia constant of generator k and $A_i$ the set of generators of the AC area which station VSC-$i$ is connected.

This strategy was motivated by POD-Q-WAF controller proposed in [66] for VSC-MTDC systems embedded in an AC system, which used as frequency set point the weighted-average frequency of the VSC-MTDC system. However, the application and the controller proposed here are different, since the VSC-HVDC are now interconnecting asynchronous AC areas, and the frequency of the COI of each AC area is used as the frequency set point for the POD-Q controller placed in that area. In POD-Q-FCOI controller, each VSC compares the frequency set point with $\omega_i^* = \omega_{COI,i}$ with its own frequency

($\omega_i$). Notice that the usefulness of the speed of the COI for power-system-stability-tailored controllers was illustrated in [129].

### 7.2.3 Design of POD-Q controllers

The method of design of POD-Q controllers is based on the work in [25], which uses the concept of eigenvalue sensitivities [122]. The work in [66] used this approach for the design of POD controllers in VSC-HVDC systems. In this work, the concept of *numerical eigenvalue sensitivity* has been used (instead of the theoretical eigenvalue sensitivity), as it can facilitate the design of POD controllers in cases with limited information of the state matrices of the linearised system.

It is assumed that a linearised model of the power system is available. A POD-Q controller in VSC-$j$ will be used to damp a target electromechanical mode $i$:

$$\lambda_i^0 = \sigma_i^0 \pm j\omega_i^0 \tag{7.6}$$

with a damping ratio $\zeta_i^0$. If the required damping ratio is $\zeta_i^d$, the estimated target electromechanical mode can be approximated as:

$$\lambda_i^d = -\zeta_i^d\omega_i^0 \pm j\omega_i^0 \tag{7.7}$$

The sensitivity of electromechanical mode $i$ to changes in the gain of POD-Q controller $j$, $K_{Q,j}$, is defined as [122]:

$$S_{ij} = \frac{\partial\lambda_i}{\partial K_{Q,j}} \tag{7.8}$$

Similarly, the (non-compensated) sensitivity of mode $i$ to changes in the gain of the non-compensated POD-Q controller $j$ ($S_{ij}^{NC}$) is defined as:

$$\begin{aligned} S_{ij}^{NC} &= S_{ij}(T_{Q1,j}=0) = \left.\frac{\partial\lambda_i}{\partial K_{Q,j}}\right|_{T_{Q1,j}=0} \\ &= |S_{ij}^{NC}|\angle\varphi_{ij}^{NC} \end{aligned} \tag{7.9}$$

Therefore, the sensitivity of the non-compensated eigenvalue can be approximated, numerically, by:

$$\hat{S}_{ij}^{NC} = \frac{\lambda_i^{NC} - \lambda_i^0}{\Delta K_{Q,j}} \tag{7.10}$$

where $\lambda_i^{NC}$ is the non-compensated eigenvalue, i.e., the new eigenvalue with the POD-Q implemented without its lead/lag filter ($T_{Q1,j=0}$) and with a small gain $\Delta K_{Q,j}$. Naturally, $\hat{S}_{ij}^{NC} \approx S_{ij}^{NC}$.

Fig. 7.4 shows the geometric interpretation of eigenvalue sensitivities [25, 66]. An effective POD-Q will move the target electromechanical mode to the left-hand side of the complex plane, as illustrated in Fig. 7.4. The lead/lag filter is used to ensure that the eigenvalue sensitivity has a phase as close to 180° as possible, while gain $K_{Q,j}$ (see Fig. 7.3) is used to move the eigenvalues further to the left-hand side of the complex plane and to achieve the required damping ratio.

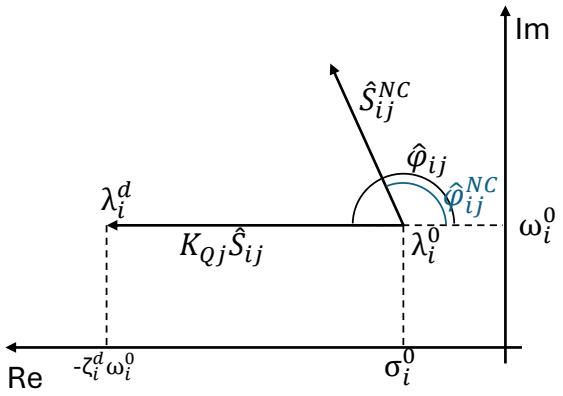


Figure 7.4: Geometric interpretation of eigenvalue sensitivities.

The design of the POD-Q controller of each VSC-$j$ consists of two steps:

1. *Design of the lead/lag filter:* Its objective is to obtain a phase of the eigenvalue sensitivity ($\hat{S}_{ij}$) as close to 180° as possible [25]:

   phase lead ($\hat{\varphi}_{ij}^{NC} \geq 0$):

$$a_{Q,j} = \frac{1 - \sin\phi_{ij}}{1 + \sin\phi_{ij}} \leq 1,\ \phi_{ij} = \frac{\pi - \hat{\varphi}_{ij}^{NC}}{N_{QS,j}}. \tag{7.11}$$

   phase lag ($\hat{\varphi}_{ij}^{NC} < 0$):

$$a_{Q,j} = \frac{1 + \sin\phi_{ij}}{1 - \sin\phi_{ij}} > 1,\ \phi_{ij} = \frac{\pi + \hat{\varphi}_{ij}^{NC}}{N_{QS,j}}. \tag{7.12}$$

with $\hat{\varphi}_{ij}^{NC} = \angle(\hat{S}_{ij}^{NC})$.

Finally, the time constants of the lead/lag filter ($T_{Q1,j}$ and $T_{Q2,j}$) are selected to achieve maximum lead/lag phase compensation at the frequency of the target electromechanical mode [130]:

$$T_{Q1,j} = \frac{1}{\omega_i^0 \sqrt{a_{Q,j}}}, \text{ and } T_{Q2,j} = a_{Q,j} T_{Q1,j}. \tag{7.13}$$

The resulting numerical eigenvalue sensitivity can be then calculated as:

$$\hat{S}_{ij} = \hat{S}_{ij}^{NC} \Big[ \frac{1 + sT_{Q1,j}}{1 + sa_{Q,j}T_{Q1,j}} \Big]_{s=\lambda_i^0}^{N_{QS,j}} = |\hat{S}_{ij}| \angle \hat{\varphi}_{ij} \tag{7.14}$$

2. *Calculation of the controller gain:* Gain $K_{Q,j}$ is calculated to obtain the required damping ratio of the target electromechanical mode:

$$\lambda_i^d \approx \lambda_i^0 + K_{Q,j} \hat{S}_{ij}. \tag{7.15}$$

$$K_{Q,j} = \gamma_j \frac{|\lambda_i^d - \lambda_i^0|}{|\hat{S}_{ij}|} \tag{7.16}$$

with $K_{Q,j} \in [-K_{Q,j}^{max}, K_{Q,j}^{max}]$ and $\gamma_j = 1$ if a positive gain is required and $\gamma_j = -1$ if a negative gain is required.

## 7.3 Case study and results

The Nordic 44 test system [131] (already used in Chapter 6) was used to analyse DC segmentation and the supplementary controllers described in Section 7.2.

The starting point for the work of this chapter is the DC-segmented system proposed in Chapter 6, as shown in Fig. 7.5. VSC-HVDC link A has a rating of 3500 MVA, while VSC-HVDC link B has a rating of 800 MVA. Supplementary controllers for frequency support among the two AC areas (FC) and power-oscillation damping for the intra-area modes by means of Q-modulation at the VSC stations (POD-Q controllers) will now be analysed (see Section 7.2).

Four cases will be analysed and compared:

- **AC base case**: The initial Nordic 44 test system. It corresponds to the case of Fig. 7.5 with AC lines instead of the DC links.

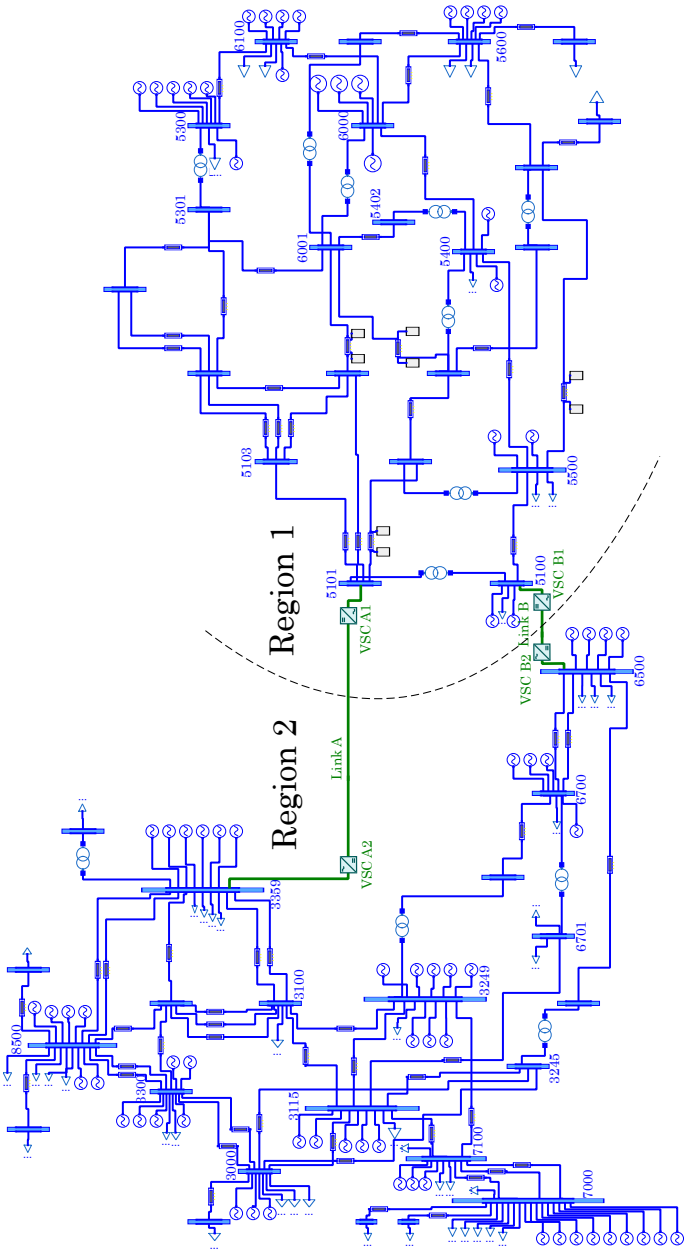


Figure 7.5: DC-segmented N44 test system under Dymola.

- **DCs constant PQ**: The DC-segmented case without supplementary controllers.
- **DCs f-support, POD-Q-LF**: The DC-segmented case with frequency support (FC) and POD-Q using local frequency (POD-Q-LF).
- **DCs f-support, POD-Q-FCOI**: The DC-segmented case with frequency support (FC) and POD-Q using the frequency of the centre of inertia of each AC area (POD-Q-FCOI).

Details of the four cases can be found in Appendix C. For the DC-segmented cases, the operating point considered for the VSC-HVDC links was when they transmit the same active-power as the AC lines in the AC-base case, while reactive power injections were equal zero at both converter stations on both links:

- VSC-HVDC link A (VSC A1 at bus 5101, VSC A2 at bus 3359): Active power of 1548 MW from VSC A1 to VSC A2.
- VSC-HVDC link B (VSC B1 at bus 5100, VSC B2 at bus 6500): Active power of 447 MW from VSC B1 to VSC B2.

The parameters of Frequency Controller (FC) (Fig. 7.2) are $K_{FC,i} = 100$ pu, $T_{FC,i} = 0.1$ s and $\pm\Delta P_{ac,i}^{max} = \pm 1$ pu.

The effects of the DC segmentation and supplementary controllers proposed were investigated using Dymola [114]. VSC-HVDC links were modelled as proposed in Section 3.3 and models were implemented in Modelica language to be tested in combination with the OpenIPSL library [92]. The four cases have been compared by means of small-signal stability analysis (see Section 7.3.2) and non-linear time-domain simulations (see Section 7.3.3).

### 7.3.1 Design of POD-Q controllers

Table 7.1 presents the main modes of the Nordic 44 test system in the AC case and in the DC-segmented case without supplementary controllers. All the electromechanical modes with a damping lower than 20% in at least one of the cases have been included. The table also indicates the location of each mode. Results show that the critical inter-area mode (mode 1), which has a low damping ratio, has been mitigated with the DC segmentation obtained following the algorithm proposed in [132]. Nevertheless, there are still intra-area modes in each asynchronous AC area. POD-Q controllers

(POD-Q-LF and POD-Q-FCOI described in Section 7.2.2) have been used in every VSC station to increase the damping ratio of some intra-area modes. POD-Q controllers will be designed following the methodology presented in Section 7.2.3.

Table 7.1: Poorly-damped electromechanical modes of the two initial cases.

| | AC base case | | DCs constant PQ | | Region of |
|---|---|---|---|---|---|
| N0. | $\zeta$ (%) | Freq (Hz) | $\zeta$ (%) | Freq (Hz) | the mode |
| 1 | 1.85 | 0.39 | - | - | Inter-area |
| 2 | 5.45 | 0.83 | 5.70 | 0.80 | R1 |
| 3 | 11.68 | 0.88 | 11.92 | 0.87 | R2 |
| 4 | 12.11 | 0.75 | 11.73 | 0.72 | R2 |
| 5 | - | - | 12.06 | 1.12 | R2 |
| 6 | 12.12 | 1.07 | 12.14 | 1.07 | R1 |
| 7 | 12.22 | 0.54 | 12.38 | 0.50 | R2 |
| 8 | 13.12 | 0.98 | 13.12 | 0.95 | R2 |
| 9 | 13.57 | 1.23 | 17.37 | 1.27 | R1 |
| 10 | 15.69 | 1.10 | 14.81 | 1.12 | R1 |

The POD-Q controllers are set to damp the least damped (in the case with DC segmentation with constant P&Q) local mode of the region they are connected to. Thus, VSCs of region 1 (i.e. VSC-A1 or 5101 and VSC-B1 or 5100) will target mode 2 (with a damping ratio of $\zeta = 5.7$ % and a frequency of 0.80 Hz) while the VSCs of region 2 (i.e. VSC-A2 or 3359 and VSC-B2 or 6500) will target mode 4 (with a damping ratio of $\zeta = 11.92$ % and a frequency of 0.72 Hz). Each POD-Q controller will be designed independently to obtain a 15 % damping for the targeted mode. The gain step used for the calculation of the numerical eigenvalue sensitivity is $\Delta K_{Q,j} = 20$ pu (nominal pu). Pre-defined parameters of the POD-Q controllers are: $T_{Qf,j} = 0.1$ s, $T_{QW,j} = 5$ s, $N_{QS,j} = 2$ and $\pm Q_{ac,i}^{max} = \pm 0.1$ pu. Maximum allowed POD-Q gain is set to $K_{Q,j}^{max} = \pm 400$ pu.

Table 7.2 shows the parameters obtained for POD-Q-LF (local) and POD-Q-FCOI (global) controllers with the design method of Section 7.2.3. Notice that POD-Q gains reach their maximum allowed value. This is due to the fact that POD controllers in VSC-HVDC systems can only be very effective if the VSC stations are well located to damp electromechanical oscillations [66]. However, POD-Q controllers in a DC-segmented system may not be in the best location to damp electromechanical oscillations. Precisely, the aim of this work is to analyse the capability of damping intra-area electromechanical modes in DC-segmented system with a pre-defined scheme. It is also worth

highlighting that some POD-Q gains have opposite signs, which is related to the location of the VSC stations in each AC area.

Table 7.2: Parameters of the POD-Q controllers.

| Case | VSC | $K_{Q,j}$ (pu) | $T_{Q1,j}$ (s) | $a_{Q,j}$ |
|---|---|---|---|---|
| POD-Q-LF | A1 (5101) | -400 | 0.2847 | 0.486 |
| | B1 (5100) | -400 | 0.2847 | 0.486 |
| | A2 (3359) | 400 | 0.2223 | 0.999 |
| | B2 (6500) | 400 | 0.2975 | 0.558 |
| POD-Q-FCOI | A1 (5101) | -400 | 0.2750 | 0.521 |
| | B1 (5100) | -400 | 0.2776 | 0.511 |
| | A2 (3359) | 400 | 0.2402 | 0.856 |
| | B2 (6500) | 400 | 0.2889 | 0.592 |

### 7.3.2 Small-signal stability analysis

Table 7.3 shows the main electromechanical modes of the system for the 4 cases.

Table 7.3: Poorly-damped electromechanical modes of the four scenarios.

| | AC base case | | DCs constant PQ | | DCs f-support POD-Q-LF | | DCs f-support POD-Q-FCOI | | Region of the |
|---|---|---|---|---|---|---|---|---|---|
| N0. | $\zeta$ (%) | Freq (Hz) | $\zeta$ (%) | Freq (Hz) | $\zeta$ (%) | Freq (Hz) | $\zeta$ (%) | Freq (Hz) | mode |
| 1 | 1.85 | 0.39 | - | - | - | - | - | - | Inter-area |
| 2 | 5.45 | 0.83 | 5.70 | 0.80 | 11.53 | 0.84 | 12.40 | 0.83 | R1 |
| 3 | 11.68 | 0.88 | 11.92 | 0.87 | 12.30 | 0.88 | 12.33 | 0.88 | R2 |
| 4 | 12.11 | 0.75 | 11.73 | 0.72 | 15.52 | 0.74 | 15.40 | 0.74 | R2 |
| 5 | - | - | 12.06 | 1.12 | 12.44 | 1.10 | 12.16 | 1.07 | R2 |
| 6 | 12.12 | 1.07 | 12.14 | 1.07 | 12.15 | 1.07 | 12.48 | 1.10 | R1 |
| 7 | 12.22 | 0.54 | 12.38 | 0.50 | 15.02 | 0.48 | 16.45 | 0.47 | R2 |
| 8 | 13.12 | 0.98 | 13.12 | 0.95 | 16.05 | 0.97 | 15.61 | 0.97 | R2 |
| 9 | 13.57 | 1.23 | 17.37 | 1.27 | 20.68 | 1.31 | 20.68 | 1.31 | R1 |
| 10 | 15.69 | 1.10 | 14.81 | 1.12 | 14.30 | 1.21 | 14.55 | 1.20 | R1 |

Results show that:

- The inter-area mode (mode 1 with a damping ratio of 1.85 % and a frequency of 0.39 Hz) has been suppressed by the DC segmentation.
- The damping of the main intra-area mode of region 1 (mode 2 with a damping ratio of 5.7 % and a frequency of 0.8 Hz in the DC-segmented

case without control) was improved by the POD-Q controllers (+5.97 % with POD-Q-LF and +7.04 % with POD-Q-FCOI).

- The main intra-area mode of region 2 (mode 4 with a damping ratio of 11.73 % and a frequency of 0.72 Hz in the DC-segmented case without control) is well damped by the POD-Q controllers (15.52 % with POD-Q-LF and 15.40 % with POD-Q-FCOI).
- Meanwhile, the damping ratios of the rest of the electromechanical modes do not change significantly.

Notice that in the DC-segmented case, results obtained with POD-Q-FCOI (global measurements) are slightly better than the ones obtained with POD-Q-LF (local measurements). For this reason, taking into account that the implementation of POD-Q using local measurements is much easier, for this test system the use of POD-Q-LF seems to be a better solution than POD-Q-FCOI.

### 7.3.3 Non-linear time-domain simulation

#### Small perturbation

Two small perturbations were simulated, one at each region of the system, namely:

- Disconnection of line 6001-5301 (Region 1) at $t = 1$ s.
- Disconnection of line 3249-7100 (Region 2) at $t = 1$ s.

The purpose of these simulations is to analyse electromechanical oscillations.

Fig. 7.6 shows the frequency of two representative generators (5600 in Region 1 and 7000 in Region 2) and Fig. 7.7 shows the Q injections of the VSCs of Region 1 after the disconnection of the line in Region 1. A poorly-damped inter-area oscillation can be clearly observed in AC base case, which corresponds to mode 1 of Table 7.3 (see Fig. 7.6). Results confirm the suppression of the inter-area mode in the 3 DC-segmented cases and the limitation of the first local mode of Region 1 (mode 2 of the Table 7.3) in the two DC-segmented cases with both POD-Q-LF and POD-Q-FCOI. Furthermore, POD-Q-LF and POD-Q-FCOI controllers damped intra-area oscillations successfully (see Fig. 7.6) by means of reactive-power modulation (Fig. 7.7). Notice also that in the DC-segmented case with constant power control, the perturbation, that occurs at Region 1 is not propagated to Region 2 and,

therefore, the frequency at buses in Region 2 remain constant to 50 Hz (see Fig. 7.6b). On the contrary, a small transient on the frequency at Region 2 is observed in the DC-segmented cases with supplementary controllers. This is due to the effect of the frequency controllers in the VSC-HVDC links.

Fig. 7.8 shows the frequency of the two representative generators above, and Fig. 7.9 the Q injections at the VSCs of Region 2 after the disconnection of a line in Region 2. Again, results confirm the suppression of critical inter-area mode in the 3 DC-segmented cases. However, the improvements on the damping ratio of the first local mode of Region 2 (mode 4 of Table 7.3) with the two POD-Q is not clear. This is due to the fact that mode 3 has a similar damping ratio than mode 4 and it has not been improved by POD-Q controllers.

Finally, it is worth to highlight that the frequency controller (FC) in the DC link does not propagate the critical inter-area oscillation which was present in the AC base case (see Figs. 7.6 and 7.8) because DC segmentation eliminates the critical inter-area oscillation of the AC base case by removing the synchronising constraint of the two AC regions. Therefore, although the FC controller is somehow coupling the two asynchronous AC areas, the critical inter-area oscillation is no longer present in the system and thus, it cannot be propagated. Results also show that the FC does not produce negative effects related to the propagation of other intra-area oscillations.

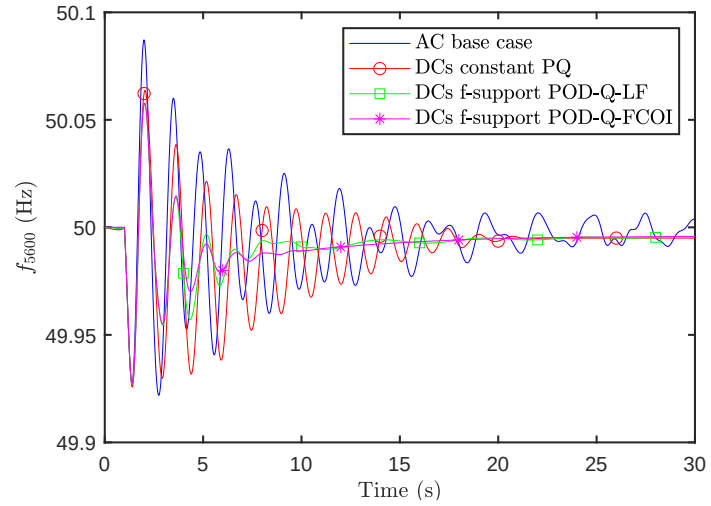


(a) Region 1

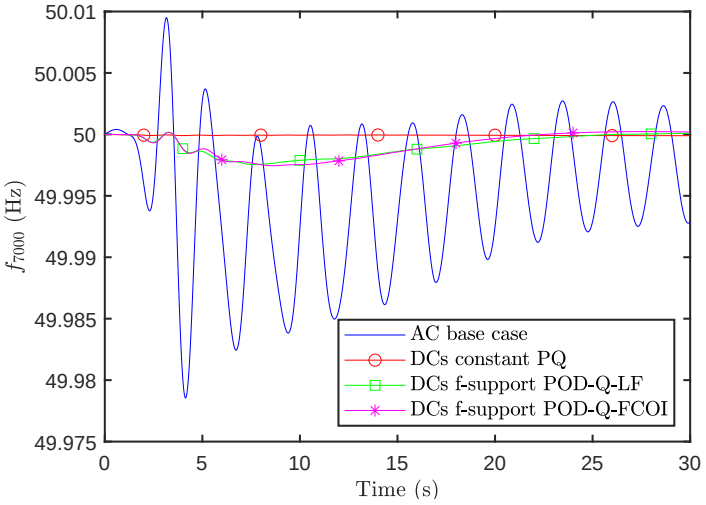


(b) Region 2

Figure 7.6: Frequency of two representative generators after the disconnection of line 6001-5301 (Region 1).

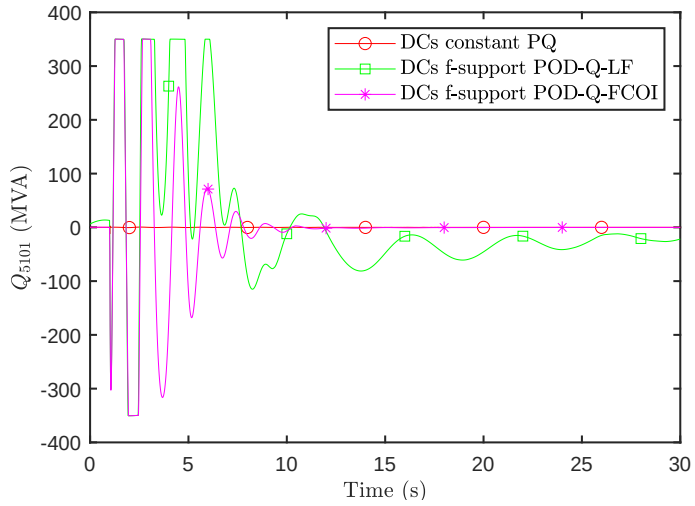


(a) VSC A1 (5101)

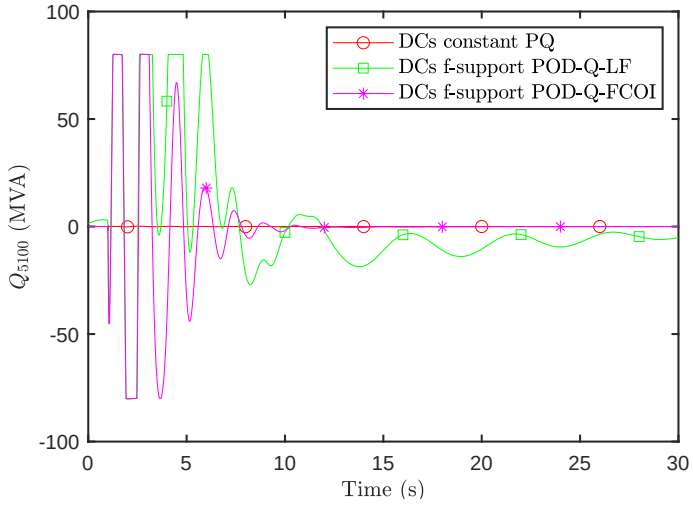


(b) VSC B1 (5100)

Figure 7.7: Reactive power injection at the two VSC of Region 1 after the disconnection of line 6001-5301 (Region 1).

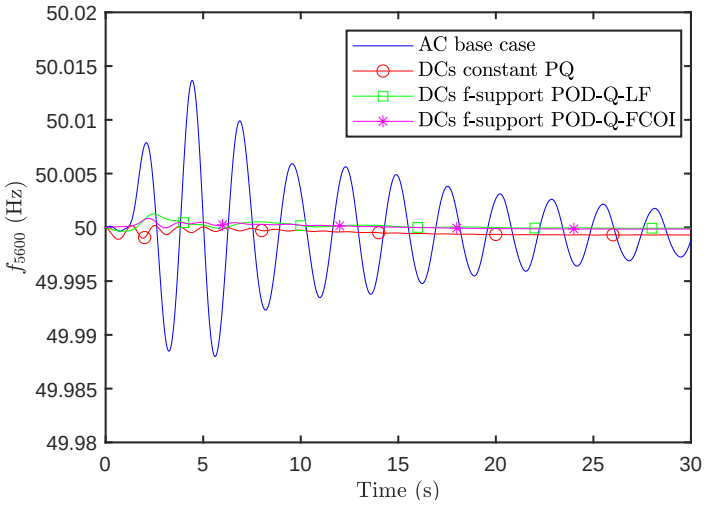


(a) Region 1

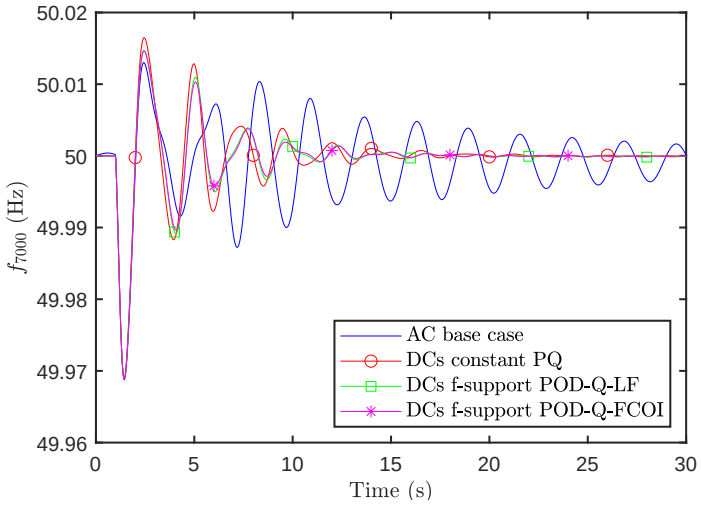


(b) Region 2

Figure 7.8: Frequency of two representative generators after the disconnection of line 3249-7100 (Region 2).

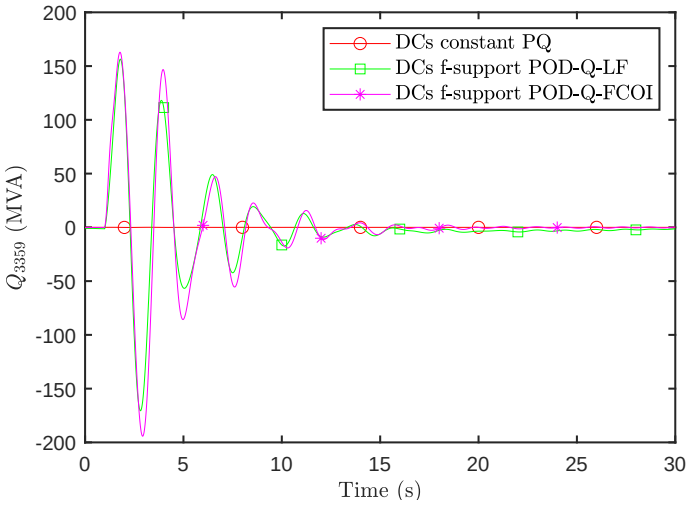


(a) VSC A2 (3359)

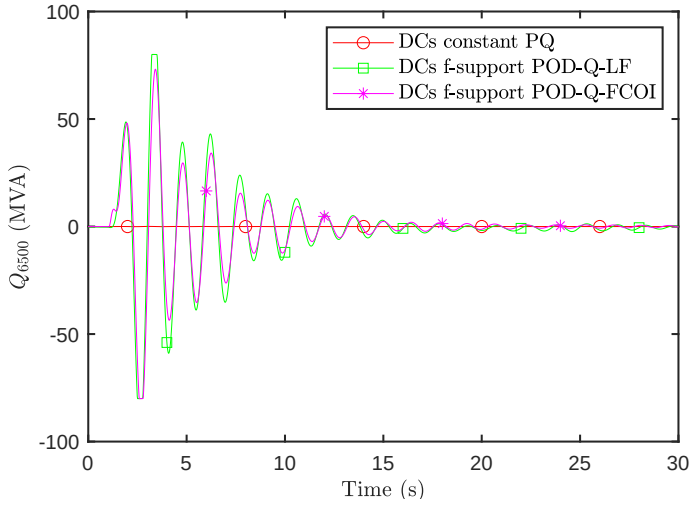


(b) VSC B2 (6500)

Figure 7.9: Reactive power injection at the two VSC of Region 2 after the disconnection of line 3249-7100 (Region 2).

**Disconnection of generator**

The disconnection of a generation in each area has been simulated. The purpose of these simulations is to analyse frequency stability. The generators selected for the contingency were those with the largest power injection before the event:

- Disconnection of a generator at bus 5300 (Region 1) at $t = 1$ s. This generator has a nominal power of 1200 MVA and it was injecting 723 MW before the event.
- Disconnection of a generator at bus 3300 (Region 2) at $t = 1$ s. This generator has a nominal power of 1100 MVA and it was injecting 757 MW before the event.

Fig. 7.10 shows the frequency of the two representative generators (5600, 7000) used above after the disconnection of the generator in Region 1, while Fig. 7.11 shows the active power exchange between the two regions (from Region 1 to Region 2). In the AC base case, the frequency nadir ($f_{min}$) and the final frequency are higher than the ones obtained in Region 1, because the two areas are connected synchronously through AC branches and the total frequency-support capability is greater. Naturally, in the AC base case the frequencies at regions 1 and 2 are in synchronism. In the DC segmented case with constant power control, the frequency nadir is low. This is because Region 1 only has frequency support from its synchronous generators and the VSC-HVDC links do not provide frequency support. Notice also that in the case of DC segmentation with constant power the frequency at Region 2 remains constant, because it is decoupled from Region 1 by the VSC-HVDC links. On the contrary, in the DC-segmented cases with supplementary controllers, FC in the VSC-HVDC links produces frequency support among the two regions. This causes the frequency nadir of region 1 to be higher than the one obtained in the DC-segmented case with constant power. The effects of frequency support through the VSC-HVDC links can be observed in Fig. 7.11, where it reduces the power exchange between Region 1 and 2. As a consequence, in the DC-segmented cases with supplementary controllers, the frequency at Region 2 also changes, due to the effect of FC in the VSC-HVDC links.

Figs. 7.12 and 7.13 shows the results for the case of disconnection of a generator in Region 2 and analogous behaviour can be observed.

Table 7.4 shows the frequency nadir ($f_{min}$) and final steady-state frequency ($f_{final}$) after the disconnection of generator G5300-1 in Region 1.

Note that the results of the table may not correspond exactly to the ones in Fig. 7.10 for the final frequency since the steady state has not been reached in the figure. Results for the disconnection of a generator in Region 2 are also included in the table (G3300-1), which has a nominal power of 1100 MVA and it was injecting 757 MW before the event. As a conclusion, in the DC-segmented cases with supplementary controllers, overall frequency stability is improved, in comparison with the DC-segmented case with constant power.

Table 7.4: Frequency Nadir and steady state after a disconnection of generator in Region 1 or 2 in the four cases.

| Disconnection of generator in: | Frequency (Hz) | AC case | DCs constant PQ | DCs f-support POD-Q-LF | DCs f-support POD-Q-FCOI |
|---|---|---|---|---|---|
| Region 1 | $f_{min,region1}$ (Hz) | 49.85 | 49.68 | 49.74 | 49.75 |
| | $f_{min,region2}$ (Hz) | 49.86 | 50.00 | 49.96 | 49.96 |
| | $f_{final,region1}$ (Hz) | 49.97 | 49.94 | 49.94 | 49.94 |
| | $f_{final,region2}$ (Hz) | 49.97 | 50.00 | 50.00 | 50.00 |
| Region 2 | $f_{min,region1}$ (Hz) | 49.86 | 50.00 | 49.96 | 49.96 |
| | $f_{min,region2}$ (Hz) | 49.86 | 49.76 | 49.79 | 49.79 |
| | $f_{final,region1}$ (Hz) | 49.97 | 50.00 | 50.00 | 50.00 |
| | $f_{final,region2}$ (Hz) | 49.97 | 49.93 | 49.94 | 49.94 |

Additionally, DC segmentation with and without frequency support significantly reduces the power-exchange oscillations in the inter-area link (Fig. 7.11 & 7.13). This could avoid unwanted tripping of the line in cases where the link is close to its maximum capacity, this could be of interest in cases in where this aspect is critical.

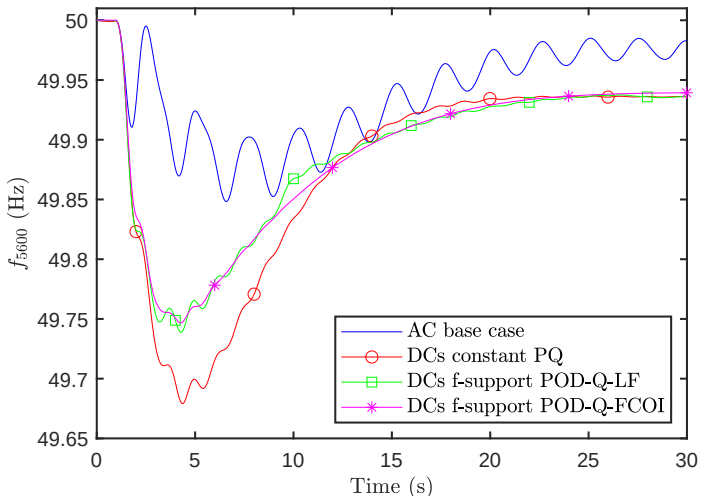


(a) Region 1

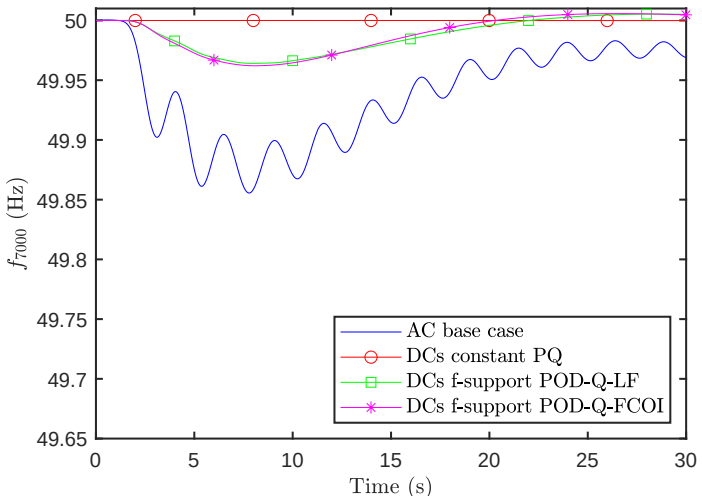


(b) Region 2

Figure 7.10: Frequency of two representative generators after the disconnection of a generator at bus 5300 (Region 1).

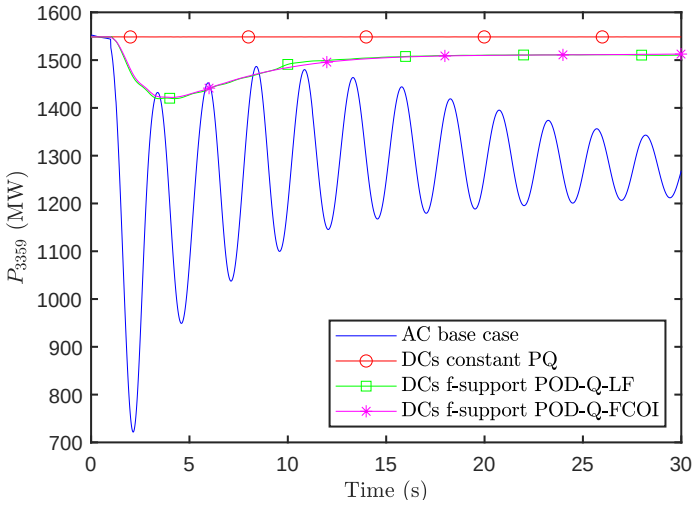


(a) Link A (5101-3359)

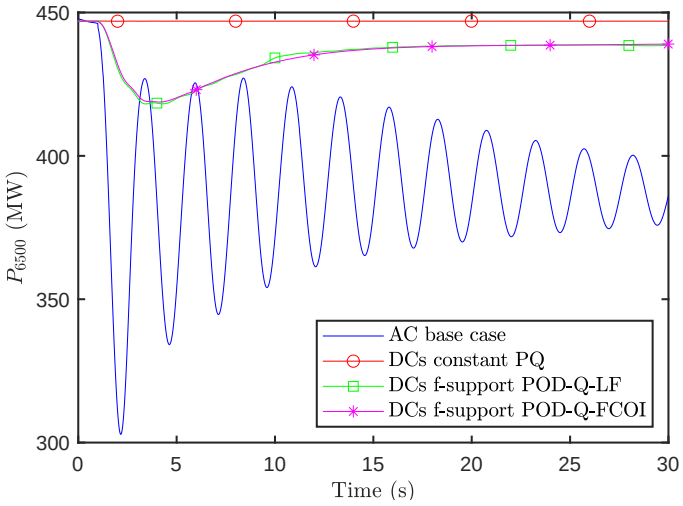


(b) Link B (5100-6500)

Figure 7.11: Active power exchange from region 1 to region 2 after the disconnection of a generator at bus 5300 (Region 1).

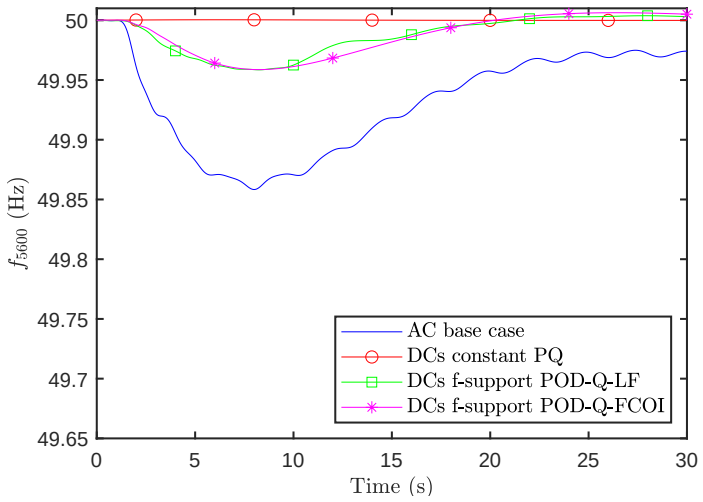


(a) Region 1

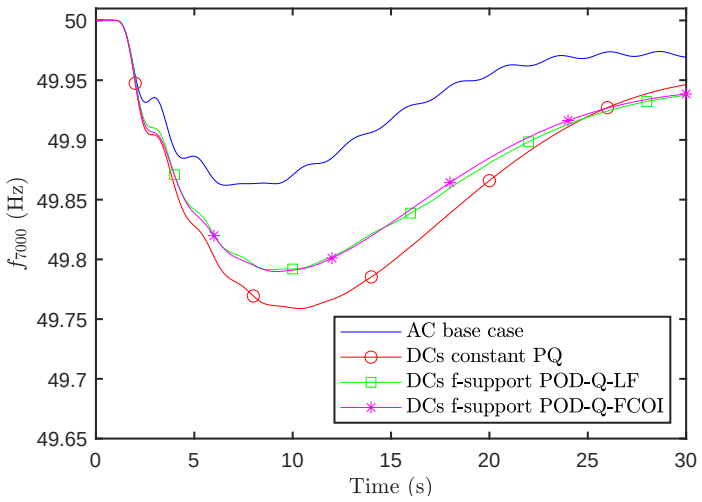


(b) Region 2

Figure 7.12: Frequency of two representative generators after the disconnection of a generator at bus 3300 (Region 2).

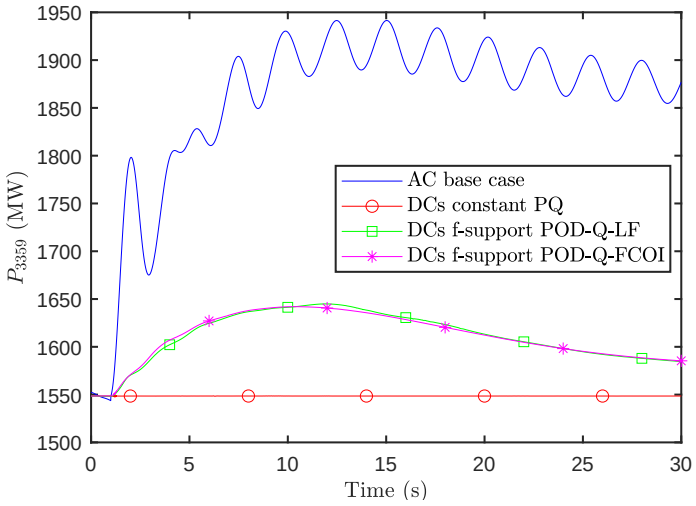


(a) Link A (5101-3359)

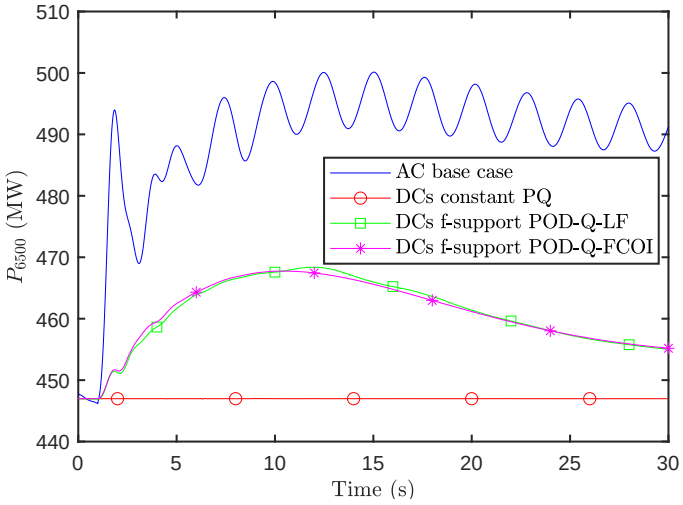


(b) Link B (5100-6500)

Figure 7.13: Active power exchange from Region 1 to Region 2 after the disconnection of a generator at bus 3300 (Region 2).

**Short circuit**

Two short circuits were simulated, one on each region of the system:

- Short circuit of duration 500 ms at bus 5103 (region 1) at $t = 1$ s.
- Short circuit of duration 500 ms at bus 8500 (region 2) at $t = 1$ s.

The purpose of these simulations is to analyse transient stability.

Figs. 7.14-7.16, show the results for the fault at Region 1, while Figs. 7.17-7.19 show the results for the fault at Region 2. Results show that transient stability is improved with DC segmentation. This can be clearly observed looking the angle difference between generators during the transient, where the angle difference during the first swing is much greater in the AC base case than in the DC-segmented cases (see Figs. 7.14-7.16 and Figs. 7.17-7.19). This is mainly due to the fact that DC segmentation decouples the two AC areas, which have large power flows between one to the other. Although supplementary controllers (FC and POD-Q) are for other applications, they contribute slightly to improve transient stability too.

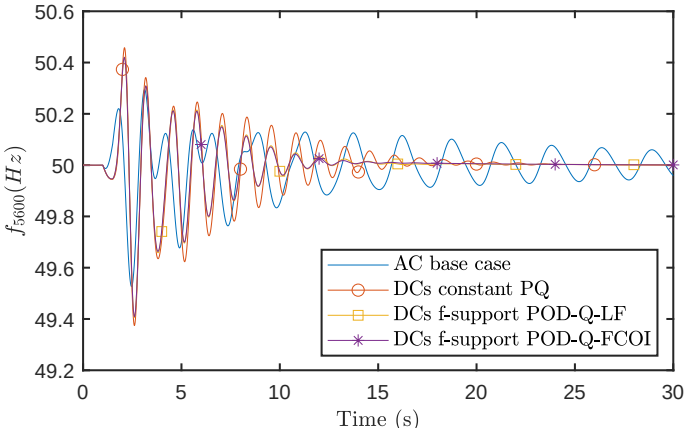


(a) Region 1

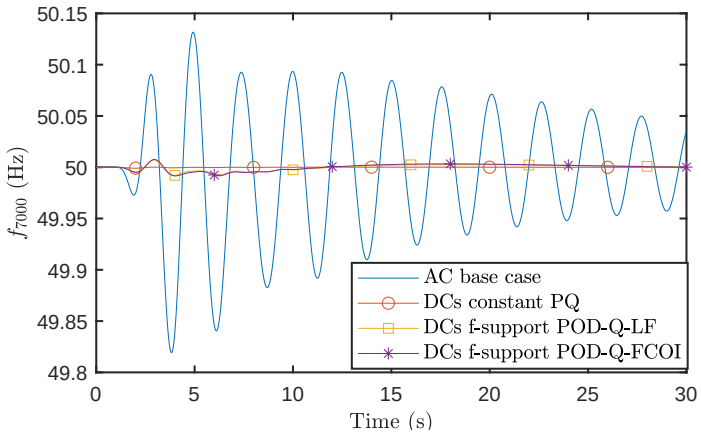


(b) Region 2

Figure 7.14: Frequency of two representative generators after a short circuit at bus 5103 (Region 1).

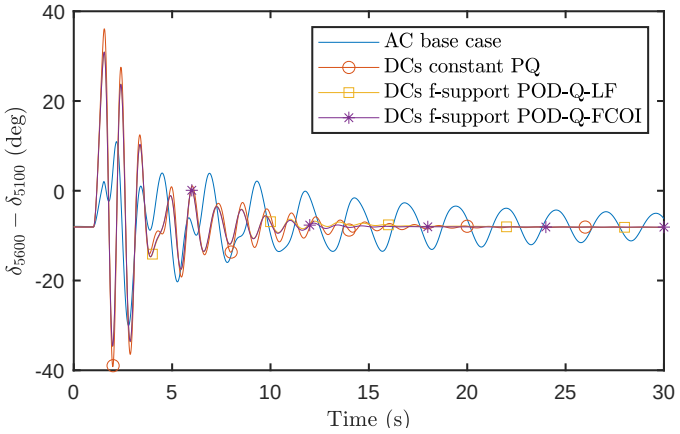


(a) Region 1

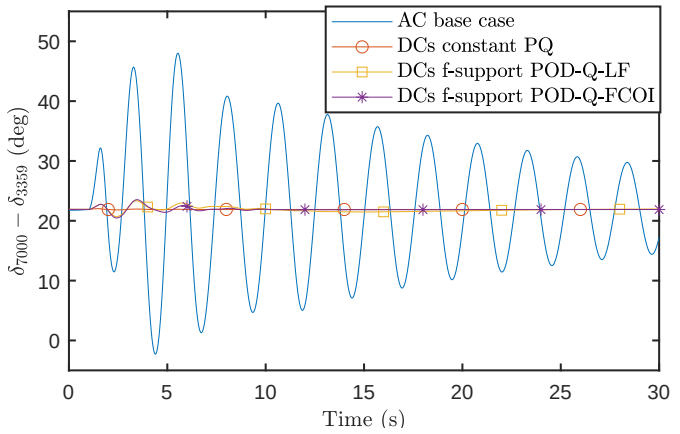


(b) Region 2

Figure 7.15: Angle difference between representative generators of a same region after a short circuit at bus 5103 (Region 1).

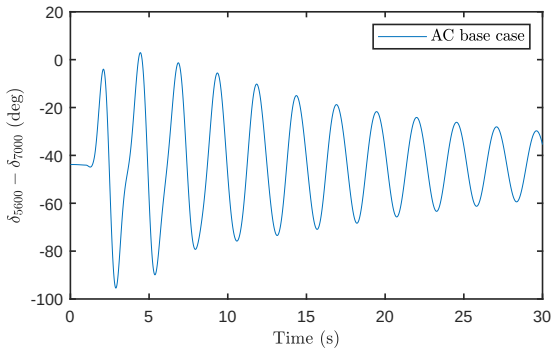


Figure 7.16: Angle difference between representative generators of the two regions after a short circuit at bus 5103 (Region 1).

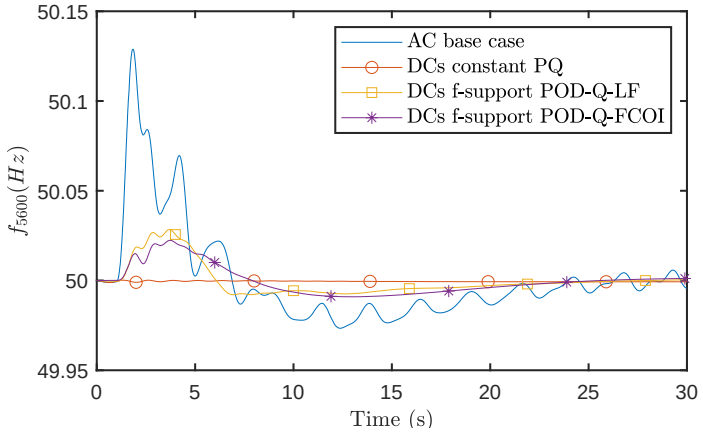


(a) Region 1

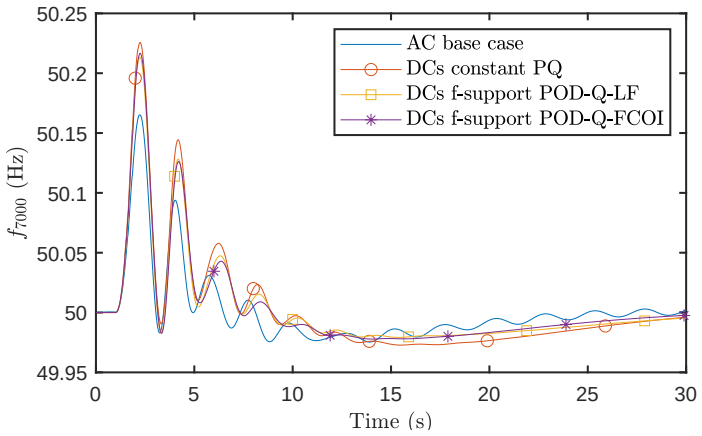


(b) Region 2

Figure 7.17: Frequency of two representative generators after a short circuit at bus 8500 (Region 2).

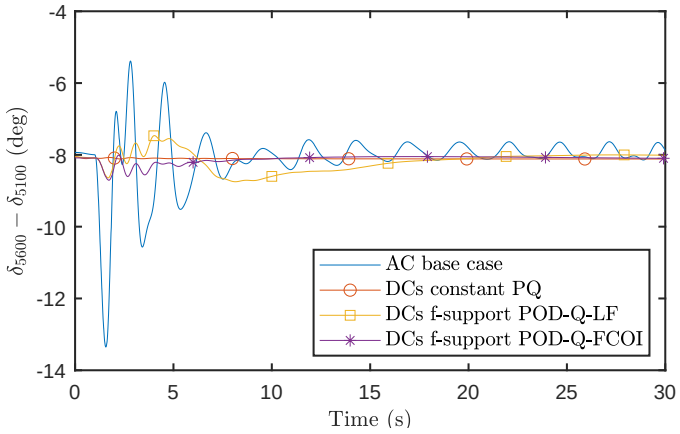


(a) Region 1

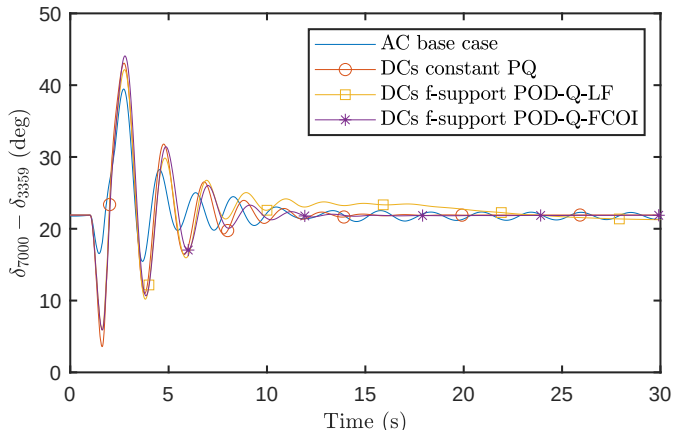


(b) Region 2

Figure 7.18: Angle difference between representative generators of a same region after a short circuit at bus 8500 (Region 2).

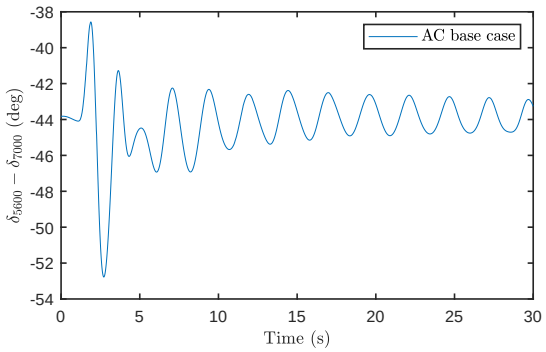


Figure 7.19: Angle difference between representative generators of the two regions after a short circuit at bus 8500 (Region 2).

### 7.3.4 Impact of communication latency

The implementation of the POD-Q-FCOI requires a communication system between the generators and the VSCs and its impact on the performance of the controller is analysed here.

Let us consider the case where the input error signal of POD-Q-FCOI of Fig. 7.3 with a communication delay reads:

$$u_i = e^{-s\tau}(\omega_{COI,i} - \omega_i) \tag{7.17}$$

where $\tau$ is the total communication delay.

The delay of (7.17) has been implemented using a first-order Padé's approximation. Realistic values of communication latency delays are analysed below ($\tau = 50$ ms and $\tau = 100$ ms).

Table 7.5 shows the main electromechanical modes of the system for DCs f-support POD-Q-FCOI for different values of communication latency delays. The modes considered are the ones of Table 7.3. Results show that the communication delays reduce the damping ratio of the target modes slightly (from 12.40% to 9.95% for mode 2 and from 15.40% to 14.37% for mode 4 with a delay of $\tau = 0.1s$) without significant impact on other modes. Therefore, results prove that POD-Q-FCOI controller is quite robust against communication latency. Independently of this, as previously discussed, since POD-Q-LF controller uses local signals and both controllers produce similar results, POD-Q-LF controller appears to be a better alternative than POD-Q-FCOI controller, for the test system used in this work.

Table 7.5: Poorly-damped electromechanical modes of the DCs f-support, POD-Q-FCOI with various communication delays.

| | No delay | | $\tau = 0.05$s | | $\tau = 0.1$s | | Region of |
|---|---|---|---|---|---|---|---|
| N0. | $\zeta$ (%) | Freq (Hz) | $\zeta$ (%) | Freq (Hz) | $\zeta$ (%) | Freq (Hz) | the mode |
| 2 | 12.40 | 0.83 | 11.14 | 0.84 | 9.95 | 0.84 | R1 |
| 3 | 12.33 | 0.88 | 12.19 | 0.88 | 12.04 | 0.88 | R2 |
| 4 | 15.40 | 0.74 | 14.86 | 0.74 | 14.37 | 0.75 | R2 |
| 5 | 12.16 | 1.07 | 12.19 | 1.07 | 12.22 | 1.07 | R2 |
| 6 | 12.48 | 1.10 | 12.65 | 1.10 | 12.79 | 1.10 | R1 |
| 7 | 16.45 | 0.47 | 17.41 | 0.48 | 18.28 | 0.48 | R2 |
| 8 | 15.61 | 0.97 | 15.10 | 0.98 | 14.11 | 0.99 | R2 |
| 9 | 20.68 | 1.31 | 20.68 | 1.31 | 20.68 | 1.31 | R1 |
| 10 | 14.55 | 1.20 | 13.84 | 1.20 | 13.18 | 1.19 | R1 |

## 7.4 Summary and conclusions

This chapter has investigated supplementary controllers for DC segmented power systems in order to improve the effects of DC segmentation. Namely, a frequency controller (FC) has been used to improve frequency stability that was initially jeopardised due to the DC segmentation. Furthermore, two power-oscillation-damping controllers for the reactive power injections of the converter stations of VSC-HVDC systems (POD-Q controllers) have been implemented in a DC-segmented system to damp intra-area modes. One POD-Q controller (POD-Q-LF) is based on local measurements, and was derived from previous work, while the the other one is based on global measurements (POD-Q-FCOI), and has been proposed in this work for the first time. Both controllers were tested and compared on the Nordic 44 test system.

The following conclusions have been obtained from the results presented in this chapter:

- DC segmentation can be very effective to suppress critical inter-area oscillation in stressed AC power systems. However, if VSC-HVDC systems are controlled with constant power: (a) overall frequency stability will be jeopardised, since each asynchronous AC cluster will have a lower amount of frequency support and inertia and (b) intra-area electromechanical oscillations in the AC clusters may have similar damping ratio to those obtained in the AC base case, with room for further improvement.

- Frequency controllers (FC) in the VSC-HVDC links of a DC-segmented system allows frequency support among the different AC clusters, improving overall frequency stability, in comparison with DC segmentation with constant power control.

- Power oscillation damping controllers for the reactive-power injections (POD-Q) in the VSC-HVDC links of a DC-segmented system can be used to damp intra-area oscillations of the asynchronous AC clusters, in addition to the mitigation of the critical inter-area oscillation due to DC segmentation. Two effective POD-Q controllers were analysed and compared: POD-Q-LF (using local measurements), based on previous proposals and POD-Q-FCOI (using global measurements), newly proposed in this work.

- POD-Q-LF (local) and POD-Q-FCOI (global) controllers produced comparable results, and the latter proved to be reasonably robust when subject to communication latencies. Nevertheless, taking into account that implementation of POD controllers using remote signals is more complex and expensive than POD controllers using local signals, POD-Q-LF controller seems to be a more practical solution than POD-Q-FCOI controller, at least for the test system considered.
- Eigenvalue sensitivities were calculated numerically using finite differences when designing POD-Q controllers in the DC-segmented power system. This approach has proved useful when no alternative was in hand. However, the robustness and numerical conditioning of this procedure has not been explored in detail.
- The use of DC segmentation, frequency support and POD-Q control brought an important improvement of the overall stability of the test system compared to the initial AC case.

# Chapter 8

# Conclusions and contributions

This PhD thesis aimed at investigating the effects of DC segmentation on power system stability and how to improve it. The work focused on (a) angle stability under small disturbances (electromechanical oscillations), (b) angle stability under large disturbances (transient stability) and (c) frequency stability.

Traditionally, AC power systems have been planned to be as large as possible in order to improve their robustness and resiliency. This PhD has analysed DC segmentation and its potential to improve power system stability. It is important to highlight that this does not mean that DC segmentation would always be a good option, however, we have shown that it may be an interesting alternative for some cases in the context of stressed large-scale power systems in which angle stability is a critical phenomenon.

This chapter summarises the conclusions and contributions of the work and suggests potential directions for future research.

## 8.1 Conclusions

The main conclusions and findings obtained in this PhD thesis are classified and summarised below.

### 8.1.1 Impact of DC segmentation on power system stability

- DC segmentation with constant power set points can improve small-signal angle stability of the system (electromechanical oscillations) by removing the inter-area oscillations without affecting the damping of the local modes.

- DC segmentation with constant power set points can also improve angle stability under large disturbances (transient stability) of the overall system by removing the inter-area synchronism constrain by decoupling the two areas.
- However, it jeopardises the overall frequency stability of the overall system.

### 8.1.2 Dominant electromechanical-oscillation paths

- The proposed algorithm for the detection of the dominant inter-area oscillation path in an AC power system (Chapter 5) is fully automated and obtains the desired path systematically.
- The proposed algorithm for the detection of the dominant inter-area-oscillation path in an AC power system (Chapter 5) showed to be useful for the DC-segmentation algorithm proposed in this PhD thesis (Chapter 6), but it could also be used for further applications on the analysis of electromechanical oscillations in power systems.

### 8.1.3 Proposed algorithm for DC segmentation to mitigate electromechanical oscillations

- The proposed algorithm obtains, systematically, a DC-segmentation scheme of the initial AC power system.
- In the resulting DC-segmented scheme, the critical inter-area oscillation of the initial AC power system is suppressed, without jeopardising the damping ratio of the intra-area modes.
- The concept of dominant inter-area oscillation path is a remarkably useful tool to determine where to segment the system with DC technology, at least when tackling electromechanical oscillations.

### 8.1.4 Supplementary controllers in DC-segmented power systems

- Frequency controllers (FCs) in the VSC-HVDC links of a DC-segmented system allows frequency support among the different AC clusters, improving overall frequency stability, in comparison with DC segmentation with constant power control.

- Power oscillation damping controllers using reactive-power injections (POD-Q) in the VSC-HVDC links of a DC-segmented system can be used to damp intra-area oscillations of the asynchronous AC clusters, in addition to the mitigation of the critical inter-area oscillation due to DC segmentation.

- POD-Q-LF controller (local), based on previous proposals, and POD-Q-FCOI controller (global), proposed in this PhD thesis were shown effective in damping intra-area modes in a DC-segmented power system. Both POD-Q controllers produced comparable results, and the latter proved to be reasonably robust when subject to communication latencies. Nevertheless, taking into account that implementation of POD controllers using remote signals is more complex and expensive than POD controllers using local signals, POD-Q-LF controller seems to be a more practical solution than POD-Q-FCOI controller, at least for the test system considered.

- The use of DC segmentation, frequency support and POD-Q control brought an important improvement of the overall stability of the test system compared to the initial AC case.

Based on the conclusions presented above, general conclusions can be illustrated and summarised in Table 8.1, which assumes a stressed large AC power system vulnerable to angle stability.

Table 8.1: DCs: DC-segmented case. EO: Electromechanical oscillations. ✗: poor results, o: intermediate results, ✓: excellent results.

| Phenomenon | AC case | DCs constant PQ | DCs f-support POD-Q-LF | DCs f-support POD-Q-FCOI |
|---|---|---|---|---|
| EO - inter-area modes | ✗ | ✓ | ✓ | ✓ |
| EO - intra-area modes | o | o | ✓ | ✓ |
| Transient stability | ✗ | ✓ | ✓ | ✓ |
| Frequency stability | ✓ | ✗ | o | o |

## 8.2 Contributions

The main scientific contributions of this PhD thesis are summarised below.

### 8.2.1 Impact of DC segmentation on power system stability

- Analysis of the impact of DC segmentation with constant power set points on electromechanical oscillations.
- Analysis of the impact of DC segmentation with constant power set points on transient stability.
- Analysis of the impact of DC segmentation with constant power set points on frequency stability.

### 8.2.2 Dominant electromechanical-oscillation paths

- Proposal of an algorithm for the detection of the dominant inter-area oscillation path in an AC power system.

### 8.2.3 An algorithm for DC segmentation to mitigate electromechanical oscillations

- Proposal of an algorithm for DC segmentation to mitigate electromechanical oscillations.
- Identification of the key aspects to be considered in DC segmentation when targeted to mitigate electromechanical oscillations.

### 8.2.4 Supplementary controllers in DC-segmented power systems

- Implementation of frequency controllers (FC) in the VSC-HVDC systems of a DC-segmented system, based on previous work, to improve frequency stability.
- Implementation of a local POD-Q controller (POD-Q-LF) in the VSC-HVDC systems of a DC-segmented system, based on previous proposals, to damp intra-area oscillations.
- Proposal and implementation of a global POD-Q controller (POD-Q-FCOI) in the VSC-HVDC systems of a DC-segmented system, to damp intra-area oscillations.

The supplementary controllers implemented in this PhD thesis are similar to those presented in previous work for VSC-HVDC systems. They have been used here to add value to DC segmentation. To the best of our knowledge, it is the first time that such controllers are implemented in the context of DC-segmentation with VSC-HVDC systems.

### 8.2.5 Modelling and simulation tools

- Modelling of VSC-HVDC systems in Dymola (used for small-signal analysis and non-linear time-domain simulation).
- Modelling of VSC-HVDC systems in SSST (used for small-signal analysis and to obtain observability factors).
- Incorporation of supplementary controllers in VSC-HVDC systems in Dymola.
- Implementation of the algorithms proposed in this PhD thesis in Matlab scripts and linking them with the information provided with the different simulation tools used.

## 8.3 Publications

**Journal papers**

- M. Robin, J. Renedo, J. C. Gonzalez-Torres, A. Garcia-Cerrada, A. Benchaib, and P. Garcia-Gonzalez, "An algorithm for DC Segmentation of AC Power Systems to Mitigate Electromechanical Oscillations," IEEE Access, vol. 11, pp. 64651–64667, 2023.
- M. Robin, J. Renedo, J. C. Gonzalez-Torres, A. Garcia-Cerrada, L. Rouco, A. Benchaib, and P. Garcia-Gonzalez, "Addressing intra-area oscillations and frequency stability after DC segmentation of a large AC power system," pre-print, arxiv: arXiv:2406.18514, pp. 1-11, 2024. [133][1]
  submitted to Journal of Modern Power Systems and Clean Energy (under review), 2024.

**Conference paper**

- M. Robin, J. Renedo, J.-C. Gonzalez-Torres, A. Garcia-Cerrada, A. Benchaib, and P. Garcia-Gonzalez, "DC segmentation: A promising solution to improve angle stability of stressed power systems," in The 17th International Conference on AC and DC Power Transmission (ACDC 2021), Online Conference, 2021, pp. 84–90.

[1] https://arxiv.org/abs/2406.18514

## 8.4 Proposals for further research

### 8.4.1 Extension and further applications of the proposed algorithm for DC segmentation of power systems

In general, the choice of investment on new VSC-HVDC links or converting AC lines into VSC-HVDC links would depend on a cost/benefit analysis. In this context, the demonstrated effect of DC segmentation of an existing power system can be one-among-others argument to be taken into account.

Further extensions of the algorithm could be investigated:

- Since the tool presented is based on a linearisation of the system in one operating point, an obvious extension of the tool would be the application to different scenarios and their selections. Nevertheless experience in real systems show that the same critical inter-area modes may be present in a good number of scenarios.
- Extension of the algorithm to tackle electromechanical oscillation taking into account more than two coherent groups of oscillating generators.
- Extension of the algorithm to damp several critical electromechanical modes.
- Since the proposed algorithm only takes into account technical aspects, a choice was made when segmenting the AC lines: they were converted into VSC-HVDC links. However, other options could also be considered, such as back-back or multi-terminal VSC-HVDC configurations. Naturally, this would require the consideration of not only technical aspects, but also a cost-benefit analysis.
- DC segmentation taking into account controllers in the VSC-HVDC links to improve power system stability. Although this aspect would not impact the choice of the DC segments, the overall stability of the DC-segmented system could be improved.

The proposed algorithm for DC segmentation (targeted to damp electromechanical oscillations) could be combined with other applications of DC segmentation:

- DC segmentation to improve transient stability (angle stability under large disturbances).

- DC segmentation taking into account frequency stability. This would mean requiring a minimum amount of primary frequency support and inertia in each synchronous AC cluster.
- DC segmentation to reduce the risk of black-outs and disturbance propagation.
- The information provided by the algorithm proposed in this work could be used to determine corrective actions. For example, considering a power system with embedded VSC-HVDC links presenting problems related to inter-area oscillations. The information provided by the algorithm could be used to identify disconnection of certain AC lines (in parallel with certain VSC-HVDC links) to obtain temporary DC-segmented configurations in emergency situations to damp inter-area oscillations.

### 8.4.2 Supplementary controllers

In this PhD thesis, the uses of active power frequency control (FC) and reactive power oscillation damping (POD-Q) targeting intra-area modes has been tested and gave satisfactory results on the stability of the DC-segmented system. However, numerous other supplementary controllers could be studied for DC segmented systems such as: AC voltage control, emergency power control, power oscillation damping on active power, synthetic inertia. Finally, if numerous supplementary controller brings stability benefits then their coordinated control should also be studied.

### 8.4.3 Further applications of the algorithm for the identification of dominant electromechanical-oscillation paths

In this PhD thesis, the proposed algorithm for the identification of the dominant electromechanical-oscillation path has been used for DC segmentation (Chapter 6). Nevertheless, it should be highlighted that this algorithm proposed could be used for other applications such as:

- Placement of phasor measurement units (PMUs) along the dominant electromechanical-oscillation path.
- Placement of different types of power oscillation control devices such as Power System Stabilizers (PSS) in synchronous machines, controllers in

renewable power plants, Energy Storage Systems (ESS), Flexible Alternating Current Transmission Systems (FACTS), or embedded HVDC systems based on Line Commutated Converters (LCC-HVDC) and VSC-HVDC.

# Bibliography


[1] "Synchronous grid of Continental Europe," *Wikipedia*, Apr. 2024.

[2] S. Akkari, "Control of a multi-terminal HVDC (MTDC) system and study of the interactions between the MTDC and the AC grids." Ph.D. dissertation, Université Paris Saclay (COmUE), France, 2016.

[3] N. Hatziargyriou, J. V. Milanovic, C. Rahmann, V. Ajjarapu, C. Cañizares, I. Erlich, D. Hill, I. Hiskens, I. Kamwa, B. Pal, P. Pourbeik, J. J. Sanchez- Gasca, A. Stankovic, T. Van Cutsem, V. Vittal, and C. Vournas, "Stability Definitions and Characterization of Dynamic Behavior in Systems with High Penetration of Power Electronic Interfaced Technologies," IEEE Power & Energy Society, Tech. Rep. PES-TR7, Apr. 2020.

[4] N. Hatziargyriou, J. Milanovic, C. Rahmann, V. Ajjarapu, C. Canizares, I. Erlich, D. Hill, I. Hiskens, I. Kamwa, B. Pal, P. Pourbeik, J. Sanchez-Gasca, A. Stankovic, T. Van Cutsem, V. Vittal, and C. Vournas, "Definition and Classification of Power System Stability – Revisited & Extended," *IEEE Transactions on Power Systems*, vol. 36, no. 4, pp. 3271–3281, Jul. 2021.

[5] B. Luscan, S. Bacha, A. Benchaib, A. Bertinato, L. Chedot, J. C. Gonzalez-Torres, S. Poullain, M. Romero-Rodriguez, and K. Shinoda, "A Vision of HVDC Key Role Toward Fault-Tolerant and Stable AC/DC Grids," *IEEE Journal of Emerging and Selected Topics in Power Electronics*, vol. 9, no. 6, pp. 7471–7485, Dec. 2021.

[6] D. van Hertem, O. Gomis-Bellmunt, and J. Liang, Eds., *HVDC Grids: For Offshore and Supergrid of the Future*, ser. IEEE Press Series on Power Engineering. Piscataway, NJ : Hoboken, New Jersey: IEEE Press ; Wiley, 2016.

[7] D. Van Hertem and M. Ghandhari, "Multi-terminal VSC HVDC for the European supergrid: Obstacles," *Renewable and Sustainable Energy Reviews*, vol. 14, no. 9, pp. 3156–3163, Dec. 2010.

[8] A. Lesnicar and R. Marquardt, "An innovative modular multilevel converter topology suitable for a wide power range," in *2003 IEEE Bologna Power Tech Conference Proceedings,*, vol. 3. Bologna, Italy: IEEE, 2003, pp. 272–277.

[9] S. Kouro, M. Malinowski, K. Gopakumar, J. Pou, L. G. Franquelo, Bin Wu, J. Rodriguez, M. A. Pérez, and J. I. Leon, "Recent Advances and Industrial Applications of Multilevel Converters," *IEEE Transactions on Industrial Electronics*, vol. 57, no. 8, pp. 2553–2580, Aug. 2010.

[10] K. Sharifabadi, L. Harnefors, N. Hans-Peter, S. Norrga, and R. Teodorescu, *Design, Control, and Application of Modular Multilevel Converters for HVDC Transmission Systems.* John Wiley & Sons, Chinchester, UK, 2016.

[11] J. Rocabert, A. Luna, F. Blaabjerg, and P. Rodríguez, "Control of Power Converters in AC Microgrids," *IEEE Transactions on Power Electronics*, vol. 27, no. 11, pp. 4734–4749, Nov. 2012.

[12] F. Milano, F. Dorfler, G. Hug, D. J. Hill, and G. Verbic, "Foundations and Challenges of Low-Inertia Systems (Invited Paper)," in *2018 Power Systems Computation Conference (PSCC).* Dublin: IEEE, Jun. 2018, pp. 1–25.

[13] M. Paolone, T. Gaunt, X. Guillaud, M. Liserre, S. Meliopoulos, A. Monti, T. Van Cutsem, V. Vittal, and C. Vournas, "Fundamentals of power systems modelling in the presence of converter-interfaced generation," *Electric Power Systems Research*, vol. 189, p. 106811, Dec. 2020.

[14] C. Cardozo, T. Prevost, S.-H. Huang, J. Lu, N. Modi, M. Hishida, X. Li, A. Abdalrahman, P. Samuelsson, T. V. Cutsem, Y. Laba, Y. Lamrani, F. Colas, and X. Guillaud, "Promises and Challenges of Grid Forming: Transmission System Operator, Manufacturer and Academic View Points," in *Proc. {Power} Systems Computation Conference ({PSCC}), Paris, France*, 2024, pp. 1–25.

[15] J. L. Domínguez-García, O. Gomis-Bellmunt, F. D. Bianchi, and A. Sumper, "Power oscillation damping supported by wind power: A review," *Renewable and Sustainable Energy Reviews*, vol. 16, no. 7, pp. 4994–5006, Sep. 2012.

[16] L. M. Castro and E. Acha, "On the Provision of Frequency Regulation in Low Inertia AC Grids Using HVDC Systems," *IEEE Transactions on Smart Grid*, vol. 7, no. 6, pp. 2680–2690, Nov. 2016.

[17] R. Lemaire, "HVDC-VSC Newsletter," May 2024.

[18] O. Stanojev, J. Garrison, S. Hedtke, C. M. Franck, and T. Demiray, "Benefit Analysis of a Hybrid HVAC/HVDC Transmission Line: A Swiss Case Study," in *2019 IEEE Milan PowerTech*. Milan, Italy: IEEE, Jun. 2019, pp. 1–6.

[19] D. Hart, A. Xemard, S. Poullain, Z. Rubinic, T. Dolenc, K. Pavic, I. Uglesic, V. Milardic, G. Levacic, and M. Mesic, "Transformation of an AC transmission line into a DC transmission line: A study case," in *CIGRE International Symposium 2021 "Reshaping the Electric Power System Infrastructure"*. Ljubljana: CIGRE, Jun. 2021, pp. 1–17.

[20] P. Kundur, J. Paserba, V. Ajjarapu, G. Andersson, A. Bose, C. Canizares, N. Hatziargyriou, D. Hill, A. Stankovic, C. Taylor, T. Van Cutsem, and V. Vittal, "Definition and Classification of Power System Stability IEEE/CIGRE Joint Task Force on Stability Terms and Definitions," *IEEE Transactions on Power Systems*, vol. 19, no. 3, pp. 1387–1401, Aug. 2004.

[21] ENTSO-E, "Continental Europe Synchronous Area Separation on 24 July 2021," ENTSO-E, Brussels, Belgium, Tech. Rep., Nov. 2021.

[22] Project Group Turkey, "Report on Blackout in Turkey on 31st March 2015," TEIAS, ENTSO-E, Brussels, Belgium, Tech. Rep., 2015.

[23] ENTSO-E, "Analysis of CE Inter-Area Oscillations of 1st December 2016," ENTSO-E, Brussels, Belgium, SG SPD REPORT, 2017.

[24] P. Kundur, *Power System Stability And Control*. McGraw Hill Education, 1993.

[25] L. Rouco, "Coordinated design of multiple controllers for damping power system oscillations," *International Journal of Electrical Power & Energy Systems*, vol. 23, no. 7, pp. 517–530, Oct. 2001.

[26] K. Uhlen, L. Vanfretti, M. M. De Oliveira, V. H. Aarstrand, and J. O. Gjerde, "Wide-Area Power Oscillation Damper implementation and testing in the Norwegian transmission network," in *2012 IEEE Power and Energy Society General Meeting*. San Diego, CA: IEEE, Jul. 2012, pp. 1–7.

[27] A. M. Vural, "Contribution of high voltage direct current transmission systems to inter-area oscillation damping: A review," *Renewable and Sustainable Energy Reviews*, vol. 57, pp. 892–915, May 2016.

[28] L. Sigrist, E. Lobato, F. Echavarren, I. Egido, and L. Rouco, *Island Power Systems*. CRC Press - Taylor and Francis Group, Boca Raton, FL, USA, 2016.

[29] B. A. Carreras, D. E. Newman, and I. Dobson, "Does size matter?" *Chaos: An Interdisciplinary Journal of Nonlinear Science*, vol. 24, no. 2, p. 023104, Jun. 2014.

[30] H. K. Clark, M. M. El-Gasseir, H. D. Kenneth Epp, and A.-A. Edris, "The application of segmentation and grid shock absorber concept for reliable power grids," in *2008 12th International Middle-East Power System Conference*. Aswan, Egypt: IEEE, Mar. 2008, pp. 34–38.

[31] ENTSO-E, "HVDC Links in System Operations," ENTSO-E, Brussels, Belgium, Technical Paper, Dec. 2019.

[32] H. Clark, A.-A. Edris, M. El-Gasseir, K. Epp, A. Isaacs, and D. Woodford, "Softening the blow of disturbance," *IEEE power & energy magazine*, vol. vol. 6, no. no. 1, pp. 30–41, 2008.

[33] "Electrical interconnection between Baixas - Santa Llogaia | Drupal," https://www.inelfe.eu/en/projects/baixas-santa-llogaia, Jun. 2024.

[34] "The electricity interconnection across the Biscay Gulf | Drupal," https://www.inelfe.eu/en/projects/bay-biscay, Jun. 2024.

[35] P. Fairley, "Why Southern China broke up its power grid," *IEEE SPECTRUM*, pp. 13–14, Dec. 2016.

[36] X. Fang and J. H. Chow, "BTB DC link modeling, control, and application in the segmentation of AC interconnections," in *2009 IEEE Power & Energy Society General Meeting*. Calgary, Canada: IEEE, Jul. 2009, pp. 1–7.

[37] U. T. Shami, R. Naeem, and M. S. Chaudhary, "Analysis of Different Power Grid Segmentation and Transmission Schemes for Power System Security Improvement," *University of Engineering and Technology Taxila. Technical Journal*, vol. 20, no. I, pp. 39–49, 2015.

[38] O. A. Mousavi, L. Bizumic, and R. Cherkaoui, "Assessment of HVDC grid segmentation for reducing the risk of cascading outages and blackouts," in *2013 IREP Symposium Bulk Power System Dynamics and Control - IX Optimization, Security and Control of the Emerging Power Grid*. Rethymno, Greece: IEEE, Aug. 2013, pp. 1–10.

[39] D. Gomila, B. Carreras, J. Reynolds-Barredo, P. Colet, and O. Gomis-Bellmunt, "Analysis of the blackout risk reduction when segmenting large power systems using lines with controllable power flow," *International Journal of Electrical Power & Energy Systems*, vol. 148, p. 108947, Jun. 2023.

[40] M. El-Gasseir and H. D. Kenneth Epp, "Electricity Marketoriented Dc-Segmentation Design And Optimial Scheduling For Electrical Power Transmission," US Patent US 2012/0 143 388A1, 2012.

[41] R. G. Roshanagh and S. N. Ravadanegh, "A way to evaluate segmentation: An examination of AC line elimination in a parallel AC/DC transmission system," in *2013 21st Iranian Conference on Electrical Engineering (ICEE)*. Mashhad, Iran: IEEE, May 2013, pp. 1–4.

[42] B. Cheng, Z. Xu, and W. Xu, "Optimal DC-Segmentation for Multi-Infeed HVDC Systems Based on Stability Performance," *IEEE Transactions on Power Systems*, vol. 31, no. 3, pp. 2445–2454, May 2016.

[43] Y. Chompoobutrgool and L. Vanfretti, "Identification of Power System Dominant Inter-Area Oscillation Paths," *IEEE Transactions on Power Systems*, vol. 28, no. 3, pp. 2798–2807, Aug. 2013.

[44] O. Gomis-Bellmunt, E. Sanchez-Sanchez, J. Arevalo-Soler, and E. Prieto-Araujo, "Principles of operation of grids of DC and AC

subgrids interconnected by power converters," *IEEE Transactions on Power Delivery*, vol. 36, no. 2, pp. 1107–1117, Apr. 2021.

[45] J. A. Soler, D. Groß, E. P. Araujo, and O. G. Bellmunt, "Interconnecting Power Converter Control Role Assignment in Grids With Multiple AC and DC Subgrids," *IEEE Transactions on Power Delivery*, vol. 38, no. 3, pp. 2058–2071, Jun. 2023.

[46] S. Pirooz Azad, R. Iravani, and J. E. Tate, "Dynamic Stability Enhancement of a DC-Segmented AC Power System Via HVDC Operating-Point Adjustment," *IEEE Transactions on Power Delivery*, vol. 30, no. 2, pp. 657–665, Apr. 2015.

[47] ——, "Stability Enhancement of a DC-Segmented AC Power System," *IEEE Transactions on Power Delivery*, vol. 30, no. 2, pp. 737–745, Apr. 2015.

[48] M. Klein, G. J. Rogers, and P. Kundur, "A fundamental study of inter-area oscillations in power systems," *IEEE Transactions on Power Systems*, vol. 6, no. 3, pp. 914–921, Aug./1991.

[49] R. Shah, N. Mithulananthan, and K. Y. Lee, "Large-Scale PV Plant With a Robust Controller Considering Power Oscillation Damping," *IEEE Transactions on Energy Conversion*, vol. 28, no. 1, pp. 106–116, Mar. 2013.

[50] N. Jankovic, J. Roldan-Perez, M. Prodanovic, J. A. Suul, S. D'Arco, and L. R. Rodriguez, "Power oscillation damping method suitable for network reconfigurations based on converter interfaced generation and combined use of active and reactive powers," *International Journal of Electrical Power & Energy Systems*, vol. 149, p. 109010, Jul. 2023.

[51] N. Mithulananthan, C. Canizares, J. Reeve, and G. Rogers, "Comparison of PSS, SVC, and STATCOM controllers for damping power system oscillations," *IEEE Transactions on Power Systems*, vol. 18, no. 2, pp. 786–792, May 2003.

[52] T. Smed and G. Andersson, "Utilizing HVDC to damp power oscillations," *IEEE Transactions on Power Delivery*, vol. 8, no. 2, pp. 620–627, Apr. 1993.

[53] B. J. Pierre, F. Wilches-Bernal, D. A. Schoenwald, R. T. Elliott, D. J. Trudnowski, R. H. Byrne, and J. C. Neely, "Design of the Pacific DC Intertie Wide Area Damping Controller," *IEEE Transactions on Power Systems*, vol. 34, no. 5, pp. 3594–3604, Sep. 2019.

[54] M. A. Elizondo, R. Fan, H. Kirkham, M. Ghosal, F. Wilches-Bernal, D. Schoenwald, and J. Lian, "Interarea Oscillation Damping Control Using High-Voltage DC Transmission: A Survey," *IEEE Transactions on Power Systems*, vol. 33, no. 6, pp. 6915–6923, Nov. 2018.

[55] M. Hadjikypris and V. Terzija, "Active power modulation assisting controller scheme implemented on a VSC-HVDC link establishing effective damping of low frequency power oscillations," in *2014 IEEE International Energy Conference (ENERGYCON)*. Cavtat, Croatia: IEEE, May 2014, pp. 295–302.

[56] Y. Pipelzadeh, B. Chaudhuri, and T. C. Green, "Control Coordination Within a VSC HVDC Link for Power Oscillation Damping: A Robust Decentralized Approach Using Homotopy," *IEEE Transactions on Control Systems Technology*, vol. 21, no. 4, pp. 1270–1279, Jul. 2013.

[57] R. Preece, J. V. Milanovic, A. M. Almutairi, and O. Marjanovic, "Damping of inter-area oscillations in mixed AC/DC networks using WAMS based supplementary controller," *IEEE Transactions on Power Systems*, vol. 28, no. 2, pp. 1160–1169, May 2013.

[58] P. Agnihotri, A. M. Kulkarni, A. M. Gole, B. A. Archer, and T. Weekes, "A Robust Wide-Area Measurement-Based Damping Controller for Networks With Embedded Multiterminal and Multiinfeed HVDC Links," *IEEE Transactions on Power Systems*, vol. 32, no. 5, pp. 3884–3892, Sep. 2017.

[59] J. Gonzalez-Torres, J. Mermet-Guyennet, S. Silvant, and A. Benchaib, "Power system stability enhancement via VSC-HVDC control using remote signals: Application on the Nordic 44-bus test system," in *15th IET International Conference on AC and DC Power Transmission (ACDC)*, Coventry, UK, 2019, pp. 1–6.

[60] Y. Xing, E. Kamal, B. Marinescu, and F. Xavier, "Advanced control to damp power oscillations with VSC-HVDC links inserted in meshed AC grids," *International Transactions on Electrical Energy Systems*, vol. 31, no. 12, pp. 1–22, Dec. 2021.

[61] Y. Dong, Y. Zhao, K. Alshuaibi, C. Zhang, Y. Liu, L. Zhu, E. Farantatos, K. Sun, B. Marshall, M. Rahman, O. Adeuyi, S. Marshall, and I. L. Cowan, "Adaptive Power Oscillation Damping Control via VSC-HVDC for the Great Britain Power Grid," in *2023 IEEE Power & Energy Society Innovative Smart Grid Technologies Conference (ISGT)*. Washington, DC, USA: IEEE, Jan. 2023, pp. 1–5.

[62] J. Bola, R. Rivas, R. Fernández-Alonso, G. Pérez, J. Hidalgo, LM. Coronado, C. Longas, S. Sanz, G. Lemarchand, and J. Roguin, "Operational experience of new Spain-France HVDC interconnection," in *Proceedings of the CIGRE Session, Paper B4–117*, Paris, France, 2016, pp. 1–13.

[63] J. Renedo, A. Diaz-García, G. Torresan, E. Lorenzo Cabrera, A. A. Cordón, S. Sanz Verdugo, J. Peiró, J. Pérez Castro, G. Calvo, A. Hernández Sautua, A. Petit, H. Oukhayi, S. Akkari, and H. Saad, "Tests on the POD-P controller of INELFE Spain-France VSC-HVDC interconnector," in *Proc. CIGRE B4 International SC Meeting and Colloquium, Vienna, Austria, 11-15 Sep*, 2023, pp. 1–13.

[64] L. Harnefors, N. Johansson, L. Zhang, and B. Berggren, "Interarea Oscillation Damping Using Active-Power Modulation of Multiterminal HVDC Transmissions," *IEEE Transactions on Power Systems*, vol. 29, no. 5, pp. 2529–2538, Sep. 2014.

[65] R. Eriksson, "A New Control Structure for Multiterminal DC Grids to Damp Interarea Oscillations," *IEEE Transactions on Power Delivery*, vol. 31, no. 3, pp. 990–998, Jun. 2016.

[66] J. Renedo, A. Garcia-Cerrada, L. Rouco, and L. Sigrist, "Coordinated Design of Supplementary Controllers in VSC-HVDC Multi-Terminal Systems to Damp Electromechanical Oscillations," *IEEE Transactions on Power Systems*, vol. 36, no. 1, pp. 712–721, Jan. 2021.

[67] M. Ndreko, A. Van Der Meer, B. Rawn, and M. Gibescu, "Damping Of Power System Oscillations by VSC-HVDC Multi-Terminal Transmission Networks," *WP 6.1. NSTG Project Technical Report, Part I, Delft University of Technology*, 2013.

[68] F. O. Resende, M. H. Vasconcelos, and J. A. Pecas Lopes, "Simultaneous tuning of power system stabilizers installed in the VSC-based

MTDC networks of large offshore wind farms," in *2014 Power Systems Computation Conference*. Wroclaw: IEEE, Aug. 2014, pp. 1–7.

[69] C. Barker, R. Whitehouse, A. Adamczyk, and G. Soto, "Low Frequency Active Power Oscillation Damping Using a MMCVSC HVDC link," in *13th IET International Conference on AC and DC Power Transmission (ACDC 2017)*. Manchester, UK: Institution of Engineering and Technology, 2017, pp. 12 (6 .)–12 (6 .).

[70] A. Rodriguez-Cabero, J. Roldan-Perez, M. Prodanovic, J. A. Suul, and S. D'Arco, "Coupling of AC Grids via VSC-HVDC Interconnections for Oscillation Damping Based on Differential and Common Power Control," *IEEE Transactions on Power Electronics*, vol. 35, no. 6, pp. 6548–6558, Jun. 2020.

[71] S. G. Johansson, G. Asplund, E. Jansson, and R. Rudervall, "POWER SYSTEM STABILITY BENEFITS WITH VSC DC-TRANSMISSION SYSTEMS," in *Proc. CIGRE Session, Paris, France*, 2004, pp. 1–8.

[72] H. Latorre, M. Ghandhari, and L. Söder, "Active and reactive power control of a VSC-HVdc," *Electric Power Systems Research*, vol. 78, no. 10, pp. 1756–1763, Oct. 2008.

[73] A. Fuchs, M. Imhof, T. Demiray, and M. Morari, "Stabilization of Large Power Systems Using VSC–HVDC and Model Predictive Control," *IEEE Transactions on Power Delivery*, vol. 29, no. 1, pp. 480–488, Feb. 2014.

[74] L. Sigrist, F. Echavarren, L. Rouco, and P. Panciatici, "A fundamental study on the impact of HVDC lines on transient stability of power systems," in *2015 IEEE Eindhoven PowerTech*. Eindhoven, Netherlands: IEEE, Jun. 2015, pp. 1–6.

[75] R. Eriksson, "Coordinated Control of Multiterminal DC Grid Power Injections for Improved Rotor-Angle Stability Based on Lyapunov Theory," *IEEE Transactions on Power Delivery*, vol. 29, no. 4, pp. 1789–1797, Aug. 2014.

[76] G. Tang, Z. Xu, H. Dong, and Q. Xu, "Sliding Mode Robust Control Based Active-Power Modulation of Multi-Terminal HVDC Transmissions," *IEEE Transactions on Power Systems*, vol. 31, no. 2, pp. 1614–1623, Mar. 2016.

[77] J. Renedo, A. Garcia-Cerrada, and L. Rouco, "Active Power Control Strategies for Transient Stability Enhancement of AC/DC Grids With VSC-HVDC Multi-Terminal Systems," *IEEE Transactions on Power Systems*, vol. 31, no. 6, pp. 4595–4604, Nov. 2016.

[78] ——, "Reactive-Power Coordination in VSC-HVDC Multi-Terminal Systems for Transient Stability Improvement," *IEEE Transactions on Power Systems*, vol. 32, no. 5, pp. 3758–3767, Sep. 2017.

[79] J. Renedo, L. Rouco, A. García-Cerrada, and L. Sigrist, "A communication-free reactive-power control strategy in VSC-HVDC multi-terminal systems to improve transient stability," *Electric Power Systems Research*, vol. 174, p. 105854, Sep. 2019.

[80] J. C. Gonzalez-Torres, G. Damm, V. Costan, A. Benchaib, and F. Lamnabhi-Lagarrigue, "A Novel Distributed Supplementary Control of Multi-Terminal VSC-HVDC Grids for Rotor Angle Stability Enhancement of AC/DC Systems," *IEEE Transactions on Power Systems*, vol. 36, no. 1, pp. 623–634, Jan. 2021.

[81] X. Fan, J. Shu, and B. Zhang, "Coordinated Control of DC Grid and Offshore Wind Farms to Improve Rotor-Angle Stability," *IEEE Transactions on Power Systems*, vol. 33, no. 4, pp. 4625–4633, Jul. 2018.

[82] O. Kotb, M. Ghandhari, J. Renedo, L. Rouco, and R. Eriksson, "On the design and placement of a supplementary damping controller in an embedded VSC-MTDC network," in *2017 IEEE PES Innovative Smart Grid Technologies Conference Europe (ISGT-Europe)*. Torino, Italy: IEEE, Sep. 2017, pp. 1–6.

[83] B. Silva, C. L. Moreira, L. Seca, Y. Phulpin, and J. A. Pecas Lopes, "Provision of Inertial and Primary Frequency Control Services Using Offshore Multiterminal HVDC Networks," *IEEE Transactions on Sustainable Energy*, vol. 3, no. 4, pp. 800–808, Oct. 2012.

[84] I. Martinez Sanz, B. Chaudhuri, and G. Strbac, "Inertial Response From Offshore Wind Farms Connected Through DC Grids," *IEEE Transactions on Power Systems*, vol. 30, no. 3, pp. 1518–1527, May 2015.

[85] T. M. Haileselassie and K. Uhlen, "Primary frequency control of remote grids connected by multi-terminal HVDC," in *IEEE PES General Meeting*. Minneapolis, MN: IEEE, Jul. 2010, pp. 1–6.

[86] N. R. Chaudhuri, R. Majumder, and B. Chaudhuri, "System Frequency Support Through Multi-Terminal DC (MTDC) Grids," *IEEE Transactions on Power Systems*, vol. 28, no. 1, pp. 347–356, Feb. 2013.

[87] S. Akkari, J. Dai, M. Petit, and X. Guillaud, "Interaction between the voltage-droop and the frequency-droop control for multi-terminal HVDC systems," *IET Generation, Transmission & Distribution*, vol. 10, no. 6, pp. 1345–1352, Apr. 2016.

[88] A. Sarlette, J. Dai, Y. Phulpin, and D. Ernst, "Cooperative frequency control with a multi-terminal high-voltage DC network," *Automatica*, vol. 48, no. 12, pp. 3128–3134, Dec. 2012.

[89] D. Obradovic, M. Oluic, R. Eriksson, and M. Ghandhari, "Supplementary Power Control of an HVDC System and Its Impact on Electromechanical Dynamics," *IEEE Transactions on Power Systems*, vol. 36, no. 5, pp. 4599–4610, Sep. 2021.

[90] F. Milano, *Power System Modelling and Scripting*. Springer Science & Business Media, Sep. 2010.

[91] L. Vanfretti, T. Rabuzin, M. Baudette, and M. Murad, "iTesla Power Systems Library (iPSL): A Modelica library for phasor time-domain simulations," *SoftwareX*, vol. 5, pp. 84–88, 2016.

[92] M. Baudette, M. Castro, T. Rabuzin, J. Lavenius, T. Bogodorova, and L. Vanfretti, "OpenIPSL: Open-Instance Power System Library — Update 1.5 to "iTesla Power Systems Library (iPSL): A Modelica library for phasor time-domain simulations"," *SoftwareX*, vol. 7, pp. 34–36, Jan. 2018.

[93] J. Freytes, L. Papangelis, H. Saad, P. Rault, T. Van Cutsem, and X. Guillaud, "On the modeling of MMC for use in large scale dynamic simulations," in *2016 Power Systems Computation Conference (PSCC)*. Genoa, Italy: IEEE, Jun. 2016, pp. 1–7.

[94] J. C. Gonzalez-Torres, R. Mourouvin, K. Shinoda, A. Zama, and A. Benchaib, "A simplified approach to model grid-forming controlled

MMCs in power system stability studies," in *2021 IEEE PES Innovative Smart Grid Technologies Europe (ISGT Europe)*. Espoo, Finland: IEEE, Oct. 2021, pp. 01–06.

[95] S. Cole, J. Beerten, and R. Belmans, "Generalized Dynamic VSC MTDC Model for Power System Stability Studies," *IEEE Transactions on Power Systems*, vol. 25, no. 3, pp. 1655–1662, Aug. 2010.

[96] S. Cole and R. Belmans, "A proposal for standard VSC HVDC dynamic models in power system stability studies," *Electric Power Systems Research*, vol. 81, no. 4, pp. 967–973, Apr. 2011.

[97] ——, "MatDyn, A New Matlab-Based Toolbox for Power System Dynamic Simulation," *IEEE Transactions on Power Systems*, vol. 26, no. 3, pp. 1129–1136, 2011.

[98] J. Beerten, S. Cole, and R. Belmans, "Modeling of Multi-Terminal VSC HVDC Systems With Distributed DC Voltage Control," *IEEE Transactions on Power Systems*, vol. 29, no. 1, pp. 34–42, Jan. 2014.

[99] S. Liu, Z. Xu, W. Hua, G. Tang, and Y. Xue, "Electromechanical Transient Modeling of Modular Multilevel Converter Based Multi-Terminal HVDC Systems," *IEEE Transactions on Power Systems*, vol. 29, no. 1, pp. 72–83, Jan. 2014.

[100] J. Renedo, A. Garcia-Cerrada, L. Rouco, L. Sigrist, I. Egido, and S. Sanz Verdugo, "Development of a PSS/E tool for power-flow calculation and dynamic simulation of VSC-HVDC multi-terminal systems," in *13th IET International Conference on AC and DC Power Transmission (ACDC 2017)*. Manchester, UK: Institution of Engineering and Technology, 2017, pp. 1–6.

[101] R. Wachal, A. Jindal, S. Dennetière, H. Saad, O. Rui, S. Cole, M. Barnes, L. Zhang, Z. Song, J. Jardini, J. C. Garcia, F. Mosallat, H. Suriyaarachich, P. Le-Huy, A. Totterdell, L. Zeni, S. Kodsi, T. Deepak, P. Thepparat, T. Beddard, J. Velasquez, S. D'Arco, A. Morales, Y. Kono, T. K. Vrana, and Y. Yang, "Guide for the Development of Models for HVDC Converters in a HVDC Grid," CIGRE, Tech. Rep., 2014.

[102] G. Bergna-Diaz, J. Freytes, X. Guillaud, S. D'Arco, and J. A. Suul, "Generalized Voltage-Based State-Space Modeling of Modular Multi-

level Converters With Constant Equilibrium in Steady State," *IEEE Journal of Emerging and Selected Topics in Power Electronics*, vol. 6, no. 2, pp. 707–725, Jun. 2018.

[103] O. C. Sakinci and J. Beerten, "Equivalent Multiple $dq$-Frame Model of the MMC Using Dynamic Phasor Theory in the $\alpha \beta z$-Frame," *IEEE Transactions on Power Delivery*, vol. 35, no. 6, pp. 2916–2927, Dec. 2020.

[104] H. A. Saad, "Modelisation et simulation d'une liaison HVDC de type VSC-MMC," Ph.D. dissertation, Ecole Polytechnique de Montréal, Montréal, Canada, 2015.

[105] Y. Liao, X. Wang, X. Yue, and H. Gong, "Harmonic Transfer-Function Model of Three-Phase Synchronous Reference Frame PLL under Unbalanced Grid Conditions," in *2019 IEEE Applied Power Electronics Conference and Exposition (APEC)*. Anaheim, CA, USA: IEEE, Mar. 2019, pp. 58–65.

[106] X.-P. Zhang, "Multiterminal Voltage-Sourced Converter-Based HVDC Models for Power Flow Analysis," *IEEE Transactions on Power Systems*, vol. 19, no. 4, pp. 1877–1884, Nov. 2004.

[107] M. Baradar and M. Ghandhari, "A Multi-Option Unified Power Flow Approach for Hybrid AC/DC Grids Incorporating Multi-Terminal VSC-HVDC," *IEEE Transactions on Power Systems*, vol. 28, no. 3, pp. 2376–2383, Aug. 2013.

[108] E. Acha, B. Kazemtabrizi, and L. M. Castro, "A New VSC-HVDC Model for Power Flows Using the Newton-Raphson Method," *IEEE Transactions on Power Systems*, vol. 28, no. 3, pp. 2602–2612, Aug. 2013.

[109] E. Acha and L. M. Castro, "A generalized frame of reference for the incorporation of, multi-terminal VSC-HVDC systems in power flow solutions," *Electric Power Systems Research*, vol. 136, pp. 415–424, Jul. 2016.

[110] J. Beerten, S. Cole, and R. Belmans, "Generalized Steady-State VSC MTDC Model for Sequential AC/DC Power Flow Algorithms," *IEEE Transactions on Power Systems*, vol. 27, no. 2, pp. 821–829, May 2012.

[111] R. Teixeira Pinto, C. Leon-Ramirez, M. Aragues-Penalba, A. Sumper, and E. Sorrentino, "A fast methodology for solving power flows in hybrid ac/dc networks: The European North Sea Supergrid case study," in *Proc. International Exhibition and Conference for Power Electronics, Intelligent Motion, Renewable Energy and Energy Management (PCIM Europe), Nuremberg, Germany*, 2016, pp. 1–8.

[112] J.-C. Fernandez-Perez, F. M. Echavarren Cerezo, and L. R. Rodriguez, "On the Convergence of the Sequential Power Flow for Multiterminal VSC AC/DC Systems," *IEEE Transactions on Power Systems*, vol. 33, no. 2, pp. 1768–1776, Mar. 2018.

[113] J.-C. Fernandez-Perez, F. M. Echavarren Cerezo, and L. Rouco Rodriguez, "Linear Power Flow Algorithm With Losses for Multi-Terminal VSC AC/DC Power Systems," *IEEE Transactions on Power Systems*, vol. 37, no. 3, pp. 1739–1749, May 2022.

[114] "Dymola," https://www.3ds.com/products/catia/dymola, May 2023.

[115] "Modelica," https://modelica.org/.

[116] G. Bakhos, S. Bacha, J.-C. Gonzalez-Torres, L. Vanfretti, A. Benchaib, J. Dai, and K. Shinoda, "Hybrid Ac/Dc Power System Stability: An Attempt of Global Approach," 2024.

[117] G. Bakhos, K. Shinoda, J. C. Gonzalez-Torres, A. Benchaib, L. Vanfretti, and S. Bacha, "Aspects of stability issues of HVAC/HVDC coupled grids," in *2022 24th European Conference on Power Electronics and Applications (EPE'22 ECCE Europe)*, Sep. 2022, pp. 1–10.

[118] L. Rouco, "Small signal stability toolbox (SSST): Reference Manual," *Instituto de Investigación Tecnológica (IIT), ETSI ICAI, Universidad Pontificia Comillas*, 2002.

[119] L. Rouco, I. J. Pérez-Arriaga, R. Criado, and J. Soto, "A computer package for analysis of small signal stability in large electric power systems," in *Proceedings of the 11th Power Systems Computations Conference*, 1993, pp. 1141–1148.

[120] J. Renedo, L. Sigrist, A. Garcia-Cerrada, and L. Rouco, "Modelling of VSC-HVDC multi-terminal systems for small-signal angle stability analysis," in *15th IET International Conference on AC and DC Power*

*Transmission (ACDC 2019)*. Coventry, UK: Institution of Engineering and Technology, 2019, pp. 1–7.

[121] I. J. Perez-Arriaga,, G. Verghese, and F. Schweppe, "Selective Modal Analysis with Applications to Electric Power Systems, PART I: Heuristic Introduction," *IEEE Transactions on Power Apparatus and Systems*, vol. PAS-101, no. 9, pp. 3117–3125, Sep. 1982.

[122] F. Pagola, I. J. Perez-Arriaga, and G. Verghese, "On sensitivities, residues and participations: Applications to oscillatory stability analysis and control," *IEEE Transactions on Power Systems*, vol. 4, no. 1, pp. 278–285, Feb. 1989.

[123] L. Rouco and I. J. Perez-Arriaga, "Multi-area analysis of small signal stability in large electric power systems by SMA," *IEEE Transactions on Power Systems*, vol. 8, no. 3, pp. 1257–1265, Aug./1993.

[124] G. Verghese, I. J. Perez-arriaga, and F. Schweppe, "Selective Modal Analysis With Applications to Electric Power Systems, Part II: The Dynamic Stability Problem," *IEEE Transactions on Power Apparatus and Systems*, vol. PAS-101, no. 9, pp. 3126–3134, Sep. 1982.

[125] L. Vanfretti and J. H. Chow, "Analysis of power system oscillations for developing synchrophasor data applications," in *2010 IREP Symposium Bulk Power System Dynamics and Control - VIII (IREP)*. Rio de Janeiro, Brazil: IEEE, Aug. 2010, pp. 1–17.

[126] L. Rouco, F. L. Pagola, A. Garcia-Cerrada, J. M. Rodriguez, and R. M. Sanz, "Damping of electromechanical oscillations in power systems with superconduction magnetic energy storage systems: Location and controller design," in *12th Power Systems Computation Conference*, vol. 1097–1104, Dresden, 1996-08-19/1996-08-23.

[127] C. Moler, "MATLAB Users' Guide," 1980.

[128] Q. Zhang, J. D. McCalley, V. Ajjarapu, J. Renedo, M. A. Elizondo, A. Tbaileh, and N. Mohan, "Primary Frequency Support Through North American Continental HVDC Interconnections With VSC-MTDC Systems," *IEEE Transactions on Power Systems*, vol. 36, no. 1, pp. 806–817, Jan. 2021.

[129] L. Diez-Maroto, J. Renedo, L. Rouco, and F. Fernandez-Bernal, "Lyapunov Stability Based Wide Area Control Systems for Excitation Boosters in Synchronous Generators," *IEEE Transactions on Power Systems*, vol. 34, no. 1, pp. 194–204, Jan. 2019.

[130] E. V. Larsen and D. A. Swann, "Pplying Power System Stabilizers Part II: Performance Objectives and Tuning Concepts," *IEEE Transactions on Power Apparatus and Systems*, vol. PAS-100, no. 6, pp. 3025–3033, 1981.

[131] S. H. Jakobsen, L. Kalemba, and E. H. Solvang, "The Nordic 44 test Network," *Online: https://figshare. com/projects/Nordic_44/57905*, p. 1001438 Bytes, 2018.

[132] M. Robin, J. Renedo, J. C. Gonzalez-Torres, A. Garcia-Cerrada, A. Benchaib, and P. Garcia-Gonzalez, "An Algorithm for DC Segmentation of AC Power Systems to Mitigate Electromechanical Oscillations," *IEEE Access*, vol. 11, pp. 64 651–64 667, 2023.

[133] M. Robin, J. Renedo, J. C. Gonzalez-Torres, A. Garcia-Cerrada, L. Rouco, A. Benchaib, and P. Garcia-Gonzalez, "Addressing intra-area oscillations and frequency stability after DC segmentation of a large AC power system," Jun. 2024.

[134] "Nordic44-Nordpool/N44_BC.dyr at master · ALSETLab/Nordic44-Nordpool," https://github.com/ALSETLab/Nordic44-Nordpool, Oct. 2022.

# Appendix A

# Two areas test system

## A.1 AC base case

Fig. A.1 presents the Two-area system with an AC interconnection studied in Chapter 4.

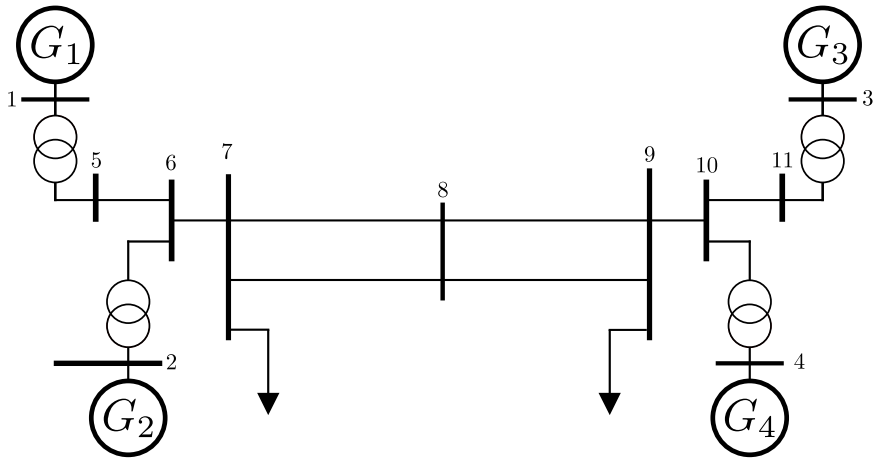


Figure A.1: AC base case: Two-area system with an AC interconnection.

Data of the HVAC test system can be found on [24] with the only difference that, here, the nominal voltage of the transmission system and the nominal frequency have been changed to 220 kV and 50 Hz, respectively.

## A.2 DC-segmented case

Fig. A.2 presents the Two-area system with a VSC-HVDC interconnection studied in Chapter 4.

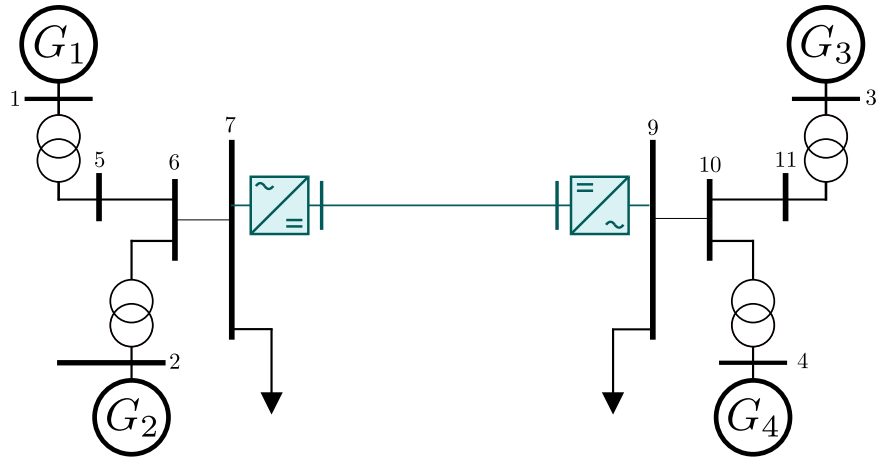


Figure A.2: DC-segmented case: Two-area system with a VSC-HVDC interconnection.

VSC of bus 7 was set in p-control mode while VSC of bus 9 was set in $V_{dc}$-control mode. The characteristics of the VSCs and DC line used to segment the two-area system are included in Table A.1.

Table A.1: Data of the HVDC link in the DC-segmented two area test system.

| Parameters (p.u's: converter rating) | Values |
|---|---|
| Rating VSC, DC voltage | 500 MVA, ± 320 kV |
| Configuration | Symmetrical monopole |
| Max active (reactive) power | ± 500 MW, (± 250 MVAr) |
| Max. current | 1.1 p.u. (q-priority) |
| Max. DC voltage $V_{dc,i}^{max}, V_{dc,i}^{min}$ | No limitation |
| Current-controller time constant ($\tau$) | 3 ms |
| Voltage- controller time constant ($\tau_{dc}$) | 40 ms |
| Voltage- controller damping ration ($\zeta_{dc}$) | 0.7 |
| Outer control gains | |
| P prop./int.($K_{p,d1}/K_{i,d1}$) | 0/0 |
| $V_{dc}$ prop./int.($K_{p,d2}/K_{i,d2}$) | 10 p.u./20 p.u./s |
| Q prop./int.($K_{p,q1}/K_{i,q1}$) | 0/0 |
| Connection imp. ($R_{s,i} + jX_{s,i}$) | 0.02 + j 0.2 p.u. |
| VSCs' loss coefficients | a = b = c = 0 p.u. |
| DC-bus capacitance ($C_i^{dc}$) | 195 $\mu F$ |
| DC-line series resistance, inductance ($R_{ij}^{dc}, L_{ij}^{dc}$) | 2.55 Ω, 1.7442 mH |
| Initial operation point | |
| P injection (bus 7/ bus 9) | -418/400 MW |
| Q injection (bus 7/ bus 9) | 100/-100 MVAr |

# Appendix B

# 6-generator test system

## B.1 Six-generator test system 1

Fig. B.1 presents the 6 generator test system studied in Chapters 5 and 6.

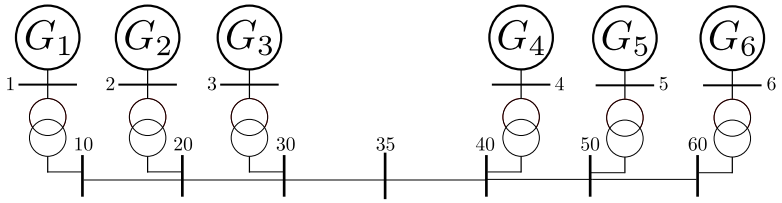


Figure B.1: Test system 1: Conceptual 6-generator system.

Each of the six generators radially connected in this system is rated at 200 MVA and 20 kV with a nominal frequency of 50 Hz. The generator parameters in per unit on the rated MVA and kV base are:

$$H = 6.5s, \;\; D = 0p.u., \;\; R = 0.0025p.u.,$$
$$T'_{d0} = 8s, \;\; T''_{d0} = 0.03s, \;\; T'_{q0} = 0.4s, \;\; T''_{q0} = 0.05s,$$
$$X_d = 1.8p.u., \;\; X_q = 1.7p.u., \;\; X'_d = 0.3p.u.,$$
$$X'_q = 0.55p.u., \;\; X''_d = 0.25p.u., \;\; X_L = 0.2p.u.$$

Each generator has an excitation system with parameters: $T_r = 0.01s$, $K_a = 200p.u.$ Each step-up transformer has an impedance of 0 + j0,15 p.u. on a 200 MVA and 20/220 kV base and has an off-nominal ratio of 1.0.

The transmission system nominal voltage is 220 kV. The inter-area lines (lines 30-35 and 35-40) have a length of 50 km while the local lines (lines

10-20, 20-30, 40-50, and 50-60) have a length of 25 km. The parameters of the lines in p.u. per km on a 100 MVA, 220 kV base are:

$$r = 0.0001\,p.u./km, \quad x_L = 0.001\,p.u./km,$$
$$b_c = 0.00175\,p.u./km$$

The system is operating with the left area exporting 600 MW to the right area and the generating units are loaded as listed in Table B.1.

Table B.1: Initial power flow data of the six-generator system.

| | $P_{G,i}$ (MW) | $Q_{G,i}$ (Mvar) | $V_i$ (p.u.) | $\theta_i$ (deg) |
|---|---|---|---|---|
| G1 | 112.9 | 11.6 | 1 | 0.0 |
| G2 | 100 | 15.2 | 1 | -2.2 |
| G3 | 100 | 24.7 | 1 | -5.2 |
| G4 | -100 | 36.7 | 1 | -32.7 |
| G5 | -100 | 30.2 | 1 | -35.8 |
| G6 | -100 | 26.9 | 1 | -37.3 |

## B.2 Six-generator + one-load test system 2

Fig. B.2 presents the 6 generator one-load test system studied in Chapter 5.

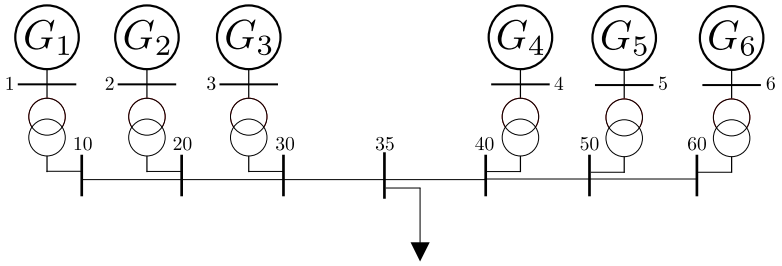


Figure B.2: Test system 2: Conceptual 6-generator system with one load.

This system is like the previous one but with a 600 MW-0 MVAr load connected at bus 35. The generating units are loaded as listed in table B.2.

## B.3 DC-segmented six-generator test system

Fig. B.3 and B.4 presents the two variation of the DC segmented 6 generator test system studied in Chapter 6.

Table B.2: Initial power flow data of the six-generator 1 load system.

| | $P_{G,i}$ (MW) | $Q_{G,i}$ (Mvar) | $V_i$ (p.u.) | $\theta_i$ (deg) |
|---|---|---|---|---|
| G1 | 112.8 | 16.7 | 1 | 0.0 |
| G2 | 100 | 22.0 | 1 | -2.2 |
| G3 | 100 | 35.4 | 1 | -5.3 |
| G4 | 100 | 34.4 | 1 | -5.7 |
| G5 | 100 | 21.1 | 1 | -2.8 |
| G6 | 100 | 15.0 | 1 | -1.3 |

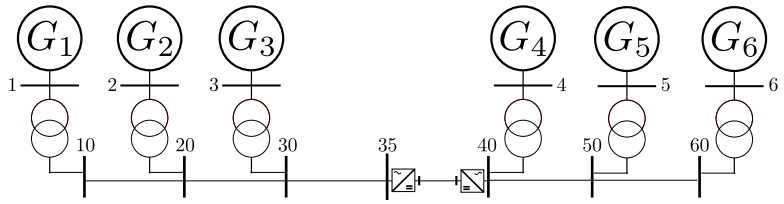


Figure B.3: Test system 1-DC 1:6-generator system with DC segmentation 1.

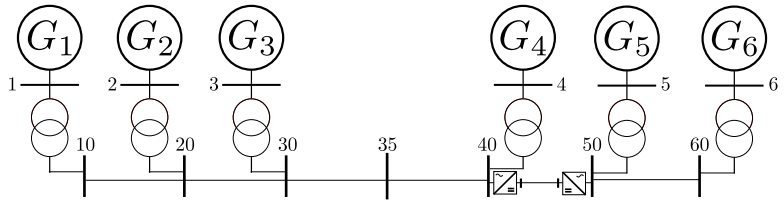


Figure B.4: Test system 1-DC 2: 6-generator system with DC segmentation 2.

The characteristics of the VSCs and the two DC lines used to segment the six-generator system are included in Table B.3.

Table B.3: Data of the HVDC links in the DC-segmented six-generator system.

| Parameters (p.u's: converter rating) | Values |
|---|---|
| Rating VSC, DC voltage | 500 MVA, ± 320 kV |
| Configuration | Symmetrical monopole |
| Max active (reactive) power | $\pm 500MW$, $(\pm 200MVAr)$ |
| Max. current | 1 p.u. |
| Max. DC voltage $V_{dc,i}^{max}, V_{dc,i}^{min}$ | 1.1 , 0.9 p.u. |
| Current-controller time constant ($\tau$) | 2 ms |
| Connection imp. $(R_{s,i} + jX_{s,i})$ | 0.02 + j 0.2 p.u. |
| Outer control gains | |
| P prop./int.$(K_{p,d1}/K_{i,d1})$ | 0/0 |
| $V_{dc}$ prop./int.$(K_{p,d2}/K_{i,d2})$ | 10 p.u./20 p.u./s |
| Q prop./int.$(K_{p,q1}/K_{i,q1})$ | 0/0 |
| VSCs' loss coefficients | a = b = c = 0 p.u. |
| DC-bus capacitance $(C_i^{dc})$ | 195 $\mu F$ |
| DC-line series resistance, inductance $(R_{ij}^{dc}, L_{ij}^{dc})$ | |
| - line 35-40 | 2.2 Ω, 77.1 mH |
| - line 40-50 | 1.1 Ω, 38.5 mH |

# Appendix C

# Nordic 44 test system

## C.1 AC base case

The Nordic 44 test system is presented in Fig. C.1.

The Nordic 44 test system is a representation of the interconnected grids of Norway, Sweden and Finland. It is based on previous models developed at The Norwegian University of Science and Technology (NTNU) [131]. It has been initially implemented within iTesla project as an application example of the OpenIPSL library, implemented in the Modelica language [91, 92]. The version used in this thesis is the one updated by the ALSETlab team. In this thesis, the simulations of the Nordic 44 system are carried out using the Dymola environment. OpenIPSL can be used for non-linear electromechanical-type simulation, but also for small-signal stability analysis, by using a numerical linearisation of the system.

Dynamic and static data of the Nordic 44 test system can be found under [134]. The initial power flow condition used in this paper correspond to the Nord Pool data of Tuesday November 10 2015 at 11:38 available at the same link.

## C.2 DC-segmented case

The DC-segmented Nordic 44 test system is presented in Fig. C.2.

The DC-segmented case was obtained from the initial Nordic 44 system by replacing AC line 5100-6500 and the two parallel lines between buses 3359 and 5101 with VSC-HVDC links. The characteristics of the four VSCs and the two DC lines are included in Table C.1. VSC 5100, 6500, 5101 and 3359

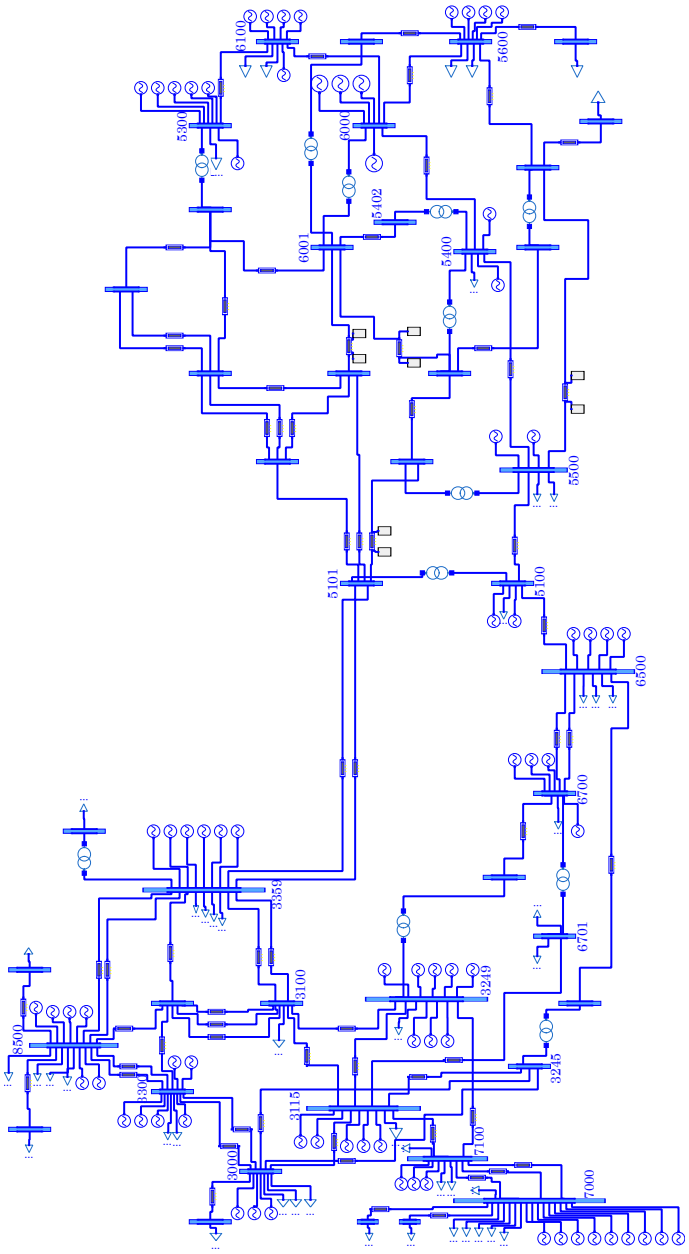


Figure C.1: Nordic 44 test system under Dymola.

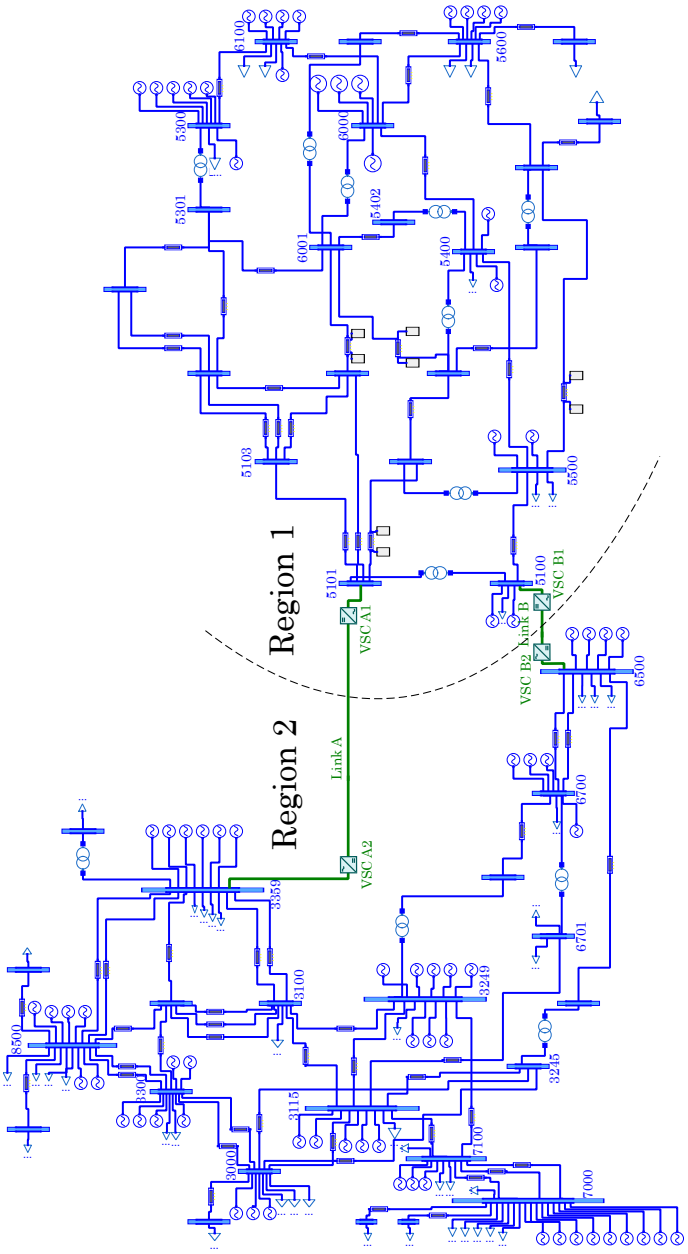


Figure C.2: DC-segmented Nordic 44 test system under Dymola.

are renamed VSC 1, 2, 3 and 4 in the table for simplicity.

Table C.1: Data of the HVDC links in the DC-segmented Nordic 44 system.

| Parameters<br>(p.u's: converter rating) | Values |
|---|---|
| Rating VSC (VSCA1-2/ VSCV1-2) | 3500/800 MVA |
| DC voltage (VSCA1-2/ VSCV1-2) | ± 535/320 kV |
| Configuration | Symmetrical monopole |
| Max active power (VSCA1-2/ VSCV1-2) | $\pm 3500/800 MW$ |
| Max reactive power (VSCA1-2/ VSCV1-2) | $\pm 1400/320 MVAr$ |
| Max. current | 1 p.u. |
| Max. DC voltage $V_{dc,i}^{max}, V_{dc,i}^{min}$ | 1.1, 0.9 p.u. |
| Current-controller time constant ($\tau$) | 2 ms |
| Connection imp. ($R_{s,i} + jX_{s,i}$) | 0.004 + j 0.2 p.u. |
| Outer control gains | |
| P prop./int.($K_{p,d1}/K_{i,d1}$) | 0/0 |
| $V_{dc}$ prop./int.($K_{p,d2}/K_{i,d2}$) | 10 p.u./20 p.u./s |
| Q prop./int.($K_{p,q1}/K_{i,q1}$) | 0/0 |
| VSCs' loss coefficients | a = b = c = 0 p.u. |
| DC-bus capacitance ($C_{dc,i}$) (VSCA1-2/ VSCV1-2) | 305/195 $\mu F$ |
| DC-line series resistance, inductance ($R_{dc,ij}, L_{dc,ij}$) | |
| - line A (5101-3359) | 1.6 Ω, 67 mH |
| - line B (5100-6500) | 7.2 Ω, 258 mH |

VSCs 6500 and 3359 were set in $V_{dc}$-control mode while VSCs 5100 and 5101 were set in $P$-control mode.